# The Anomalous Magnetic Moment of Baryons in Cavity QCD

R. J. Lindebaum
Department of Physics
University of Cape Town

A thesis submitted in partial fulfillment
of the requirements for
the degree of Master of Science in Theoretical Physics

16 September 1992

## Abstract

Using a generalised form of the Gell-Mann and Low theorem, all the diagrams in cavity QCD to order $\alpha_S$ that contribute to the magnetic moment are calculated. The calculations are performed for massive quarks so a mass renormalisation scheme has been developed to cope with the new divergances this brings into the self-energy insert diagrams.

The results of this work show that no improvement on the simple SU(3) model is made by including these corrections. These calculations point to a smaller value of $\alpha_S$ than that which is ususally used.

# Contents

# Introduction

Quantum chromodynamics (QCD) is generally believed to be the theory describing strong interactions. The major discovery that led to QCD as the theory of strong interactions was the discovery of the asymptotic freedom of non-Abelian gauge field theories. The need for an asymptotically free theory became apparent in 1969 when Bjorken reported that the deep inelastic region of electron–nucleon scattering where the momentum transfer squared $q^2$ and the energy transfer $\nu$ both are very large, then the structure function should depend only on the ratio $q^2/\nu$ and not on these independent variables separately. Immediately after Bjorken made his proposal, experimental confirmation was found for it. This proposal is most easily understood if one assumes that the electrons scatter off almost free point–like particles inside the nucleus, and hence the need to find a quantum field theory that has an effective coupling constant that becomes smaller for large momentum, ie. an asymptotically free theory. A search was made of all the known quantum field theories in four dimensions, and only Yang–Mills theory was found via the renormalization group technique to have an ultra–violet fixed point at zero momentum and hence being asymptotically free. In the meanwhile it had frequently been suggested that quarks must carry a new quantum number called colour and exhibit a colour symmetry to resolve the following problems in the quark model :

- Construction of baryon wavefunctions
- Non–observability of isolated quarks
- The discrepancy between the predictions and experimentally determined values for the total cross section of $e^+e^- \rightarrow$ hadrons and the decay rates for $\pi^0 \rightarrow 2\gamma$.

Fritzch and Gell–Mann proposed that the extra symmetry in the Yang–Mills or non–Abelian gauge field theory be identified with the colour symmetry. Fortunately at this time t'Hooft had already proven the renormalizability of non–Abelian gauge field theory. The problem of quark confinement may be overcome by assuming that only colourless states are physically realizable. It may also be possible to explain this assumption as a

dynamical effect in QCD, perhaps due to the serious infrared divergences found in QCD due to the massless gluons. The infrared divergences in QCD are much worse than the infrared divergences in QED due to the self–coupling of the gluons.

The asymptotic freedom of QCD allows one to safely use perturbation theory to discuss the short distance reactions. To uniquely extract the purely short distance part of an operator to be calculated, the operator product expansion may be used. Perturbative QCD has been successful in calculating many processes such as $e^+e^-$ annihilation, Drell–Yan processes and jets.

The computation of higher order effects in perturbative QCD have been done, but some predictive power is lost due to the renormalization scheme dependence of the results. At the present energy scale available experimentally the strong coupling constant $\alpha_S$ is approximately 1/10 which leads to non negligible renormalization scheme dependence in the results calculated.

One major requirement of a theory of strong interactions is that it must produce confinement. Confinement appears to be a non–perturbative part of QCD which is at present not calculable. The calculation of the properties of the hadrons such as magnetic moment, charge radius squared and the ratio $g_A/g_V$ is beyond the scope of perturbative QCD. One can resort to lattice QCD to calculate these properties, which gives some quite promising results. Despite this, quite a lot of work needs to be done to reduce the lattice spacing and increase the lattice size to avoid unphysical finite spacing and finite size effects. To do this requires faster computers and better algorithms.

Another technique that can be used is to make some simplifying assumptions about the confinement mechanism before any QCD calculations are done. One model of this nature was the M.I.T. bag model [14] which was quite popular for a while. This model introduces confinement by imposing boundary conditions on the colour carrying particles. The advantage of imposing confinement in this way is that there is only minimal modification to the underlying gauge field theory. The results to lowest order of perturbation theory are quite good despite the fact that confining the particles to a static sphere breaks the translational and Lorentz invariance, as well as the chiral symmetry of the theory. Calculation of higher order terms in this theory is rather difficult, especially the divergent loop diagrams. A number of other non–renormalizable bag models such as the chiral [1] and the cloudy [2] bag introduce an elementary pion field into the theory to restore the chiral symmetry. This is a bit disturbing as the pionic interactions should already be contained in QCD.

Models of this nature are supported by work done by T. D. Lee [4] who analysed QCD in a finite volume and found that the effective colour dielectric constant became very small for large volumes. The bag models can thus be seen in the light of a region in which the colour dielectric constant is 1 surrounded by a region where the colour

dielectric constant is 0.

Buser *et al.* [3] has approached this topic form a different angle by showing that QCD can be formulated consistently in a finite volume subject to the M.I.T. bag model boundary conditions. Stoddart *et al.* [13] has introduced a method of renormalizing this theory based on dimensional regularisation in free space. The result is that cavity QCD is a fully fledged field theory in its own right. This finite volume field theory can be used as an approximation to the real world. Calculations of the quark self–energy for massless [13] and massive [6] quarks, the gluon self energy [5], magnetic moments of the proton and neutron [7] and the ratio $g_A/g_V$ [27] have been done.

In this thesis the magnetic moment of baryons are calculated. The calculation is similar to that of O'Connor [7] who calculated the magnetic moment of the proton and neutron, but it has the added complexity of massive quarks and hence mass renormalization. Magnetic moments of the baryons are useful to calculate as they are well known experimentally. Most of the magnetic moments known involve baryons containing strange quarks and hence the need to include massive quarks is clear. The techniques used to handle massive quarks developed in this thesis, especially the mass renormalization, can easily be adapted to calculation of other observables in cavity QCD.

If one views cavity QCD as an approximation to the real world, centre of mass corrections need to be performed due to the breaking of the Lorentz invariance of the theory. Centre of mass corrections have not been attempted in this work due to the unreliability of the usual Peierl– Yoccoz method of calculating them, especially in the case of the magnetic moment [2].

In chapter 1 QCD is developed in order to develop the notation used in this work. The Gell–Mann and Low theorem is discussed as it forms the basis of the calculations done here. The field operators and propagators in cavity QCD are discussed.

In chapter 2 the renormalization techniques used in this thesis are developed. This is done by first looking at the free space renormalization of these diagrams. The divergences in the free space diagrams are then Fourier transformed to the cavity and can be used to renormalize the cavity diagrams.

In chapter 3 the diagrams contributing to the magnetic moment are found via the Gell–Mann and Low theorem and evaluated in the cavity. The last section shows how in this formalism the unwanted diagrams cancel out naturally.

In chapter 4 the techniques and numerical routines used to obtain the results are discussed.

In chapter 5 the results of this calculation are displayed and compared with the results of other similar calculations and conclusions are drawn.

The bulk of the details of the calculations done here are found in the appendices at the end of this work.

# Chapter 1

# Background

This chapter serves as an brief introduction to both free space QCD and cavity QCD. This work is well known, but is included in here to develop the notation used in this thesis and to serve as an easy reference.

## 1.1 Canonical Quantization

It is not known how to implement the usual path integral method in a cavity, so the canonical operator formalism is used instead. This section is a brief review of this formalism which also serves to develop the notation used in this thesis. The notation is essentially the same as that used by Buser *et al.* [3] The Lagrange density of QCD is

$$\mathcal{L} = \bar{\psi}\left(i\gamma_\mu D^\mu - M\right)\psi - \frac{1}{2}i\partial_\mu\left(\bar{\psi}\gamma^\mu\psi\right) - \frac{1}{4}\boldsymbol{F}_{\mu\nu}\cdot\boldsymbol{F}^{\mu\nu} - \frac{1}{2}\lambda\partial_\mu\boldsymbol{A}^\mu\cdot\partial_\nu\boldsymbol{A}^\nu + i\boldsymbol{\chi}\cdot\partial_\mu\mathcal{D}^\mu\boldsymbol{\omega} \quad (1.1)$$

where the covariant derivative determines the interaction between quarks and gluons

$$D^\mu\psi = \left(\partial^\mu - ig\boldsymbol{\lambda}/2\cdot\boldsymbol{A}^\mu\right)\psi \quad (1.2)$$

The covariant derivative in the adjoint representation of the gauge group determines the interaction between the ghosts and gluons

$$\mathcal{D}_\mu\boldsymbol{\omega} = \partial_\mu\boldsymbol{\omega} + g\boldsymbol{A}_\mu\times\boldsymbol{\omega} \quad (1.3)$$

The chromoelectromagnetic field strength tensor $\boldsymbol{F}^{\mu\nu}$ can be written as

$$\boldsymbol{F}^{\mu\nu} = \partial^\mu\boldsymbol{A}^\nu - \partial^\nu\boldsymbol{A}^\mu + g\boldsymbol{A}^\mu\times\boldsymbol{A}^\nu \quad (1.4)$$

The field strength tensor $\boldsymbol{F}^{\mu\nu}$ and the covariant derivative are connected via the Bianchi identity.

$$[D^\mu, D^\nu] = -\frac{1}{2} ig \boldsymbol{\lambda} \cdot \boldsymbol{F}^{\mu\nu} \tag{1.5}$$

We have made use of the eight dimensional scalar and vector products in colour space

$$\boldsymbol{A} \cdot \boldsymbol{B} = \sum_{a=1}^{8} A_a B_a \tag{1.6}$$

$$(\boldsymbol{A} \times \boldsymbol{B})_a = \sum_{b,c=1}^{8} f_{abc} A_b B_c \tag{1.7}$$

where $f_{abc}$ are the structure constants of $\mathrm{SU}(3)_{\mathrm{colour}}$ and the $\lambda_a$ are the Gell-Mann matrices. The first two terms in the Lagrange density describe the locally gauge invariant interacting quark and gluon fields. The third term is the covariant gauge fixing term which is globally gauge invariant, which is required in the quantized theory to make the canonical conjugate momentum $\boldsymbol{\Pi}^0$ of $\boldsymbol{A}^0$ non vanishing. The fourth term is the Faddeev–Popov ghost term which makes the Lagrange density invariant under a BRS transformation, which is a transformation on the fields $\psi, \boldsymbol{A}_\mu, \omega, \chi$ that resembles the local gauge transformation on the quark and gluon fields. The Lagrange density can be separated into a part independent of the coupling constant $g$, which describes the free quark, gluon and ghost fields

$$\begin{aligned} \mathcal{L}_0 = {} & \bar{\psi} \left( \frac{1}{2} i \gamma_\mu \overleftrightarrow{\partial^\mu} - M \right) \psi - \frac{1}{4} (\partial_\mu \boldsymbol{A}_\nu - \partial_\nu \boldsymbol{A}_\mu) \cdot (\partial^\mu \boldsymbol{A}^\nu - \partial^\nu \boldsymbol{A}^\mu) \\ & - \frac{1}{2} \lambda \partial_\mu \boldsymbol{A}^\mu \cdot \partial_\nu \boldsymbol{A}^\nu - i \partial_\mu \boldsymbol{\chi} \cdot \partial^\mu \boldsymbol{\omega} \end{aligned} \tag{1.8}$$

and a $g$ dependent part or interaction part

$$\begin{aligned} \mathcal{L}_{\mathrm{int}} = {} & \frac{1}{2} g \bar{\psi} \gamma_\mu \boldsymbol{\lambda} \psi \cdot \boldsymbol{A}^\mu - \frac{1}{2} g (\partial^\mu \boldsymbol{A}^\nu - \partial^\nu \boldsymbol{A}^\mu) \cdot (\boldsymbol{A}_\mu \times \boldsymbol{A}_\nu) \\ & - \frac{1}{4} g^2 (\boldsymbol{A}^\mu \times \boldsymbol{A}^\nu) \cdot (\boldsymbol{A}_\mu \times \boldsymbol{A}_\nu) - i g \partial_\mu \boldsymbol{\chi} \cdot (\boldsymbol{A}^\mu \times \boldsymbol{\omega}) \end{aligned} \tag{1.9}$$

In order to write out the Hamiltonian density one needs the canonical conjugate momentum of all the fields

$$\Psi = \frac{\partial \mathcal{L}}{\partial \dot{\psi}} = -\frac{1}{2} i \psi^\dagger \tag{1.10}$$

$$\bar{\Psi} = \frac{\partial \mathcal{L}}{\partial \dot{\bar{\psi}}} = -\frac{1}{2} i \bar{\psi}^\dagger \tag{1.11}$$

$$\boldsymbol{\Pi}^k = \frac{\partial \mathcal{L}}{\partial \dot{\boldsymbol{A}}_k} = \boldsymbol{F}^{k0} \qquad k = 1,2,3 \tag{1.12}$$

$$\boldsymbol{\Pi}^0 = \frac{\partial \mathcal{L}}{\partial \dot{\boldsymbol{A}}_0} = -\lambda \partial_\mu \boldsymbol{A}^\mu \tag{1.13}$$

$$\boldsymbol{X} = \frac{\partial \mathcal{L}}{\partial \dot{\boldsymbol{\chi}}} = -i\mathcal{D}_0 \boldsymbol{\omega} \tag{1.14}$$

$$\boldsymbol{\Omega} = \frac{\partial \mathcal{L}}{\partial \dot{\boldsymbol{\omega}}} = i\dot{\boldsymbol{\chi}} \tag{1.15}$$

The Hamilton density is then

$$\mathcal{H} = -\frac{\partial \mathcal{L}}{\partial \dot{\psi}}\dot{\psi} + \dot{\bar{\psi}}\frac{\partial \mathcal{L}}{\partial \dot{\bar{\psi}}} + \dot{\boldsymbol{A}}_\mu \cdot \frac{\partial \mathcal{L}}{\partial \dot{\boldsymbol{A}}_\mu} + \dot{\boldsymbol{\chi}} \cdot \frac{\partial \mathcal{L}}{\partial \dot{\boldsymbol{\chi}}} + \dot{\boldsymbol{\omega}} \cdot \frac{\partial \mathcal{L}}{\partial \dot{\boldsymbol{\omega}}} - \mathcal{L} \tag{1.16}$$

where the minus sign on the first term is due to the Grassman nature of the quark fields. The Hamilton density is a function of the fields, spatial derivatives of the fields and the canonical momenta. This can also be split into its free $g$ independent parts

$$\begin{aligned} \mathcal{H}_0 = {} & \bar{\psi}\left(-\frac{1}{2}i\gamma_k \overleftrightarrow{\partial^k} + M\right)\psi + \frac{1}{4}\left(\partial_k \boldsymbol{A}^l - \partial_l \boldsymbol{A}^k\right) \cdot \left(\partial_k \boldsymbol{A}^l - \partial_l \boldsymbol{A}^k\right) + \frac{1}{2}\boldsymbol{\Pi}^k \cdot \boldsymbol{\Pi}^k \\ & -\frac{1}{2\lambda}\boldsymbol{\Pi}^0 \cdot \boldsymbol{\Pi}^0 + \boldsymbol{\Pi}^k \cdot \partial_k \boldsymbol{A}^0 - \boldsymbol{\Pi}^0 \cdot \partial_k \boldsymbol{A}^k - i\boldsymbol{\Omega} \cdot \boldsymbol{X} - \partial_k \boldsymbol{\chi} \cdot \partial_k \boldsymbol{\omega} \end{aligned} \tag{1.17}$$

and an interaction part that depends explicitly on $g$

$$\begin{aligned} \mathcal{H}_{\text{int}} = {} & -\frac{1}{2}g\bar{\psi}\gamma_\mu \boldsymbol{\lambda}\psi \cdot \boldsymbol{A}^\mu - \frac{1}{2}g\left(\partial_k \boldsymbol{A}^l - \partial_l \boldsymbol{A}^k\right) \cdot \left(\boldsymbol{A}^k \times \boldsymbol{A}^l\right) \\ & -g\boldsymbol{\Pi}^k \cdot \left(\boldsymbol{A}^k \times \boldsymbol{A}^0\right) + \frac{1}{4}g^2(\boldsymbol{A}_k \times \boldsymbol{A}_l) \cdot \left(\boldsymbol{A}^k \times \boldsymbol{A}^l\right) \\ & +g\boldsymbol{\Omega} \cdot \left(\boldsymbol{A}^0 \times \boldsymbol{\omega}\right) + ig\partial_k \boldsymbol{\chi} \cdot \left(\boldsymbol{A}^k \times \boldsymbol{\omega}\right) \end{aligned} \tag{1.18}$$

The terms in eq. (1.18) describe the two quark and one gluon interaction, the three gluon interaction, the four gluon interaction and the two ghost one gluon interactions respectively. The Hamiltonian can be formed by integrating the Hamilton density over space and time

$$H = \int d^4x\, \mathcal{H}_0 + \mathcal{H}_{\text{int}} \tag{1.19}$$

This Hamiltonian is quantized by interpreting the fields in the classical theory as field operators and imposing equal time anti-commutation relations on the fields that are

Grassman in the classical theory, and commutation relations on the Hermitian gluon field operators.

$$\left\{\psi_{c,f,\alpha}(\vec{x},t),\psi^{\dagger}_{c',f',\alpha'}(\vec{y},t)\right\} = \delta_{cc'}\delta_{ff'}\delta_{\alpha\alpha'}\delta^3(\vec{x}-\vec{y}) \quad (1.20)$$

$$\{\omega_a(\vec{x},t),\Omega_b(\vec{y},t)\} = -i\delta_{ab}\delta^3(\vec{x}-\vec{y}) \quad (1.21)$$

$$\{\chi_a(\vec{x},t),X_b(\vec{y},t)\} = -i\delta_{ab}\delta^3(\vec{x}-\vec{y}) \quad (1.22)$$

$$[A^{\mu}_a(\vec{x},t),\Pi^{\nu}_b(\vec{y},t)] = ig^{\mu\nu}\delta_{ab}\delta^3(\vec{x}-\vec{y}) \quad (1.23)$$

This quantization procedure has made the fields become field operators in the Heisenberg picture which satisfy the Heisenberg equation of motion

$$i\frac{\partial}{\partial t}F(\vec{x},t) = [F(\vec{x},t),H] \quad (1.24)$$

while the state vectors defining the Fock space are time independent. It is useful to transform to the interaction or Dirac picture. This is done using a unitary transformation $U(t)$ in the Fock space which satisfies the differential equation

$$i\frac{\partial}{\partial t}U(t) = U(t)H_{\rm int}(t) \quad (1.25)$$

and transforms a Heisenberg state $|\psi\rangle$ into a Dirac state $|\hat{\psi}(t)\rangle$

$$|\hat{\psi}(t)\rangle = U(t)|\psi\rangle \quad (1.26)$$

A general field operator is transformed from the Heisenberg picture $F(\vec{x},t)$ to the Dirac picture $\hat{F}(\vec{x},t)$ by

$$\hat{F}(\vec{x},t) = U(t)F(\vec{x},t)U^{-1}(t) \quad (1.27)$$

The commutation relations (1.20)-(1.23) still hold in the Dirac picture. The equation of motion in the Dirac picture is

$$i\frac{\partial}{\partial t}\hat{F}(\vec{x},t) = \left[\hat{F}(\vec{x},t),H_0\right] \quad (1.28)$$

and the Dirac states satisfy

$$i\frac{\partial}{\partial t}|\hat{\psi}(t)\rangle = \hat{H}_{\rm int}|\hat{\psi}(t)\rangle \quad (1.29)$$

The field operators of the non interacting Hamiltonian satisfy the non interacting field equations

$$(i\gamma_\mu\partial^\mu - M)\hat{\psi} = \hat{\bar{\psi}}(i\gamma_\mu\overleftarrow{\partial^\mu} - M) = 0 \quad (1.30)$$

$$\Box\hat{\boldsymbol{A}}^{\mu} + (\lambda-1)\partial^\mu\partial_\nu\hat{\boldsymbol{A}}^{\nu} = 0 \quad (1.31)$$

$$\Box\hat{\omega} = \Box\hat{\chi} = 0 \quad (1.32)$$

These equations are important as the asymptotic states will be constrained to be soloutions of the non–interacting field equations.

It is well known that canonical quantization of gauge fields leads to a Fock space with an indefinite metric. This indefinite metric means that there are states with negative norm. This endangers the probabilistic nature of the quantum theory. The solution to this problem lies in the fact the whole Fock space is too large to describe the physicial world. A constraint on the Hilbert space, such as the Gupta– Bleuler condition in QED

$$\partial_\mu A^{\mu(+)}|\psi_{\text{phys}}\rangle = 0 \tag{1.33}$$

is required to guarentee a subspace $|\psi_{\text{phys}}\rangle$ which has a positive definite norm. The corresponding relation in QCD is that the physical states must have no BRS charge i.e.

$$Q_B|\psi_{\text{phy}}\rangle = 0 \tag{1.34}$$

The BRS charge is the spatial integral of the zeroth component of the conserved current which arises due to the BRS invariance of the Lagrange density and Noether's theorem. (See Buser *et al* [3] for more details of the definition of the BRS charge.)

## 1.2 The Gell–Mann and Low Theorem

Observables are often expressed in terms of energy shifts between the interacting and non interacting systems. The usual way of calculating energy shifts is via the Gell–Mann and Low theorem. The Gell–Mann and Low theorem is expressed in terms of the time–evolution operator $U(t,t')$ which is related to the unitary transformation $U(t)$ of the previous section by

$$U(t,t') = U(t)U^{-1}(t') \tag{1.35}$$

and it satisfies the same differential equation as $U(t)$

$$i\frac{\partial U(t,t')}{\partial t} = H_{\text{int}}(t)U(t,t') \tag{1.36}$$

together with the initial condition $U(t,t) = 1$. The reason $U(t,t')$ is called the time evolution operator becomes clear when it acts on a state in the Dirac picture

$$|\hat{\psi}(t)\rangle = U(t,t')|\hat{\psi}(t')\rangle \tag{1.37}$$

All the physics of the quantum field theory is contained in the operator $U(t,t')$. This can be seen by multiplying equation (1.36) by $|\hat{\psi}(t')\rangle$ and using equation (1.37) which gives

the equation of motion (1.28). The solution of equation (1.36) together with the initial condition is given in terms of Dyson's expansion which expresses $U(t,t')$ as a series of time ordered products of $\hat{H}_{\rm int}(t)$ (see the well known book by Fetter and Walecka [21].)

$$U^{\epsilon}(t,t') = \sum_{n=0}^{\infty} \frac{(-i)^n}{n!} \int_{t'}^{t} dt_1 \cdots \int_{t'}^{t} dt_n \; T\left(\hat{H}^{\epsilon}_{\rm int}(t_1) \cdots \hat{H}^{\epsilon}_{\rm int}(t_n)\right) \tag{1.38}$$

where we have introduced an adiabatic switch on of the interaction by defining

$$\hat{H}^{\epsilon}_{\rm int}(t) = e^{-\epsilon|t|}\hat{H}_{\rm int}(t) \tag{1.39}$$

where $\epsilon$ is a small positive number.

Let $|\hat{\phi}_k\rangle$ is a set of complete and orthonormal eigenvectors of the non interacting Hamiltonian. The Gell-Mann and Low theorem states that if a state vector

$$|\psi_k\rangle = \lim_{\epsilon\to 0} \frac{U^{\epsilon}(0,-\infty)|\hat{\phi}_k\rangle}{\langle\hat{\phi}_k|U^{\epsilon}(0,\infty)|\hat{\phi}_k\rangle} \tag{1.40}$$

exists to all orders, then it is an eigenstate of the full Hamilton operator at $t = 0$. This can also be expressed as

$$E_k - E_k^0 = \lim_{\epsilon\to 0} \frac{\langle\hat{\phi}_k|\hat{H}^{\epsilon}_{\rm int}U^{\epsilon}(0,-\infty)|\hat{\phi}_k\rangle}{\langle\hat{\phi}_k|U^{\epsilon}(0,-\infty)|\hat{\phi}_k\rangle} \tag{1.41}$$

An alternative but equivalent form of the Gell-Mann and Low theorem due to Sucher [8] exists. It has been shown by O'Connor [7] to be quite useful to use in cavity calculations In this formulation the energy shift is given by

$$E_k - E_k^0 = \lim_{\substack{\eta\to 1\\ \epsilon\to 0}} \frac{i\epsilon}{2} \frac{\partial\langle\hat{\phi}_k|S^{\epsilon}_{\eta}|\hat{\phi}_k\rangle_c/\partial\eta}{\langle\hat{\phi}_k|S^{\epsilon}_{\eta}|\hat{\phi}_k\rangle_c} \tag{1.42}$$

where the subscript $c$ means take only the connected diagrams. $S^{\epsilon}_{\eta}$ is the adiabatic $S$-matrix and can be written as

$$S^{\epsilon}_{\eta} = 1 + \sum_{n=1}^{\infty} S^{\epsilon(n)}_{\eta} \tag{1.43}$$

where

$$S^{\epsilon(n)}_{\eta} = \frac{(i\eta)^n}{n!} \int_{-\infty}^{\infty} dt_1 \cdots \int_{-\infty}^{\infty} dt_n \; e^{-\epsilon(|t_1|+\cdots+|t_n|)} T\left[\hat{H}^{\epsilon}_{\rm int}(t_1) \cdots \hat{H}^{\epsilon}_{\rm int}(t_n)\right] \tag{1.44}$$

The benefit of this formalism is that the Feynman diagrams no longer need to be decomposed into time ordered diagrams, as in the Gell-Mann and Low theorem, due to the symmetry of the limits of the time integrations. This formalism does however have its disadvantages in that the time integrations are more complicated.

The magnetic moment of a particle may be defined in terms of the energy shift via $\Delta E = -\vec{\mu} \cdot \vec{B}$ where $\Delta E$ is the energy shift due to the interaction with an external magnetic field $\vec{B}$. In this thesis all corrections to $O(eg^2)$ to the magnetic moment are calculated. The terms which contribute to eq. (1.42) to this order can be found by substituting in eq. (1.43) into eq. (1.42) and taking the limit $\eta \to 1$. It is found that

$$\Delta E = \lim_{\epsilon \to 0} \frac{i\epsilon}{2} \frac{\langle S_\epsilon^{(1)} \rangle + 2\langle S_\epsilon^{(2)} \rangle + 3\langle S_\epsilon^{(3)} \rangle + \cdots}{1 + \langle S_\epsilon^{(1)} \rangle + \langle S_\epsilon^{(2)} \rangle + \langle S_\epsilon^{(3)} \rangle + \cdots} \tag{1.45}$$

Using the expansion $1/(1+x) = 1 - x + x^2 \cdots$ one finds that the energy shift $\Delta E$ to $O(eg^2)$ can be written as

$$\Delta E = \lim_{\epsilon \to 0} \frac{i\epsilon}{2} \left[ \langle S_\epsilon^{(1)} \rangle + 2\langle S_\epsilon^{(2)} \rangle + 3\langle S_\epsilon^{(3)} \rangle - \langle S_\epsilon^{(1)} \rangle^2 + \langle S_\epsilon^{(1)} \rangle^3 - 3\langle S_\epsilon^{(1)} \rangle \langle S_\epsilon^{(2)} \rangle \right] \tag{1.46}$$

Ignoring those terms that are not connected to the asymptotic states of the baryons and do not contribute to the magnetic moment, the energy shift can be written as

$$\Delta E = \lim_{\epsilon \to 0} \frac{i\epsilon}{2} \left[ \langle S_\epsilon^{(1)} \rangle + 3\langle S_\epsilon^{(3)} \rangle - 3\langle S_\epsilon^{(1)} \rangle \langle S_\epsilon^{(3)} \rangle + 2\langle S_\epsilon^{(2)} \rangle \right] \tag{1.47}$$

The first term in eq. (1.47) gives the zeroth order contribution. The second term gives the $O(eg^2)$ contribution. The third term also gives $O(eg^2)$ but it comes from the denominator of equation (1.45) and serves to cancel the poles in the Feynman diagrams due to the second term, which will be discussed in more detail later. The last term is required if a mass counterterm renormalization is used.

## 1.3 Cavity QCD

Up until this point all the properties that have been discussed have been of a general nature and do not depend on the volume of the space the fields occupy. We now restrict the fields to occupy a static spherical cavity by imposing boundary conditions on a spherical surface $S$. These boundary conditions are chosen such that no colour charge can escape through the surface, thus imposing confinement on the quarks. The boundary conditions chosen are those of the M.I.T. bag model [14], as they are linear

in the field operators and independent of the strong coupling constant. The boundary conditions also preserve the important BRS symmetry [3] of the theory that is vital to the proof of renormalizability QCD in free space. The M.I.T. bag model boundary conditions are

$$\left(in_k\gamma^k - 1\right)\hat{\psi}\Big|_S = i\,\hat{\bar{\psi}}\left(in_k\gamma^k + 1\right)\Big|_S = 0 \tag{1.48}$$

$$n_k\left(\partial^k\hat{\boldsymbol{A}}^\nu - \partial^\nu\hat{\boldsymbol{A}}^k\right)\Big|_S = n_k\hat{\boldsymbol{A}}^k\Big|_S = n_k\partial^k\left(\partial_\nu\hat{\boldsymbol{A}}^\nu\right)\Big|_S = 0 \tag{1.49}$$

$$n_k\partial^k\hat{\omega}\Big|_S = n_k\partial^k\hat{\chi}\Big|_S = 0 \tag{1.50}$$

The solution of the non interacting field equations (1.30)–(1.32) subject to the above boundary conditions are the familiar cavity modes discussed in appendix A.

The quark field operator can be expanded in terms of the quark cavity modes by

$$\hat{\psi}_{cf}(x) = \sum_{\substack{\kappa\mu \\ \nu>0}}\left(\hat{a}_{cfn}u_n(\vec{x})e^{-i\epsilon_n t} + \hat{b}^\dagger_{cfn}u_{-n}(\vec{x})e^{i\epsilon_n t}\right) \tag{1.51}$$

where n is the set of quantum numbers $n = \{\nu, \kappa, \mu\}$, the radial, Dirac and magnetic quantum numbers. It is assumed that there is also an implicit dependance of the cavity modes on the flavour of the quark. $\hat{a}^\dagger_{cfn}$ and $\hat{a}_{cfn}$ are the quark creation and annihilation operators which create or annihilate a quark with quantum numbers $c, f, n$. $\hat{b}^\dagger_{cfn}$ and $\hat{b}_{cfn}$ are the antiquark creation and annihilation operator which create or annihilate an antiquark with the quantum numbers $c, f, n$. The spinors $u_n(x)$ are the quark cavity modes given in appendix A. The quark field operator must satisfy the anticommutation relation (1.20) which reduces to the following constraint on the quark creation and annihilation operators

$$\left\{\hat{a}_{cfn}, \hat{a}^\dagger_{c'f'n'}\right\} = \left\{\hat{b}_{cfn}, \hat{b}^\dagger_{c'f'n'}\right\} = \delta_{cc'}\delta_{ff'}\delta_{nn'} \tag{1.52}$$

The cavity quark propagator is defined in terms of a time–ordered product of the fields as

$$iS(x,x') = \left\langle\hat{0}\left|\mathrm{T}\left[\hat{\psi}_{cf}(x)\hat{\bar{\psi}}_{c'f'}(x')\right]\right|\hat{0}\right\rangle \tag{1.53}$$

Substituting the expansion for the quark field operator (1.51) into this expression and using the anticommutation relations (1.52) one finds

$$iS(x,x') = \delta_{cc'}\delta_{ff'}\sum_{\substack{\kappa\nu \\ \nu>0}}\left[u_n(\vec{x})\bar{u}_n(\vec{x}')\theta(t-t') - u_{-n}(\vec{x})\bar{u}_{-n}(\vec{x}')\theta(t'-t)\right]e^{-i\epsilon_n|t-t'|} \tag{1.54}$$

Using the integral representation of the theta function

$$\theta(t) = \lim_{\epsilon \to 0} \frac{-1}{2\pi i} \int_{-\infty}^{\infty} d\omega \, \frac{e^{-i\omega t}}{\omega + i\varepsilon} \tag{1.55}$$

the propagator can be written as

$$iS(x,x') = i\delta_{cc'}\delta_{ff'} \sum_{\kappa\nu\mu} u_n(\vec{x})\bar{u}_n(\vec{x}') \int \frac{d\omega}{2\pi} \frac{e^{-i\omega(t-t')}}{\omega - \epsilon_n \pm i0} \tag{1.56}$$

where we now sum over both positive and negative radial quantum numbers. The usual Feynman prescription for the poles is used. All poles with positive (negative) energy acquire a small negative (positive) imaginary part.

The gluon field operator may be expanded in terms of the gluon cavity modes as

$$\hat{A}^{\mu}_{a}(x) = \sum_{m\Sigma} \frac{1}{\sqrt{2\Omega^{\Sigma}_{m}}} \left[ \hat{c}^{\Sigma}_{am} a^{\mu}_{m\Sigma}(\vec{x}) e^{-i\Omega^{\Sigma}_{m} t} + \hat{c}^{\Sigma\dagger}_{am} a^{\mu *}_{m\Sigma}(\vec{x}) e^{i\Omega^{\Sigma}_{m} t} \right] \tag{1.57}$$

where $m$ is the set of quantum numbers $m = \{N, J, M\}$. $N$ is the radial quantum number while $J$ and $M$ are the angular momentum quantum numbers. $a^{\mu}_{m\Sigma}$ are the gluon cavity modes. $\hat{c}^{\Sigma\dagger}_{am}$ and $\hat{c}^{\Sigma}_{am}$ are the gluon creation and annihilation operators which create or annihilate a gluon with quantum numbers $a, m$ and polarisation $\Sigma$. The gluon field operator must satisfy the commutation relation (1.23) which means that the gluon creation and annihilation operators must satisfy

$$\left[ \hat{c}^{\Sigma}_{am}, \hat{c}^{\Sigma'\dagger}_{a'm'} \right] = -g^{\Sigma\Sigma'} \delta_{aa'} \delta_{mm'} \tag{1.58}$$

where $g^{\Sigma\Sigma'}$ is the metric tensor in polarisation space and is given by

$$g^{\mathcal{SS}} = -g^{\mathcal{LL}} = -g^{\mathcal{MM}} = -g^{\mathcal{EE}} = 1 \tag{1.59}$$

and

$$g^{\Sigma\Sigma'} = 0 \qquad \text{if} \qquad \Sigma \neq \Sigma' \tag{1.60}$$

where $\mathcal{S}$ is the scalar, $\mathcal{L}$ the longitudinal, $\mathcal{M}$ is the transverse magnetic and $\mathcal{E}$ the transverse electric polarisation.

The gluon propagator is defined as the vacuum expectation of the time-ordered product of the gluon field operators

$$iD^{\mu\nu}_{ab}(x,x') = \left\langle \hat{0} \left| \mathrm{T} \left[ \hat{A}^{\mu}_{a} \hat{A}^{\nu}_{b} \right] \right| \hat{0} \right\rangle \tag{1.61}$$

Using the gluon field expansion (1.57) and the anticommutation relations (1.58) one finds

$$iD_{ab}^{\nu\mu}(x,x') = -\delta_{ab}\sum_{m\Sigma}\frac{g^{\Sigma\Sigma}}{2\Omega_m^{\Sigma}}a_{m\Sigma}^{\mu}(\vec{x})a_{m\Sigma}^{\nu *}(\vec{x}')e^{-i\Omega_m^{\Sigma}|t-t'|} \tag{1.62}$$

Using the integral representation of the theta function this may be written as

$$iD_{ab}^{\nu\mu}(x,x') = -i\delta_{ab}\sum_{m\Sigma}g^{\Sigma\Sigma}a_{m\Sigma}^{\mu}(\vec{x})a_{m\Sigma}^{\nu *}(\vec{x}')\int\frac{d\omega}{2\pi}\frac{e^{i\omega(t'-t)}}{\omega^2-(\Omega_m^{\Sigma})^2+i0} \tag{1.63}$$

Using the gluon cavity modes in the Feynman gauge as given in appendix A one has an expression for the Feynman propagator in the Feynman gauge. An expression for the Feynman propgator in an arbitrary gauge has been formulated by Stoddart [13], but since the sum of all the graphs we are calculating is gauge independent, [7] we need not consider the Feynman propagator in an arbitrary gauge.

# Chapter 2

# Renormalization

The Feynman diagrams in figure (2) are all the divergent diagrams that contribute to the magnetic moment to order $\alpha_S$. The vertex correction diagram figure (2a) and the vertex diagram with self–energy inserts figures (2b) and (2c) are ultra–violet divergent and have to be regularised and renormalized before any sensible result can be obtained. The remaining diagrams that contribute to the magnetic moment to this order are the two one–gluon exchange diagrams which are finite so they will not be discussed here.

Since ultra–violet divergences are a short distance phenomenon, it is expected that the presence of the cavity boundary will not have a large effect on the divergences. More explicitly, if one parametrizes the divergence of a Feynman diagram in free space, then it is expected that the same parametrization should also be valid in the cavity.

The renormalization technique used in this thesis is based on the technique developed by Stoddart *et al.* [13] and is similar to that in O'Connor [7], but with the added complexity of mass renormalization. Briefly this technique involves dimensionally regularising the free space theory and separating out the divergent part of the diagram. This divergent part can then be Fourier transformed into cavity mode space and can be subtracted from the cavity diagram which has a similarly parametrized divergence to yield a finite result. The exact renormalization scheme used is unknown since the divergence in the cavity may differ from the free space divergence by some constant.

The divergence in the vertex correction graph will be shown to cancel exactly the remaining divergence in the two self–energy type diagrams after mass renormalization. This cancellation is guaranteed in free space due to the Ward identity which equates these two renormalization constants. Thus in free space the sum of these three diagrams depends only on the mass renormalization scheme. In free space we can choose the mass renormalization scheme to be on shell, however in the cavity the on shell condition is somewhat more complicated and will be discussed later.

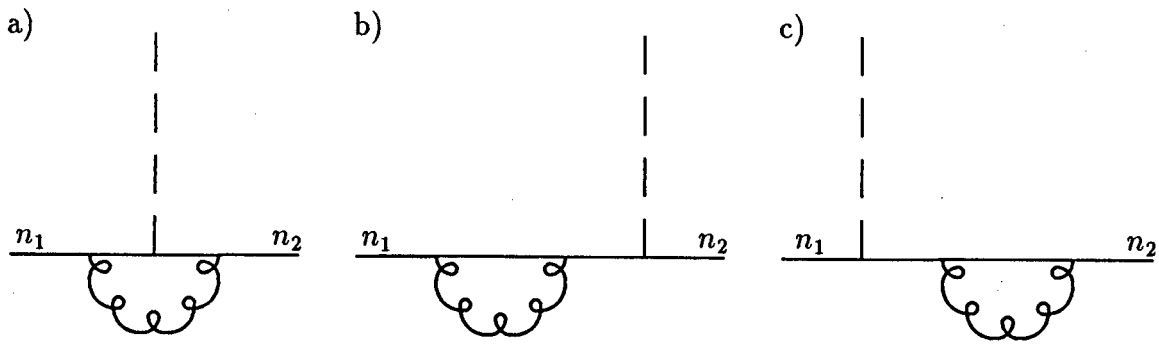


Figure 2.1: *The divergent Feynman diagrams contributing to the magnetic moment to order* $\alpha_S$.

## 2.1 Vertex Correction Diagram in Free Space

In this section the vertex correction diagram in figure (2a) will be examined in free space using dimensional regularisation to parametrize the divergence. The Feynman amplitude for this diagram is

$$\mathcal{M} = eC\bar{u}(p')\left(-i\Lambda_\mu(p',p,q)\right)U(p)A^\mu_{\rm ext}(q) \tag{2.1}$$

Where $C$ is the colour factor $C = 4/3$ and $A^\mu_{\rm ext}$ is the potential due to the external magnetic field. The vertex function in D dimensions is

$$-i\Lambda_\mu(p',p,q) = g^2\mu^{4-D}\int\frac{d^Dk}{(2\pi)^D}(i\gamma_\alpha)iS(p'-k)(i\gamma_\mu)iS(p-k)(i\gamma_\beta)iD^{\alpha\beta}(k) \tag{2.2}$$

where $S(p)$ is the quark propagator

$$S(p) = \frac{1}{\not{p}-m} \tag{2.3}$$

and $D^{\alpha\beta}(k)$ is the gluon propagator which is given by

$$D^{\alpha\beta}(k) = -\frac{g^{\alpha\beta}}{k^2+i0} - \frac{1-\lambda}{\lambda}\frac{k^\alpha k^\beta}{k^4+i0} \tag{2.4}$$

where $\lambda$ is the gauge parameter. Since the sum of all the graphs are gauge independent, throughout this thesis we shall work in the Feynman gauge $\lambda = 1$ and hence shall ignore the second term in equation (2.4). It is sufficient to calculate $\Lambda_\mu(p',p,q)$ for the case

$q = 0$ in order to find the divergent part of $\Lambda_\mu$. Substituting the quark propagator and the Feynman gauge gluon propagator into equation (2.2) where $q$ has been set to zero one finds

$$-i\Lambda_\mu(p,p) = g^2\mu^{4-D}\int \frac{d^Dk}{(2\pi)^D}\gamma_\alpha \frac{1}{\not p - \not k - m}\gamma_\mu \frac{1}{\not p - \not k - m}\gamma_\beta \frac{g^{\alpha\beta}}{k^2} \tag{2.5}$$

$$= g^2\mu^{4-D}\int \frac{d^Dk}{(2\pi)^D}\frac{\gamma_\nu(\not p - \not k - m)\gamma_\mu(\not p - \not k - m)\gamma^\nu}{((p-k)^2 - m^2)^2k^2} \tag{2.6}$$

where $\Lambda_\mu(p,p) = \Lambda_\mu(p,p,0)$. Looking at the numerator of (2.6) in D dimensions and with the help of some Diracology we find three terms

$$\gamma_\nu \not a \gamma_\mu \not a \gamma^\nu = (2-D)(2a_\mu \not a - \gamma_\mu a^2) \tag{2.7}$$

$$\gamma_\nu \not a \gamma_\mu m \gamma^\nu + \gamma_\nu m \gamma_\mu \not a \gamma^\nu = 2Dma_\mu \tag{2.8}$$

$$m^2\gamma_\nu\gamma_\mu\gamma^\nu = (2-D)m^2\gamma_\mu \tag{2.9}$$

The first term is divergent and the other two terms are finite in four dimensions. Using standard techniques the integral can be evaluated in D dimensions. Setting $D = 4 - 2\varepsilon$ where $\varepsilon$ is small and discarding all powers of $\varepsilon^n$ where $n \geq 1$.

$$\begin{aligned}\Lambda_\mu(p,p) = \frac{-g^2}{16\pi^2}\Bigg[&\gamma_\mu\left(\frac{1}{\varepsilon} - \gamma + 1 - \ln\left(\frac{m^2-p^2}{4\pi\mu^2}\right) + \frac{m^4}{p^4}\ln\left(\frac{m^2-p^2}{m^2}\right) + \frac{m^2}{p^2}\right)\\ &-\frac{2p_\mu \not p}{p^6}\left(2m^4\ln\left(\frac{m^2-p^2}{m^2}\right) + 2m^2p^2 + p^4\right)\\ &+\frac{8mp_\mu}{p^4}\left(m^2\ln\left(\frac{m^2-p^2}{m^2}\right) + p^2\right)\Bigg]\end{aligned} \tag{2.10}$$

where $\gamma$ is Euler's constant. The singular part of the vertex function, $\Lambda_\mu^S$, in the $\overline{\text{MS}}$ scheme can now be separated out and parametrized as

$$\Lambda_\mu^S = \frac{-g^2\gamma_\mu}{16\pi^2}\left(\frac{1}{\varepsilon} - \gamma\right) = \frac{-g^2\gamma_\mu}{16\pi^2}\int_0^\infty dz\,\frac{e^{-z}}{z} \tag{2.11}$$

This divergent expression can then be Fourier transformed into cavity mode space and be used to renormalize the cavity vertex correction diagram.

## 2.2 Self–Energy Diagram in Free Space

The Feynman amplitude for the self–energy insert diagrams in figures (2b) and (2c) are given by

$$\mathcal{M}_a = eC\bar{u}(p')\left(-i\Sigma(p')\right)iS(p')i\gamma_\mu u(p)A^\mu_{\text{ext}}(q) \tag{2.12}$$

$$\mathcal{M}_b = eC\bar{u}(p')i\gamma_\mu iS(p)\left(-i\Sigma(p)\right)u(p)A^\mu_{\rm ext}(q) \tag{2.13}$$

respectively The self–energy $\Sigma(p)$ can be written in D dimensions as

$$-i\Sigma(p) = g^2\mu^{4-D}\int \frac{d^Dk}{(2\pi)^D} i\gamma_\alpha iS(p-k)i\gamma_\beta iD^{\alpha\beta}(k) \tag{2.14}$$

This can be evaluated in the standard way. Setting $D = 4 - 2\varepsilon$ where $\varepsilon$ is small and dropping all terms of order $\varepsilon^n$ where $n \geq 1$ we find

$$\begin{aligned}\Sigma(p) = \frac{-g^2}{16\pi^2}\Bigg[\not{p}\left(\frac{1}{\varepsilon} - \gamma + 1 - \ln\left(\frac{m^2-p^2}{4\pi\mu^2}\right) + \frac{m^4}{p^4}\ln\left(\frac{m^2-p^2}{m^2}\right) + \frac{m^2}{p^2}\right) \\ -4m\left(\frac{1}{\varepsilon} - \gamma + \frac{3}{2} - \ln\left(\frac{m^2-p^2}{4\pi\mu^2}\right) + \frac{m^2}{p^2}\ln\left(\frac{m^2-p^2}{m^2}\right)\right)\Bigg]\end{aligned} \tag{2.15}$$

The form of the momentum dependent divergence in the self–energy $\Sigma(p)$ is the same as that in the vertex correction diagram. This is expected since the Ward identity relates $\Lambda_\mu(p,p)$ to $\Sigma(p)$ via

$$\Lambda_\mu(p,p) = \frac{\partial\Sigma(p)}{\partial p^\mu} \tag{2.16}$$

This can be shown explicitly by differentiating equation (2.15) and comparing the result with equation (2.10).

Let us look at the renormalization of the self–energy more closely. The two point Green's function is given by the sum of over irreducible self–energy inserts.

$$G(p) = \frac{i}{\not{p} - m_B} + \frac{i}{\not{p} - m_B}\left(-i\Sigma(p)\right)\frac{i}{\not{p} - m_B} + \cdots \tag{2.17}$$

This series can be summed to give

$$G(p) = \frac{i}{\not{p} - m_B - \Sigma(p)} \tag{2.18}$$

In an on shell renormalization scheme $\Sigma(p)$ is usually expressed as a Taylor series around $\not{p} = m$

$$\Sigma(p) = \Sigma(m) + (\not{p} - m)\frac{\partial\Sigma}{\partial\not{p}}\bigg|_{\not{p}=m} + \Sigma_T(p) \tag{2.19}$$

where $\Sigma_T(p)$ are all the higher order terms in the series. The first two terms are infinite while the third term is finite and vanishes as $\not{p} \to m$. Using this expansion we can define

the following quantities

$$\delta m = \Sigma(m) \tag{2.20}$$

$$\left(Z_2^{-1} - 1\right) = \frac{\partial \Sigma}{\partial \not{p}}\Big|_{\not{p}=m} \tag{2.21}$$

$$Z_2^{-1}\Sigma_R(p) = \Sigma_T(p) \tag{2.22}$$

The self–energy can then be written as

$$\Sigma(p) = \delta m + (Z_2^{-1} - 1)(\not{p} - m) + Z_2^{-1}\Sigma_R(p) \tag{2.23}$$

The renormalized mass $m$ is defined in terms of the bare mass $m_B$ and the divergent quantity $\delta m$ by

$$m = m_B + \delta m \tag{2.24}$$

The two point Greens function then becomes

$$G(p) = \frac{Z_2}{\not{p} - m - \Sigma_R(p)} \tag{2.25}$$

An important point to note is that an on shell scheme is defined so that the 2–point Green's function has a pole at $\not{p} = m$.

One way of performing the quark mass renormalization is to write the Hamiltonian in terms of the renormalized quark mass and then to include a mass counter–term

$$H_{\text{int}} \rightarrow H_{\text{int}} - \delta m \bar{\psi}(x)\psi(x) \tag{2.26}$$

The non interacting fermion now has the physical mass and satisfies

$$(i\not{\partial} - m)\psi(x) = 0 \tag{2.27}$$

and the Feynman propagator is

$$iS = \frac{i}{\not{p} - m + i0} \tag{2.28}$$

The presence of the new interaction term introduces a new two quark vertex with which we must associate the factor of

$$i\delta m = i\Sigma(p)|_{\not{p}=m} \tag{2.29}$$

Each Feynman graph containing a quark self–energy loop must be considered together with an identical graph where the self–energy loop is replaced by the two quark vertex

which is also of order $g^2$. The net effect of considering both of these graphs together is the following replacement

$$-i\Sigma(p) \rightarrow -i\Sigma(p) + i\delta m = -i(Z_2^{-1} - 1)(\not{p} - m) - i\Sigma_R(p) \tag{2.30}$$

Looking at the expression of $\Sigma(p)$ as $\not{p} \rightarrow m$ we find that

$$\delta m = \frac{-g^2 3m}{16\pi^2}\left(\frac{1}{\epsilon} - \gamma + \frac{4}{3} + \ln(4\pi\mu^2) - \ln(m^2)\right) \tag{2.31}$$

which can be parametrized as

$$\delta m = \frac{-g^2 3m}{16\pi^2}\left(\int_0^\infty \frac{e^{-z}}{z}\,dz + \frac{4}{3} + \ln(4\pi\mu^2) - \ln(m^2)\right) \tag{2.32}$$

Returning to the Feynman amplitudes, we must now look at the sum of the Feynman amplitudes of the self–energy insert graph and the corresponding graph with a two quark vertex replacing the self–energy loop. This results in

$$\mathcal{M}_b = eg^2 C\bar{u}(p')i\gamma_\mu iS(p)i\left[-\Sigma(p) + \delta m\right]u(p)A^\mu_{\text{ext}}(q) \tag{2.33}$$

The singular part of $-\Sigma(p) + \delta m$ is then given by

$$-\Sigma_S(p) + \delta m_S = \frac{g^2}{16\pi^2}(\not{p} - m)(\frac{1}{\epsilon} - \gamma) = \frac{g^2}{16\pi^2}(\not{p} - m)\int_0^\infty dz\,\frac{e^{-z}}{z} \tag{2.34}$$

If we now calculate the singular part of the Feynman amplitude (2.33) we find

$$\mathcal{M}_S^b = ieg^2 C\bar{u}(p')\gamma_\mu \frac{1}{\not{p} - m} B(\not{p} - m)u(p)A^\mu_{\text{ext}} \tag{2.35}$$

where $B = \frac{1}{16\pi^2}(1/\epsilon - \gamma)$ is a divergent constant. This expression is undefined as it stands. This can be seen by acting $\not{p} - m$ in the numerator of equation (2.35) on the free particle spinor first, resulting in the expression being zero, or by first cancelling the numerator and the denominator and obtaining a non–zero result. This problem was solved by Feynman [12]. The reason this problem occurs is that in an interacting theory no free particle spinors exist, and they must be replaced with propagators from some interactions that occurred in the remote past and the remote future. An alternative way to solve the problem is to introduce an adiabatic damping factor to the interaction which switches off the interactions $t \rightarrow \pm\infty$ by multiplying the interaction Hamiltonian by a suitable function $f(t)$. The usual factor is $f(t) = e^{-\epsilon|t|}$ where $\epsilon$ is small. This is the

factor that is used in the cavity calculations. The precise form of $f(t)$ is not important, all we require is that $f(t) \to 0$ as $t \to \pm\infty$ and $f(t)$ is very close to one for some time $T$ much longer than the interaction. The result of this is to force the asymptotic states to be non interacting free particle spinors as we require. Consider the Fourier transform

$$f(t) = \int_0^\infty F(E) e^{iEt}\, dE = \int_0^\infty F(E) e^{iqx}\, dE \tag{2.36}$$

where $q = (E, 0, 0, 0)$, with the normalisation condition

$$f(0) = \int_\infty^\infty F(E)\, dE = 1 \tag{2.37}$$

$F(E)$ looks almost like a delta function and as $F(E) \to \delta(E)$ the original theory where $f(t) = 1$ is restored. The result of having a time dependent interaction is to introduce a slight energy non-conservation at each interaction. The effect of this damping factor is to cause the following replacements

$$\frac{1}{\not p - m} \to \frac{1}{\not p - \not q - \not q' - m} \qquad \Sigma(p) \to \Sigma(p - q) \tag{2.38}$$

The Feynman amplitude then becomes

$$\mathcal{M}_S^b = ieg^2 C \bar{u}(p') \int dE\, dE'\, F(E) F(E') \gamma_\mu \frac{B}{\not p - \not q - \not q' - m} (\not p - \not q - m) U(p) A^\mu_{\text{ext}}(q) \tag{2.39}$$

To evaluate this we can subtract $\frac{1}{2}(\not p - m)$ from the numerator of equation (2.39). This is valid since $\frac{1}{2}(\not p - m)$ acts on the free particle spinor to give a zero result i.e. $\frac{1}{2}(\not p - m)u(p) = 0$. The numerator then becomes

$$\not p - \not q - \frac{1}{2}(\not p - m) = \frac{1}{2}(\not p - 2\not q - m) \tag{2.40}$$

By symmetrising the factor of $2\not q$ using $2\not q \to \not q + \not q'$ the numerator and denominator now cancel so the integral becomes simple and results in

$$\mathcal{M}_S^b = ieg^2 \bar{u}(p') \gamma_\mu \frac{B}{2} u(p) A^\mu_{\text{ext}}(q) \tag{2.41}$$

The factor of $1/2$ in this expression is important as there are two self-energy insert diagrams whose sum cancels the singular part of the vertex correction diagram whose singular part has the form

$$\mathcal{M}_S^b = -ieg^2 \bar{u}(p') \gamma_\mu B u(p) A^\mu_{\text{ext}}(q) \tag{2.42}$$

## 2.3 Cavity Renomalization

In order to renormalize the cavity diagrams, the free space divergence must be expressed in terms of cavity modes. To do this a set of Fourier transforms appropriate to the cavity are introduced as in Stoddart *et al.* [13]. For Dirac fields the appropriate Fourier set is

$$\psi_p(\omega; x) = (2\pi)^{-\frac{1}{2}} u_p(\vec{r}) e^{-i\omega t} \tag{2.43}$$

where $\psi$ is a function of $x = (t, \vec{r})$ and is labelled by $p$ and $\omega$. $u_p(\vec{r})$ denotes the usual quark cavity modes which are solutions of the time independent Dirac equation subject to the M.I.T. bag model boundary conditions (see appendix A). $\omega$ is a continuous energy parameter which is not related to the energy eigenvalues of the quark cavity modes. $p$ denotes the set of quantum numbers of the cavity mode, namely

$$p = \{\nu, \kappa, \mu\} \tag{2.44}$$

where $\nu, \kappa, \mu$ are the radial, Dirac and magnetic quantum numbers. This Fourier set consists of a set of spinors, unlike the standard Fourier set used in free space which is a set of scalars, thus the Fourier transform of a spinor will be a scalar in this set.

This set of spinor functions are orthonormal and complete in the cavity as is given by the orthonormality relation

$$\int d^4x \; \psi_p^\dagger(\omega; x)\psi_{p'}(\omega'; x) = \delta(\omega, \omega')\delta_{\nu\nu'}\delta_{\kappa\kappa'}\delta_{\mu\mu'} \tag{2.45}$$

and the completeness relation

$$\sum_p \int_{-\infty}^{\infty} d\omega \; \psi_p(\omega; x)\psi_p^\dagger(\omega; y) = \delta^4(x, y)\mathrm{I} \tag{2.46}$$

where I is the unit 4×4 matrix.

Any spinor function $f(x)$ in the cavity can be expanded in terms of the above Fourier set by

$$f(x) = \sum_p \int_{-\infty}^{\infty} d\omega \; c_p(\omega)\psi_p(\omega; x) \tag{2.47}$$

The Fourier coefficients $c_p(\omega)$ are given in terms of the overlap integral

$$c_p(\omega) = \int d^4x \; \bar{\psi}_p(w; x) f(x) \tag{2.48}$$

Similarly an adjoint spinor can be expanded as

$$\bar{f}(x) = \sum_p \int d\omega \; c_p^*(\omega)\bar{\psi}_p(\omega; x) \tag{2.49}$$

where the Fourier coefficients are

$$c_p^*(w) = \int d^4x \ \bar{f}(x)\gamma^0\psi_p(\omega;x) \tag{2.50}$$

A similar Fourier set for vector fields can be constructed from the gluon cavity modes.

To examine the cavity version of the self–energy we look at the Feynman rules in configuration space, where the Feynman rules are the same as in free space. The dressed quark propagator can be expressed in terms of the bare quark propagator $S_B$ by

$$G(x,y) = iS_B(x,y) + \int d^4x' \ d^4x'' \ iS_B(x,x')[-i\Sigma^C(x',x'')]iS_B(x'',y) \tag{2.51}$$

The bare propagator satisfies the following equation

$$(i\not{\partial}_x - m_B + i0)\, S_B(x,x') = \delta^4(x,x') \tag{2.52}$$

where $m_B$ is the bare mass. Equation (2.51) can be Fourier transformed to cavity mode space using

$$S^B_{pp'}(\omega,\omega') = \int d^4x \int d^4y \ \bar{\psi}_p(\omega;x)\gamma_0 S_B(x,y)\gamma_0\psi_{p'}(\omega',y) \tag{2.53}$$

$$\Sigma^C_{pp'}(\omega,\omega') = \int d^4x \int d^4y \ \bar{\psi}_p(\omega;x)\Sigma^C(x,y)\psi_{p'}(\omega',y) \tag{2.54}$$

the dressed quark propagator can be written as

$$-iG_{pp'}(\omega,\omega') = S^B_{pp'} + \sum_{p_1p_2}\int d\omega_1 \int d\omega_2 S^B_{pp_1}(\omega,\omega_1)\Sigma^C_{p_1p_2}(\omega_1,\omega_2)S^B_{p_2p'}(\omega_2,\omega') \tag{2.55}$$

To find an expression for the bare propagator $S^B_{pp'}(\omega,\omega')$ equation (2.52) is Fourier transformed to get

$$\sum_{p'}\int d\omega' \ O_{pp'}(\omega,\omega')S^B_{p'p''}(\omega',\omega'') = \delta_{pp''}\delta(\omega,\omega') \tag{2.56}$$

where

$$O_{pp'}(\omega,\omega') = \int d^4x \ \bar{\psi}_p(\omega;x)(i\not{\partial} - m_B)\psi_{p'}(\omega';x) \tag{2.57}$$

Due to time translational invariance, energy is conserved at each vertex and hence $G, S^B, O$ and $\Sigma$ all contain delta functions in $\omega$. In future the following shortened notation will be used

$$X_{pp'}(\omega,\omega') = \delta(\omega,\omega')X_{pp'}(w) \tag{2.58}$$

where $X$ could be any one of the above operators. Using this notation equation (2.56) can be written as

$$\sum_{p'}(\omega\delta_{pp'} - \epsilon_{pp'})S^B_{p'p''}(\omega) = \delta_{pp''} \tag{2.59}$$

Where the non–diagonal energy like term $\epsilon_{pp'}$ is given by

$$\epsilon_{pp'} = \int d\vec{r}\; \bar{u}_p(r)\left(-i\vec{\gamma}\cdot\vec{\nabla}_r + m_B\right)u_{p'}(r) \tag{2.60}$$

Thus the bare propagator can then be written as

$$S^B_{pp'}(\omega) = (\omega\delta_{pp'} - \epsilon_{pp'})^{-1} \tag{2.61}$$

where the inverse in equation (2.61) refers to matrix inversion of the discrete labels $p$ and $p'$. Substituting this form of the bare propagator into the equation (2.55) the dressed quark propagator can be written as

$$iG_{pp'}(\omega) = (\omega\delta_{pp'} - \epsilon_{pp'})^{-1} + (\omega\delta_{pp'} - \epsilon_{pp_1})^{-1}\Sigma^C_{p_1p_2}(\omega)(\omega\delta_{p_2p'} - \epsilon_{p_2p'})^{-1} + \cdots \tag{2.62}$$

This can be summed to give

$$iG_{pp'}(\omega) = \left(\omega\delta_{pp'} - \epsilon_{pp'} - \Sigma^C_{pp'}(\omega)\right)^{-1} \tag{2.63}$$

Evaluating equation (2.60) one finds

$$\epsilon_{pp'} = \delta_{pp'}\epsilon_p - \int d\vec{r}\; \bar{u}_p(r)\delta m^c u_{p'}(r) = \delta_{pp'}\epsilon_p - \delta m^c_{pp'} \tag{2.64}$$

where the superscript $c$ on $\delta m^c$ is there to denote that this is the cavity value of this constant. Thus the dressed quark propagator can be written as

$$iG_{pp'}(\omega) = \left((\omega \mp \epsilon_p)\,\delta_{pp'} - \delta m^c_{pp'} - \Sigma^C_{pp'}(\omega)\right)^{-1} \tag{2.65}$$

If we Fourier transform the free space self–energy given by equation (2.23) we find that

$$\Sigma^0_{pp'}(\omega) = \delta m^0 \int d\vec{r}\; \bar{u}_p(r)u_{p'}(r) - (Z_2^{-1} - 1)(\omega - \epsilon_p)\delta_{pp'} + Z_2^{-1}\Sigma^{0R}_{pp'}(\omega) \tag{2.66}$$

It is expected that this equation should have the same divergent structure as the cavity self–energy, but may differ from the cavity self–energy by some finite piece. To perform this Fourier transform use must be made of the following identity proved by Stoddart *et al.* [13].

$$\int d^4x\; \bar{\psi}_p(\omega;x)\,(i\not{\partial}_x - m)\,\psi_{p'}(\omega';x) = (\omega - \epsilon)\delta_{pp'}\delta(\omega,\omega') \tag{2.67}$$

This identity is not trivially true due to the equation not holding on the surface, but the surface term vanishes due to the boundary conditions. Since the cavity self–energy has the same divergent form as equation (2.66) we can write the cavity self–energy as

$$\Sigma^C_{pp'}(\omega) = \delta m^c_{pp'} - (Z_2^{-1} - 1)(\omega - \epsilon_p)\delta_{pp'} + Z_2^{-1}\Sigma^{CR}_{pp'}(\omega) \tag{2.68}$$

The exact value of $\delta m^c$ is not known as it may differ from the free space mass counterterm $\delta m^0$ by some finite constant i.e.

$$\delta m^c_{pp'} = \delta m^c \int d^3\vec{r}\ \bar{u}_p(\vec{r})u_{p'}(\vec{r}) = (\delta m^0 + c)\int d^3\vec{r}\ \bar{u}_p(\vec{r})u_{p'}(\vec{r}) \tag{2.69}$$

To determine the value of $c$ for a mass shell renormalization condition consider the definition of a mass shell renormalization condition. The dressed quark propagator must have a pole when the energy is equal to the eigenenergy of the state i.e.

$$G_{pp}(\omega)|_{\omega\to\epsilon_p} \to \infty \tag{2.70}$$

Hence we need to find the value of the constant $c$ that makes the matrix inverse of

$$\left((\omega - \epsilon_p)\,\delta_{pp'} + \left(\delta m^0 + c\right)_{pp'} - \Sigma^C_{pp'}\right) \tag{2.71}$$

have poles on the diagonal elements $pp$ when $\omega = \epsilon_p$. This is a rather complicated task as the matrix is infinite dimensional. In the calculations done in this thesis a possibly off–shell renormalization scheme is used where we chose the value $c = 0$.

To perform the mass renormalization the mass counterterm method is used as was used in the free space calculation. This means that we must write the Hamiltonian in terms of the renormalized mass and include a mass counterterm as part of the interacting Hamiltonian.

$$H_{\text{int}} \to H_{\text{int}} - \delta m\bar{\psi}(x)\psi(x) \tag{2.72}$$

This interaction term introduces a new two quark vertex which is of order $g^2$. Graphs with self–energy loops must now be considered together with an identical graph where the self–energy loop is replaced by the two quark vertex. The sum of the self–energy and mass counterterm diagrams are free of the divergence due to mass renormalisation, but is still divergant, as was the free space diagram.

The divergence remaining in the sum of the self–energy and mass conterterm diagrams can be removed by subtracting the Fourier transform of the divergence remaining in the free space diagram (2.41). The Fourier transform proceeds by first Fourier transforming equation (2.41) to configuration space and then Fourier transforming this to cavity mode space. This result must be multiplied by a factor of $-i$ to convert it to

an energy shift. Thus the divergent part of the diagram can then be subtracted from the cavity calculation to give a finite result. This result of doing this is to subtract the following divergence from the cavity diagram

$$E_S = \frac{\alpha_S}{8\pi} M_{n_1 n_2} \int_0^\infty dz \, \frac{e^{-z}}{z} \tag{2.73}$$

where $M_{n_1 n_2}$ is defined in appendix B.2.

The calculation of the cavity renormalization for the vertex correction diagram follows exactly as in the self–energy type diagram. The result is just $-2$ times the divergence for the self–energy type diagram which gives

$$\Delta E = -\frac{\alpha_S}{4\pi} M_{n_1 n_2} \int_0^\infty dz \, \frac{e^{-z}}{z} \tag{2.74}$$

which must be subtracted from the vertex correction diagram to get a finite result.

# Chapter 3

# Cavity Calculations

The energy shift contributing to the magnetic moment up to $O(eg^2)$ can be found by evaluating eq. (1.47). To this order only quark–gluon and quark–photon coupling and the mass counterterm are needed in the interaction Hamiltonian as all the other terms to this order are not connected to the asymptotic states consisting of three quarks. The interacting Hamiltonian to this order can thus be written as

$$H_{\rm int} = -\int d^3\vec{x}\ \bar{\psi}(x)\left(g\frac{\lambda_a}{2}\not{A}_a(\vec{x}) + Q\not{A}_{\rm ext}(\vec{x}) + \delta m\right)\psi(x) \tag{3.1}$$

where $Q$ is the electromagnetic charge matrix in flavour space, $A^{\mu}_{\rm ext}(\vec{x})$ is the potential due to the external magnetic field, $\delta m$ is the mass counterterm matrix in flavour space. This form of $H_{\rm int}$ can be used in eq. (1.47) to find the magnetic moment to $O(eg^2)$.

## 3.1 Zeroth Order Term

The simplest term contributing to the magnetic moment is the zeroth order $O(e)$ term. This term is given by the first term in eq. (1.47) as

$$\Delta E = \lim_{\epsilon\to 0}\frac{i\epsilon}{2}\langle S^{(1)}_{\epsilon}\rangle_c \tag{3.2}$$

This term corresponds to the Feynman diagram in figure (3.1). Substituting the part of the interaction Hamiltonian due to the external electromagnetic field into the definition of $\langle S^{(1)}_{\epsilon}\rangle_c$ one finds

$$\Delta E = -\lim_{\epsilon\to 0}\frac{i\epsilon}{2}\frac{(-i)}{1}\int_{-\infty}^{\infty} dt\ e^{-\epsilon|t|}\int d^3\vec{x}\ \langle\hat{X}|\hat{\bar{\psi}}(x)Q\not{A}_{\rm ext}\hat{\psi}(x)|\hat{X}\rangle \tag{3.3}$$

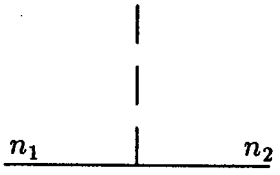


Figure 3.1: *The zeroth order diagram.*

where $|\hat{X}\rangle$ is the asymptotic state which is an eigenvector of the non-interacting Hamiltonian representing one of the baryons. This state $|\hat{X}\rangle$ can be written as a linear combination of three quark creation operators acting on the vacuum.

$$|\hat{X}\rangle \sim a^\dagger_{c_1 f_1 n_1} a^\dagger_{c_2 f_2 n_2} a^\dagger_{c_3 f_3 n_3} |\hat{0}\rangle \tag{3.4}$$

The quark field operator in eq. (3.3) can be expanded in terms of the quark and gluon cavity modes using eq. (1.51) and eq. (1.57). This gives

$$\Delta E = -\lim_{\epsilon \to 0} \frac{\epsilon}{2} \langle \hat{a}^\dagger_{c_1 f_1 n_1} Q \hat{a}_{c_2 f_2 n_2} \rangle \int_{-\infty}^{\infty} dt \; e^{-\epsilon|t|} e^{i(\varepsilon_1 - \varepsilon_2)t} \int d^3\vec{x} \; \bar{u}_{n_1}(\vec{x}) \not{A}_{\text{ext}} u_{n_2}(\vec{x}) \tag{3.5}$$

where we have used the shorthand notation for the colour flavour matrix elements

$$\langle \hat{a}^\dagger_{c_1 f_1 n_1} Q \hat{a}_{c_2 f_2 n_2} \rangle = \langle \hat{X} | \sum_{\substack{c_1 f_1 n_1 \\ c_2 f_2 n_2}} \hat{a}^\dagger_{c_1 f_1 n_1} Q \hat{a}_{c_2 f_2 n_2} | \hat{X} \rangle \tag{3.6}$$

which are evaluated in appendix E. The colour flavour matrix elements restricts the quantum numbers of the incoming and outgoing quarks to be the same ie. $c_1, f_1, n_1 = c_2, f_2, n_2$ and hence $\varepsilon_1 = \varepsilon_2$. The time integral can be evaluated and gives a result $2/\epsilon$. The energy shift can then be written in the shorthand form

$$\Delta E = -\langle \hat{a}^\dagger_{c_1 f_1 n_1} Q \hat{a}_{c_2 f_2 n_2} \rangle M_{n_1 n_2} \tag{3.7}$$

where $M_{n_1 n_2}$ is the quark–photon vertex integral defined and evaluated in appendix B.2. Using these results this expression can be is straight forward to evaluate.

## 3.2 The O($eg^2$) diagrams

The last three terms in eq. (1.47) contribute to the magnetic moment to O($eg^2$). We shall start by looking at the contribution from the $3\langle S^{(3)}_\epsilon \rangle_c$ term, as the other two terms

only serve to cancel some diagrams and divergences in this term. To this order in this term the mass counterterm does not contribute, so we can write

$$\Delta E = -\lim_{\epsilon\to 0}\frac{3i\epsilon}{2}\frac{(-i)^3}{3!}\int d^4x_1\int d^4x_2\int d^4x_3\; e^{-\epsilon(|t_1|+|t_2|+|t_3|)} \tag{3.8}$$
$$\left\langle T\left[\left(\hat{\bar{\psi}}\left(g\tfrac{\lambda_a}{2}\hat{\not{A}}_a+Q\hat{\not{A}}_{\rm ext}\right)\hat{\psi}\right)_{x_1}\left(\hat{\bar{\psi}}\left(g\tfrac{\lambda_b}{2}\hat{\not{A}}_b+Q\hat{\not{A}}_{\rm ext}\right)\hat{\psi}\right)_{x_2}\left(\hat{\bar{\psi}}\left(g\tfrac{\lambda_c}{2}\hat{\not{A}}_c+Q\hat{\not{A}}_{\rm ext}\right)\hat{\psi}\right)_{x_3}\right]\right\rangle$$

The product of field operators in eq. (3.8) gives one $O(e^3)$ term, three $O(e^2g)$ terms, three $O(eg^2)$ terms and one $O(g^3)$ term. We are only interested in the three $O(eg^2)$ terms which correspond to the interaction with the external field occurring at times $t_1$, $t_2$ and $t_3$. The symmetry of the time integration makes these terms identical, so we need only consider one case and multiply the result by three to get the full contribution. The time-ordered product can then by Wicks theorem be expressed as the normal-ordered product of the sum of all possible contractions. Some of the contractions are not connected to the asymptotic states and may be discarded, while other terms are cancelled by the remaining terms in eq. (1.47). The remaining terms with the same spatial structure can be collected into five groups of two and can be represented by the five Feynman diagrams in figure (3.2). It can be shown using the commuting/anticommuting nature of the gluon/quark field operators in the normal ordered product that both terms which have the same spatial structure give the same contribution. We consider each of the diagrams separately.

### 3.2.1 The Vertex Correction Diagram

The contribution of this graph is given by

$$\begin{aligned}\Delta E \;=\; & -\lim_{\epsilon\to 0}\frac{3i\epsilon}{2}(-i)^3\int d^4x_1\int d^4x_2\int d^4x_3 e^{-\epsilon(|t_1|+|t_2|+|t_3|)} \\ & \left\langle N\left[\underbrace{\left(\hat{\bar{\psi}}g\tfrac{\lambda_a}{2}\hat{\not{A}}_a\hat{\psi}\right)_{x_1}\left(\hat{\bar{\psi}}Q\hat{\not{A}}_{\rm ext}\hat{\psi}\right)_{x_2}\left(\hat{\bar{\psi}}g\tfrac{\lambda_c}{2}\hat{\not{A}}_c\hat{\psi}\right)_{x_3}}\right]\right\rangle\end{aligned} \tag{3.9}$$

where we have included only one possible contraction and one time ordering but multiplied by a factor of 6 to get the full contribution. Substituting the cavity mode expansion of the field operators one finds

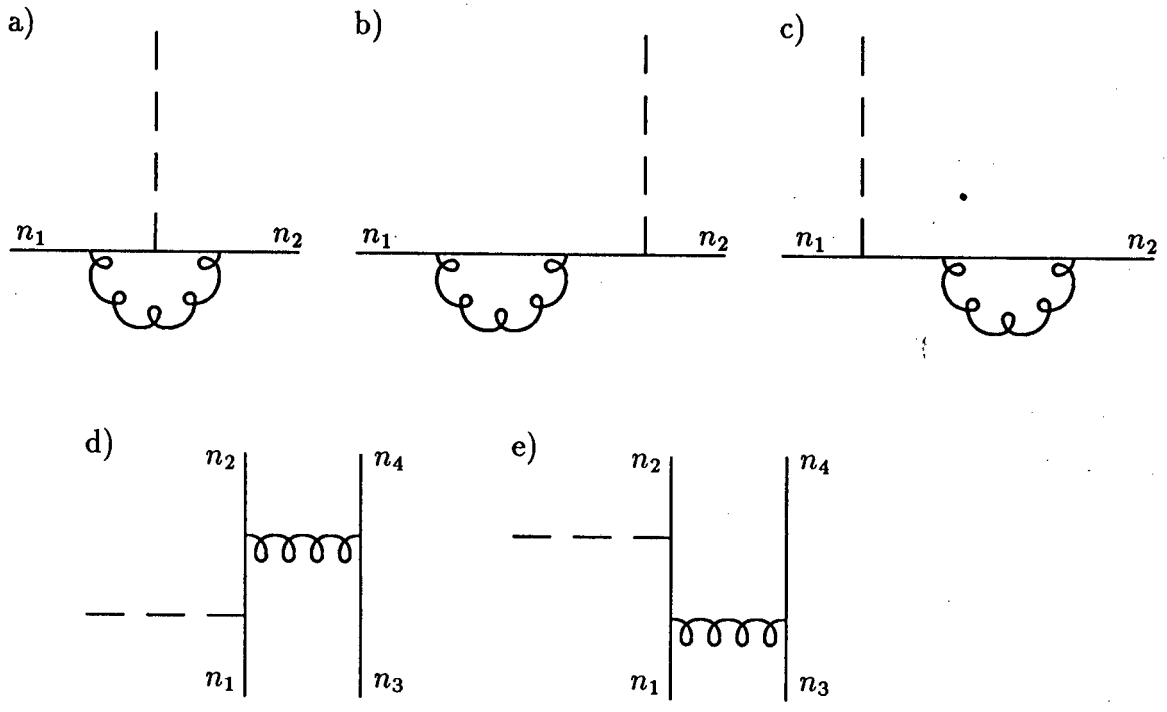


Figure 3.2: *The Feynman diagrams contributing to the magnetic moment to order $\alpha_S$ from the $\langle S_c^{(3)} \rangle$ term.*

$$\begin{aligned}\Delta E \;=\; & -\lim_{\epsilon\to 0}\frac{3i\epsilon}{2}\frac{g^2}{(2\pi)^3}\left\langle \hat{a}_{c_1 f_1 n_1}\left(\frac{\lambda^a}{2}\right)_{c_1 d}\left(\frac{\lambda^a}{2}\right)_{d c_2} Q\hat{a}_{c_2 f_2 n_2}\right\rangle \\ & \sum_{pqm\Sigma} g^{\Sigma\Sigma}\tilde{Q}^{m\Sigma}_{n_1 p}M_{pq}Q^{m\Sigma}_{qn_2}\int_{-\infty}^{\infty}dt_1\,dt_2\,dt_3\int_{-\infty}^{\infty}d\omega\,d\omega'\,d\omega'' \\ & \frac{e^{-\epsilon(|t_1|+|t_2|+|t_3|)}e^{it_1(\varepsilon_1+\omega-\omega')}e^{it_2(\omega'-\omega'')}e^{it_3(\omega''-\omega-\varepsilon_2)}}{(\omega'-\varepsilon_p\pm i0)\,(\omega''-\varepsilon_q\pm i0)\,(\omega^2-\Omega^2+i0)}\end{aligned} \tag{3.10}$$

The contour integrals over $\omega'$ and $\omega''$ are performed followed by the time integrals and after a lot of algebra one obtains

$$\Delta E = -ig^2\sum_{pqm\Sigma} g^{\Sigma\Sigma}\tilde{Q}^{m\Sigma}_{n_1 p}M_{pq}Q^{m\Sigma}_{qn_2}\int\frac{d\omega}{2\pi}\frac{\delta(\varepsilon_1,\varepsilon_2)}{(\varepsilon_1+\omega-\varepsilon_p)\,(\varepsilon_2+\omega-\varepsilon_q)\,(\omega^2-\Omega^2)} \tag{3.11}$$

where the colour flavour matrix element has been left out of this expression as it is evaluated in appendix F. The contour integral over $\omega$ can be performed directly to give

$$
\begin{aligned}
I_{pq}^{m\Sigma} &= -i\int \frac{d\omega}{2\pi}\frac{\delta(\varepsilon_1,\varepsilon_2)}{(\varepsilon_1+\omega-\varepsilon_p)(\varepsilon_2+\omega-\varepsilon_q)(\omega^2-\Omega^2)} \\
&= \begin{cases} \dfrac{1}{2\Omega(\varepsilon_1-\Omega\,\mathrm{sgn}\varepsilon_p-\varepsilon_p)(\varepsilon_1-\Omega\,\mathrm{sgn}\varepsilon_q-\varepsilon_q)} & \text{if } \mathrm{sgn}\varepsilon_p = \mathrm{sgn}\varepsilon_q \\ -\dfrac{2\Omega+|\varepsilon_p|+|\varepsilon_q|}{2\Omega(\varepsilon_1-\Omega\,\mathrm{sgn}\varepsilon_p-\varepsilon_p)(\varepsilon_1-\Omega\,\mathrm{sgn}\varepsilon_q-\varepsilon_q)(|\varepsilon_p|+|\varepsilon_q|)} & \text{if } \mathrm{sgn}\varepsilon_p \neq \mathrm{sgn}\varepsilon_q \end{cases}
\end{aligned}
\tag{3.12}
$$

If one performs the sum over the quantum numbers, the resultant energy shift is logarithmically divergent. Clearly the divergence needs to be regularized. This can be done by performing the integral over $\omega$ in a different way. Instead of contour integrating over $\omega$, the integral is done as it would be in the free space. First Wick rotate to Euclidean space by $\omega \to i\omega$, $\varepsilon_1 \to i\varepsilon_1$, $\varepsilon_2 \to i\varepsilon_2$. The denominators are squared, changing the $\pm i0$ prescription to the $+i0$ prescription, then the denominators are raised using Feynman parametrization. The Feynmann parametrization variables are transformed to make the integral over $\omega$ Gaussian. The two integrals over the transformed Feynman parametrization variables which have finite range are done leaving an integral over the last variable. (see O'Connor [7] for details) The energy shift due to the vertex correction can then be written as

$$
\Delta E = -ig^2 \sum_{pqm\Sigma} g^{\Sigma\Sigma}\tilde{Q}_{n_1p}^{m\Sigma}M_{pq}Q_{qn_2}^{m\Sigma}I_{pq}^{m\Sigma} \tag{3.13}
$$

where we have left out the colour flavour matrix element and

$$
I_{pq}^{m\Sigma} = \int_0^\infty dz\; I_{pq}^{m\Sigma}(z) \tag{3.14}
$$

where

$$
\begin{aligned}
&I_{pq}^{m\Sigma}(z) = \\
&\frac{(\varepsilon_1+\varepsilon_q)^2-\Omega^2+2\varepsilon_1\varepsilon_p}{8\varepsilon_1^2(\varepsilon_q^2-\varepsilon_p^2)\sqrt{\pi z}}e^{-z\varepsilon_q^2} - \frac{(\varepsilon_1+\varepsilon_p)^2-\Omega^2+2\varepsilon_1\varepsilon_q}{8\varepsilon_1^2(\varepsilon_q^2-\varepsilon_p^2)\sqrt{\pi z}}e^{-z\varepsilon_p^2} - \frac{1}{8\varepsilon_1^3\sqrt{\pi z}}e^{-z\Omega^2} \\
&+\frac{(\varepsilon_1^2+\varepsilon_q^2-\Omega^2+2\varepsilon_1\varepsilon_p)\left[(\varepsilon_1+\varepsilon_q)^2-\Omega^2\right]}{16\varepsilon_1^3(\varepsilon_q^2-\varepsilon_p^2)}\left[e^{-z\Omega^2}\mathrm{nerf}\left(\sqrt{z}A_+\right)+e^{-z\varepsilon_q^2}\mathrm{nerf}\left(\sqrt{z}A_-\right)\right] \\
&-\frac{(\varepsilon_1^2+\varepsilon_p^2-\Omega^2+2\varepsilon_1\varepsilon_p)\left[(\varepsilon_1+\varepsilon_p)^2-\Omega^2\right]}{16\varepsilon_1^3(\varepsilon_q^2-\varepsilon_p^2)}\left[e^{-z\Omega^2}\mathrm{nerf}\left(\sqrt{z}B_+\right)+e^{-z\varepsilon_q^2}\mathrm{nerf}\left(\sqrt{z}B_-\right)\right]
\end{aligned}
\tag{3.15}
$$

The normalised error function nerf($x$) is defined as

$$\mathrm{nerf}(x) = \frac{2}{\sqrt{\pi}} e^{x^2} \int_0^x e^{-t^2}\, dt \tag{3.16}$$

and use has been made of following definitions

$$A_+ = (\varepsilon_1^2 + \Omega^2 - \varepsilon_q^2)/2\varepsilon_1 \qquad A_- = (\varepsilon_1^2 - \Omega^2 + \varepsilon_q^2)/2\varepsilon_1 \tag{3.17}$$

$$B_+ = (\varepsilon_1^2 + \Omega^2 - \varepsilon_p^2)/2\varepsilon_1 \qquad B_- = (\varepsilon_1^2 - \Omega^2 + \varepsilon_p^2)/2\varepsilon_1 \tag{3.18}$$

The apparent singularity in eq. (3.15) when $\varepsilon_p = \varepsilon_q$ can be dealt with by setting $\varepsilon_p = \varepsilon_q$ in eq. (3.11). This gives an expression that is the same as an expression that occurs in the self–energy and will be dealt with there. Note the exponential dependence of eq. (3.15) on the square of the energy of the intermediate quarks and gluons times $-z$. This has the effect of making the terms with high intermediate state energies contribute significantly to $I_{pq}^{m\Sigma}(z)$ only when $z$ is small. If we introduce an energy cut–off to the sum over the intermediate quark states, we expect that it will only affect the region where $z$ is small. Thus if we first perform the sum over the quantum numbers up to some energy cut–off and then integrate that result over $z$, all the error due to the cut–off should be confined to a region of small $z$. This $z$–form can have a suitable renormalization factor subtracted from it in such a way that the result of the integral is finite. The final form of the energy shift due to the vertex correction diagram is

$$\Delta E = -ig^2 \int dz \sum_{pqm\Sigma} g^{\Sigma\Sigma} \tilde{Q}_{n_1 p}^{m\Sigma} M_{pq} Q_{qn_2}^{m\Sigma} I_{pq}^{m\Sigma}(z) \tag{3.19}$$

where again we have left out the colour flavour matrix element which gives the allowed values of the incoming and outgoing quark quantum numbers and weightings for each pair.

### 3.2.2 Self–Energy Inserts

The two self–energy insert graphs in figure (3.2b) and (3.2c) are also divergent and need to be written in the above form to renormalize them correctly. The contribution of figure (3.2c) is given by

$$\begin{aligned}\Delta E \;=\; & \lim_{\epsilon\to 0} \frac{3\epsilon g^2}{2} \int d^4x_1 \int d^4x_2 \int d^4x_3 e^{-\epsilon(|t_1|+|t_2|+|t_3|)} \\ & \left\langle N\left[\underbrace{\left(\hat{\bar{\psi}} Q \hat{\not{A}}_{\mathrm{ext}} \hat{\psi}\right)_{x_1}} \underbrace{\left(\hat{\bar{\psi}} \tfrac{\lambda_a}{2} \hat{\not{A}}_a \hat{\psi}\right)_{x_2}} \left(\hat{\bar{\psi}} \tfrac{\lambda_b}{2} \hat{\not{A}}_b \hat{\psi}\right)_{x_3}\right]\right\rangle \end{aligned} \tag{3.20}$$

where again we have only looked at one term and multiplied by a factor of six to get the full contribution. Substituting the cavity mode expansions of the field operators and the propagators one finds

$$\Delta E = \lim_{\epsilon\to 0}\frac{-3i\epsilon}{2}\frac{g^2}{(2\pi)^3}\sum_{pqm\Sigma} g^{\Sigma\Sigma}M_{n_1q}\tilde{Q}^{m\Sigma}_{qp}Q^{m\Sigma}_{pn_2}\int_{-\infty}^{\infty}dt_1\,dt_2\,dt_3 \qquad (3.21)$$
$$\int_{-\infty}^{\infty}d\omega\,d\omega'\,d\omega''\frac{e^{-\epsilon(|t_1|+|t_2|+|t_3|)}e^{it_1(\varepsilon_1-\omega')}e^{it_2(\omega'-\omega''+\omega)}e^{it_3(\omega''-\omega-\varepsilon_2)}}{(\omega'-\varepsilon_q\pm i0)(\omega''-\varepsilon_p\pm i0)(\omega^2-\Omega^2+i0)}$$

Note that we do not expect the same problem of ambiguity in this expression as we found in the free space calculation since we have already included the adiabatic damping factors $e^{-\epsilon|t|}$ in the cavity expression.The integrals over time and the contour integrals over $\omega'$ and $\omega''$ in eq. (3.21) can be done straight forwardly but tediously to give

$$J^{m\Sigma}_{pq} = K^{m\Sigma}_{pq} = -i\int\frac{d\omega}{2\pi}\frac{\delta(\varepsilon_1,\varepsilon_2)}{(\varepsilon_1-\varepsilon_q)(\omega+\varepsilon_1-\varepsilon_p)(\omega^2-\Omega^2)} \qquad \varepsilon_q\neq\varepsilon_2 \quad (3.22)$$

$$L^{m\Sigma}_{pq} = \frac{i}{2}\int\frac{d\omega}{2\pi}\frac{\delta(\varepsilon_1,\varepsilon_2)}{(\varepsilon_1-\varepsilon_p+\omega)^2(\omega^2-\Omega^2)} \qquad \varepsilon_q=\varepsilon_2$$
$$+\frac{3}{2\epsilon}\int\frac{d\omega}{2\pi}\frac{\delta(\varepsilon_1,\varepsilon_2)}{(\varepsilon_2-\varepsilon_p+\omega)(\omega^2-\Omega^2)} \qquad (3.23)$$

Note that the second term in the case $\varepsilon_q=\varepsilon_2$ diverges like $1/\epsilon$ in the limit $\epsilon\to 0$. This term will be exactly cancelled by a contribution from the $\langle S^{(1)}_\epsilon\rangle\langle S^{(2)}_\epsilon\rangle$ term in eq. (1.47) and can be ignored at the moment. The first term when $\varepsilon_q=\varepsilon_2$ is just $-1/2$ times the contribution from the $\omega$ integral in the vertex correction diagram when $\varepsilon_p=\varepsilon_q$ in eq. (3.11). This is important as this term is the divergent part of the vertex correction diagram and it will be cancelled by the contribution of the two diagrams with self-energy inserts. The integral over $\omega$ in eq. (3.22) can be performed in the same manner as in the vertex correction diagram resulting in $K^{m\Sigma}_{pq}$ being written in terms of a integral over a new variable $z$ so that $K^{m\Sigma}_{pq}=\int_0^\infty dz\; K^{m\Sigma}_{pq}(z)$ where

$$K^{m\Sigma}_{pq}(z) = \frac{1}{4\varepsilon_1(\varepsilon_2-\varepsilon_q)\sqrt{\pi z}}\left(e^{-z\varepsilon_p^2}-e^{-z\Omega^2}\right) \qquad (3.24)$$
$$+\frac{(\varepsilon_p+\varepsilon_1)^2-\Omega^2}{8\varepsilon_1^2(\varepsilon_2-\varepsilon_q)}\left[e^{-z\Omega^2}\mathrm{nerf}(\sqrt{z}B_+)+e^{-z\varepsilon_p^2}\mathrm{nerf}(\sqrt{z}B_-)\right]$$

$B_+$ and $B_-$ are defined in eq. (3.18). The first term in eq. (3.23) can also be integrated as above to get $L^{m\Sigma}_{pq}=\int_0^\infty dz\; L^{m\Sigma}_{pq}(z)$ where

$$
\begin{aligned}
2L^{m\Sigma}_{pq}(z) \;=\; & \frac{1}{16\varepsilon_1^4\sqrt{\pi z}}\left[(\varepsilon_1+\varepsilon_p+\Omega)^2(\varepsilon_1+\varepsilon_p-\Omega)^2 z+2\varepsilon_1^2\right] e^{-z\Omega^2} \\
& \frac{1}{16\varepsilon_1^4\sqrt{\pi z}}\left[\left((\varepsilon_1+\varepsilon_p)^2-\Omega^2\right)\left(\varepsilon_1^2-2\varepsilon_1\varepsilon_p-\varepsilon_p^2+\Omega^2\right)z+4\varepsilon_p\varepsilon_1^3 z-\varepsilon_1^2\right] \\
& \frac{1}{32\varepsilon_1^5}\left[(\varepsilon_1^2-\varepsilon_p^2+\Omega^2)((\varepsilon_1+\varepsilon_p)^2-\Omega^2)z-4\varepsilon_1^2\right]\left((\varepsilon_1+\varepsilon_p)^2-\Omega^2\right) \\
& \left[e^{-z\Omega^2}\mathrm{nerf}(\sqrt{z}B_+)+e^{-z\varepsilon_p}\mathrm{nerf}(\sqrt{z}B_-)\right] \qquad (3.25)
\end{aligned}
$$

This means that the energy shift due to the self–energy insert diagram figure (3.2c) can be written as

$$
\begin{aligned}
\Delta E \;=\; & g^2\int_0^\infty dz \sum_{\substack{pm\Sigma \\ q\neq n_2}} g^{\Sigma\Sigma} M_{n_1 q}\tilde{Q}^{m\Sigma}_{qp}Q^{m\Sigma}_{pn_2}K^{m\Sigma}_{pq}(z) \\
& +g^2\int_0^\infty dz \sum_{pm\Sigma} g^{\Sigma\Sigma} M_{n_1 n_2}\tilde{Q}^{m\Sigma}_{n_2 p}Q^{m\Sigma}_{pn_2}L^{m\Sigma}_{pq}(z) \qquad (3.26)
\end{aligned}
$$

The energy shift for the diagram with the self–energy loop on the other quark leg gives the same result as eq. (3.26) so we need only multiply by a factor of 2 to get the contribution of both graphs. Here again we first sum over the free quantum numbers and leave the integral over the $z$–form for last. This energy shift is divergent and must be considered together with the corresponding mass renormalization term. This sum is still divergent and we need to subtract the divergence in eq. (2.73) from it to find a finite contribution. An alternative way of doing this is to add the unrenormalized vertex diagram and the two self–energy and the two mass counterterm diagrams together to give a finite result. This procedure has the benefit of only having one renormalization scheme dependence which is the mass renormalization scheme.

### 3.2.3 Mass Counterterm Graphs

The mass counterterm graphs contribute to $O(eg^2)$ via the $\langle S_\epsilon^{(2)}\rangle$ term in eq. (1.47). This is also the only contribution of this term. The energy shift due to this term is

$$
\Delta E = \lim_{\epsilon\to 0} i\epsilon\langle S_\epsilon^{(2)}\rangle_c \qquad (3.27)
$$

Using the definition of $\langle S_\epsilon^{(2)}\rangle_c$ one finds

$$\Delta E = \lim_{\epsilon\to 0} i\epsilon \frac{(-i)^2}{2!} \int d^4x_1 \int d^4x_2 \; e^{-\epsilon(|t_1|+|t_2|)} \left\langle T\left[\left(\hat{\bar{\psi}}(Q\hat{\not{A}}_{\rm ext}+\delta m)\hat{\psi}\right)_{x_1}\left(\hat{\bar{\psi}}(Q\hat{\not{A}}_{\rm ext}+\delta m)\hat{\psi}\right)_{x_2}\right]\right\rangle \tag{3.28}$$

The product leads to two terms of $O(eg^2)$ corresponding to the two possible time labels for the external interaction. Due to the symmetry of the limits of the time integrals these both give the same result. The time ordered product can then be decomposed into the sum of normal ordered products of all possible contractions. There are two possible contractions that contribute to the magnetic moment and these contractions two possible contractions can be represented by the Feynman diagrams in figure (3.3). The contribution figure (3.3a) is thus


Figure 3.3: *The mass counterterm diagrams.*

$$\Delta E = -\lim_{\epsilon\to 0} i\epsilon \int d^4x_1 \int d^4x_2 \; e^{-\epsilon(|t_1|+|t_2|)} \left\langle N\left[\underbrace{\left(\hat{\bar{\psi}}Q\hat{\not{A}}_{\rm ext}\hat{\psi}\right)_{x_1}}\left(\hat{\bar{\psi}}\delta m\hat{\psi}\right)_{x_2}\right]\right\rangle \tag{3.29}$$

Substituting the quark propagator (1.56) and the cavity mode expansion of the quark field operators (1.51) one finds

$$\Delta E = \lim_{\epsilon\to 0} \epsilon \langle \hat{a}_{c_1 f_1 n_1} Q \hat{a}_{c_2 f_2 n_2}\rangle \sum_p \int dt_1 \int dt_2 \int \frac{d\omega}{2\pi} \frac{e^{-\epsilon(|t_1|+|t_2|)} e^{it_1(\varepsilon_1-\omega)} e^{-it_2(\omega-\varepsilon_2)}}{(\omega-\varepsilon_p)\; i} M_{n_1 p}\delta m_{p n_2} \tag{3.30}$$

The time and $\omega$ integrals may be performed and in the limit $\epsilon \to 0$ one obtains

$$\Delta E = \langle \hat{a}_{c_1 f_1 n_1} Q \hat{a}_{c_2 f_2 n_2}\rangle \sum_p M_{n_1 p}\delta m_{p n_2} \frac{\delta(\varepsilon_1,\varepsilon_2)}{(\varepsilon_1-\varepsilon_p)} \tag{3.31}$$

where $\delta m_{nn'}$ is defined as

$$\delta m_{nn'} = \delta m \int d^3x \; \bar{u}_n(x) u_{n'}(x) \tag{3.32}$$

The value of $\delta m$ used is the free space value of $\delta m$ in the mass shell scheme and is given by eq. (2.32). The contribution of the Feynman diagram in figure (3.3b) is found to be the same as that of figure (3.3a). The result of the calculation of these Feynman diagrams must be added to the values obtained from the self–energy insert diagrams before the integral over the $z$–form is performed. The vertex correction diagram must be added to this sum to obtain a finite result. Alternatively one can subtract the free space divergence which has been Fourier transformed into cavity mode space, given in eq. (2.73), from this sum to obtain a finite result.

### 3.2.4 One Gluon Exchange Diagrams

The remaining diagrams that contribute to the magnetic moment are the two one gluon exchange diagrams in figure (3.4). These diagrams come about due to the $\langle S_\epsilon^{(3)} \rangle$ term. These graphs are important as they are the only graphs to this order that can alter

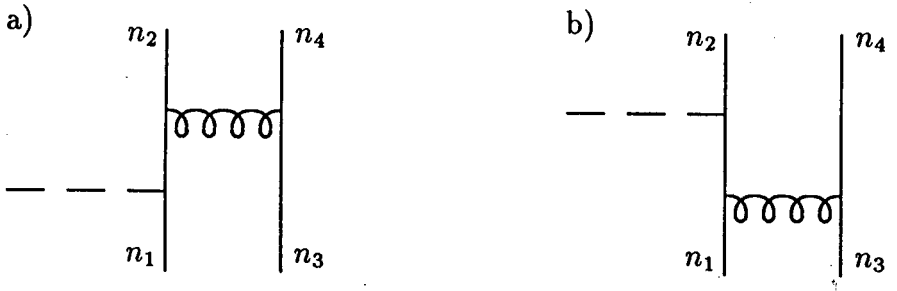


Figure 3.4: *One–gluon exchange diagrams.*

the ratio of the neutron to proton magnetic moment from the value of -2/3 which is found for each of the previous diagrams, assuming that the up and down quark masses are the same. All the diagrams considered up to now have been of a one body nature which has forced the ratio of neutron to proton magnetic moment to be -2/3. The one gluon exchange diagrams are 2 body in nature which leads to the ratio of the magnetic moments for these diagrams differ from -2/3.

The energy shift for the one gluon exchange diagrams is finite and gauge independent [7] making the diagrams easy to calculate. The energy shift for figure (3.4a) can be found

using the techniques described earlier. One finds

$$\Delta E = -\lim_{\epsilon\to 0}\frac{3i\epsilon}{2}(-i)^3 g^2 \int d^4x_1 \int d^4x_2 \int d^4x_3 e^{-\epsilon(|t_1|+|t_2|+|t_3|)} \left\langle N\left[\left(\hat{\bar{\psi}}\frac{\lambda_a}{2}\hat{\not{A}}_a\hat{\psi}\right)_{x_1}\left(\hat{\bar{\psi}}\frac{\lambda_b}{2}\hat{\not{A}}_b\hat{\psi}\right)_{x_2}\left(\hat{\bar{\psi}}\hat{\not{A}}_{\rm ext}\hat{\psi}\right)_{x_3}\right]\right\rangle \tag{3.33}$$

where again we have included only one possible contraction but have multiplied by a factor of six to get the complete contribution. Substituting the quark and gluon propagators and the quark field expansion this may be written as

$$\begin{aligned}\Delta E \;=\; & \lim_{\epsilon\to 0}\frac{3i\epsilon}{2}\left\langle \hat{a}^\dagger_{c_1 f_1 n_1}\hat{a}^\dagger_{c_3 f_3 n_3}\left(\frac{\lambda_a}{2}\right)_{c_1 c_2}\left(\frac{\lambda_a}{2}\right)_{c_3 c_4} Q\hat{a}_{c_2 f_2 n_2}\hat{a}_{c_4 f_4 g_4}\right\rangle \\ & \frac{g^2}{(2\pi)^2}\sum_{pm\Sigma} g^{\Sigma\Sigma}\tilde{Q}^{m\Sigma}_{n_1 n_2}Q^{m\Sigma}_{n_3 p}M_{pn_4}\int_{-\infty}^{\infty} dt_1\, dt_2\, dt_3 \\ & \int_{-\infty}^{\infty} d\omega\, d\omega' \,\frac{e^{-\epsilon(|t_1|+|t_2|+|t_3|)}e^{it_1(\varepsilon_1-\varepsilon_2+\omega)}e^{it_2(\varepsilon_3-\omega-\omega')}e^{it_3(\omega'-\varepsilon_4)}}{(\omega'-\varepsilon_p\pm i0)(\omega^2-\Omega^2\pm i0)}\end{aligned} \tag{3.34}$$

Since these diagrams are finite, we do not need to express the energy shift as an integral over a z–form, so both $\omega$ integrals can be performed using contour methods followed by the time integrals. This results in the expression

$$\Delta E = g^2\sum_{pm\Sigma} g^{\Sigma\Sigma}\tilde{Q}^{m\Sigma}_{n_1 n_2}Q^{m\Sigma}_{n_3 p}M_{pn_4}\frac{\delta(\varepsilon_1+\varepsilon_3,\varepsilon_2+\varepsilon_4)}{(\varepsilon_4-\varepsilon_p)\left[(\varepsilon_1-\varepsilon_2)^2-\Omega^2\right]} \tag{3.35}$$

where we have left out the colour flavour matrix element in eq.(3.35). The apparent singularity in eq. (3.35) when $\varepsilon_p = \varepsilon_4$ can be solved by letting $\varepsilon_p = \varepsilon_4$ in eq. (3.34) and evaluating the integrals. One finds

$$\Delta E = \lim_{\epsilon\to 0} g^2\sum_{m\Sigma} g^{\Sigma\Sigma}\tilde{Q}^{m\Sigma}_{n_1 n_2}Q^{m\Sigma}_{n_3 n_4}M_{n_4 n_4}\left(\frac{3}{2i\epsilon}\frac{1}{\left[(\varepsilon_1-\varepsilon_2)^2-\Omega^2\right]}+\frac{3(\varepsilon_1-\varepsilon_2)}{\left[(\varepsilon_1-\varepsilon_2)^2-\Omega^2\right]^2}\right) \tag{3.36}$$

This equation has two terms, one diverges like $1/\epsilon$ and is cancelled by a diagram in the $\langle S^{(1)}_\epsilon\rangle\langle S^{(2)}_\epsilon\rangle$ term as will be shown in the next section, the other term is finite and is in fact zero in our case where $\varepsilon_1 = \varepsilon_2$ because of the restrictions of the colour flavour matrix element. This can be seen by noting that the only way they can be not equal and still have energy conservation is to have a flavour changing interaction. Thus for this calculation the term $p = n_4$ is simply left out of the sum. There is one more contribution

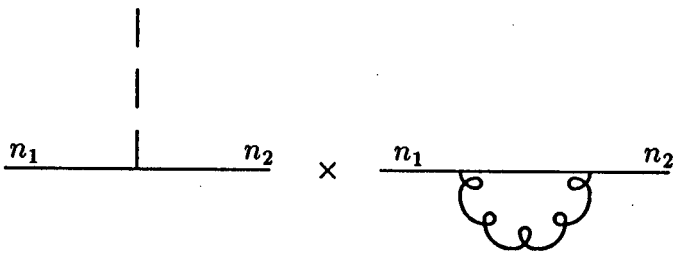


Figure 3.6: *The diagrams from the $\langle S_\epsilon^{(1)}\rangle\langle S_\epsilon^{(2)}\rangle$ term that cancels the divergence in the self energy insert graphs.*

given in figure (3.6). Using the definitions of $\langle S_\epsilon^{(1)}\rangle$ and $\langle S_\epsilon^{(2)}\rangle$, one can find the contribution of these terms which gives rise to the diagram in figure (3.6). The results are :

$$\langle S_\epsilon^{(1)}\rangle = \frac{2i}{\epsilon} M_{n_1 n_2} \tag{3.39}$$

$$\langle S_\epsilon^{(2)}\rangle = \frac{ig^2 C}{2\epsilon} \sum_{pm\Sigma} g^{\Sigma\Sigma} \tilde{Q}^{m\Sigma}_{n_1 p} Q^{m\Sigma}_{pn_2} \frac{\delta(\varepsilon_1, \varepsilon_2)}{\Omega(\varepsilon_2 - \Omega \mathrm{sgn}\, \varepsilon_p - \varepsilon_p)} \tag{3.40}$$

Using these results the energy shift due to the $\langle S_\epsilon^{(1)}\rangle\langle S_\epsilon^{(2)}\rangle$ term in eq. (1.47) can be calculated and one finds

$$\Delta E = \lim_{\epsilon\to 0} \frac{-3i\epsilon}{2} \langle S_\epsilon^{(1)}\rangle\langle S_\epsilon^{(2)}\rangle \tag{3.41}$$

$$= \lim_{\epsilon\to 0} \frac{3ig^2 C}{2\epsilon} \sum_{pm\Sigma} g^{\Sigma\Sigma} M_{n_1 n_2} \tilde{Q}^{m\Sigma}_{n_1 p} q^{m\Sigma}_{pn_2} \frac{\delta(\varepsilon_1, \varepsilon_2)}{\Omega(\varepsilon_2 - \Omega \mathrm{sgn}\varepsilon_p - e_p)} \tag{3.42}$$

This is exactly twice the energy shift of the divergent part of the one self–energy graph given in eq. (3.38). The contribution of both the self–energy inserts graphs are the same and hence the contribution of the $\langle S_\epsilon^{(1)}\rangle\langle S_\epsilon^{(2)}\rangle$ term cancels the contribution of the $1/\epsilon$ divergent part of the self–energy insert diagrams.

In all of the above calculations it has been assumed that there was only one quark in the cavity and the colour flavour matrix elements return a value of 1 for the external quarks in the $1S_{\frac{1}{2}\uparrow}$ state. If there is more than one quark in the cavity, a number of new diagrams contribute via the $\langle S_\epsilon^{(3)}\rangle$ term which diverges like $1/\epsilon$, but these contributions are cancelled by new diagrams in the $\langle S_\epsilon^{(1)}\rangle\langle S_\epsilon^{(3)}\rangle$ term. Looking at graphs with a self–energy loop in them, the $\langle S_\epsilon^{(3)}\rangle$ term gives rise to the diagrams in figure (3.7) together with all possible permutations of the labels $f_1, f_2$ and $f_3$. We have already discussed

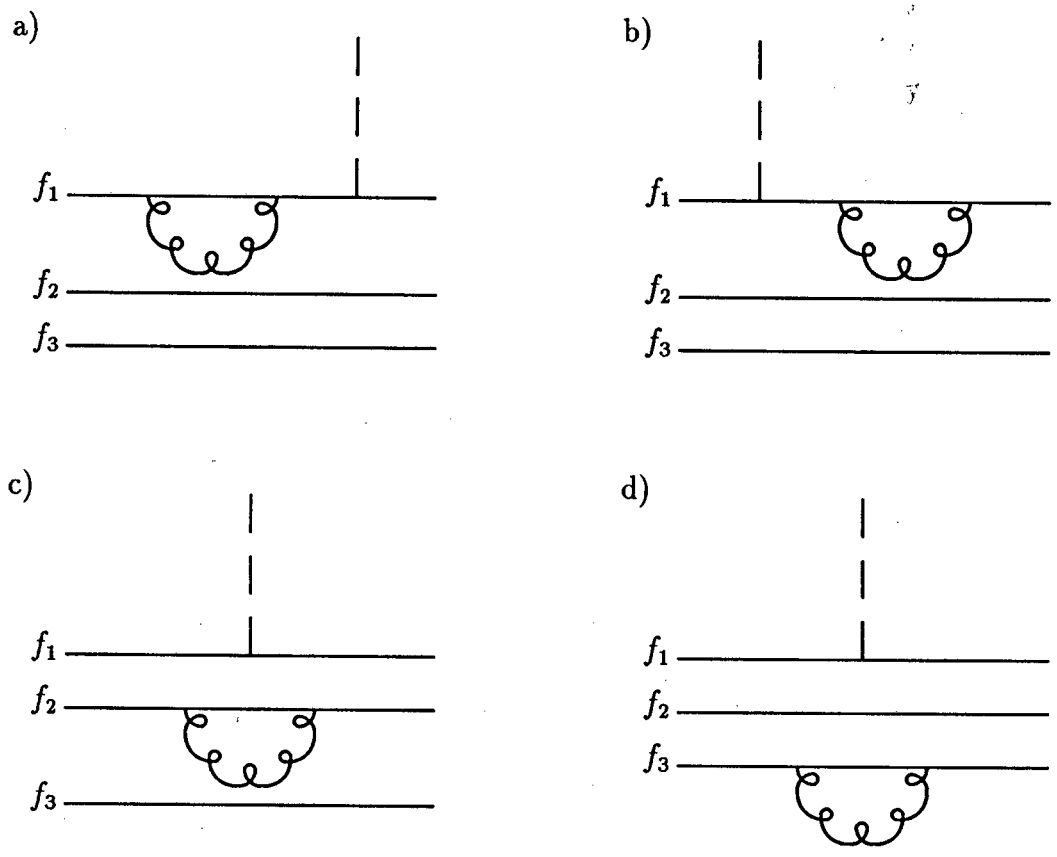


Figure 3.7: *The Feynman diagrams generated by the* $\langle S_\epsilon^{(3)} \rangle$ *term containing a self-energy loop.*

in the case of a single quark how the $1/\epsilon$ part of figures (3.5a,b) are cancelled by the diagram in figure (3.6). The other two graphs in figure (3.7c,d) diverge like $1/\epsilon$ and are cancelled by the diagrams found in the $\langle S_\epsilon^{(1)} \rangle \langle S_\epsilon^{(3)} \rangle$ term. More specifically it is found that the divergent contribution of figure (3.7a,b) is cancelled by the contribution of figure (3.8a), the contribution of figure (3.7b) and figure (3.7d) are cancelled by the contribution of figure (3.8b) and figures (3.8c) respectively.

In this analysis we see that the Gell–Mann and Low theorem forces figures (3.7c,d) not to contribute to the magnetic moment. This is in contrast with some other formalisms where these diagrams are explained away by saying that they have already been taken into account by the model parameters which were fitted to the experimental data.

A very similar procedure to the that which was used above can be applied to the

one gluon exchange diagrams, where it is also found that the only contribution to the magnetic moment is that given by the diagrams in the previous section in figure (3.4). It is also found that the divergent $1/\epsilon$ term in these diagrams is cancelled by a contribution of the $\langle S_\epsilon^{(1)} \rangle \langle S_\epsilon^{(2)} \rangle$ term.

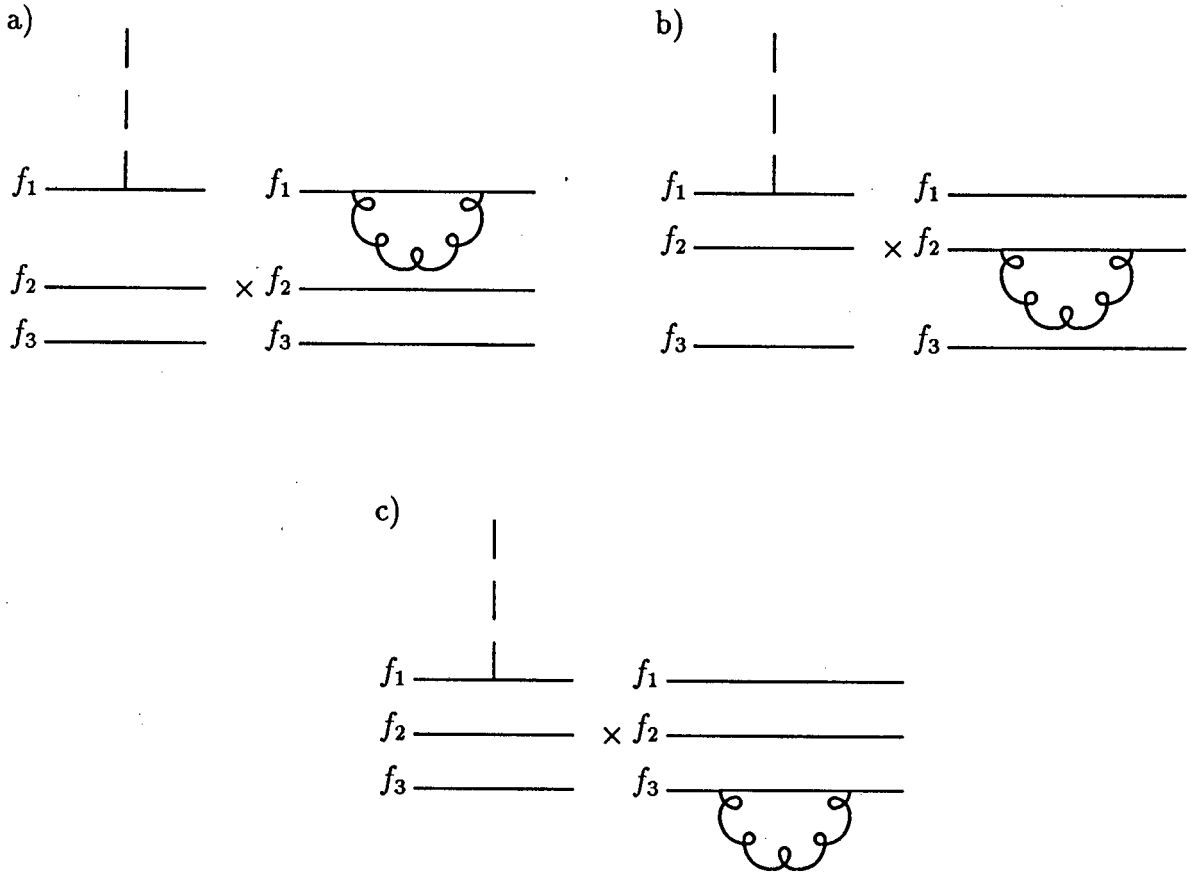


Figure 3.8: *The Feynman diagrams generated by the* $\langle S_\epsilon^{(1)} \rangle \langle S_\epsilon^{(3)} \rangle$ *term which contain a self–energy loop. These diagrams cancel the* $1/\epsilon$ *divergent parts of the Feynman diagrams generated by the* $\langle S_\epsilon^{(3)} \rangle$ *term.*

# Chapter 4

# Numerical Methods

## 4.1 Analytic Preparation for Numerical Calculations

The calculation of the magnetic moment can now proceed using the expressions for the energy shift found in chapter 3. In these expressions the colour flavour matrix elements have been left out and are evaluated separately in appendix F. The colour flavour matrix elements give a list of weights associated with each possible incoming and outgoing state The quarks are restricted to be in the $1S_{\frac{1}{2}}$ state, leaving a list of weights for each possible flavour and spin combination of the external quarks.

As an example of how the calculation is done, let us look at the contribution of the self–energy insert graph with external states $n_1$ and $n_2$.

$$\Delta E = g^2 \int_0^\infty dz \sum_{pqm\Sigma} g^{\Sigma\Sigma} M_{n_1 q} \tilde{Q}^{m\Sigma}_{qp} Q^{m\Sigma}_{pn_2} J^{m\Sigma}_{pq}(z) \tag{4.1}$$

The term $J^{m\Sigma}_{pq}(z)$ is independent of the spin of the quarks $\mu_p$ and $\mu_q$ and is also independent of the gluon magnetic quantum number $M$. The sum of the remaining factors over these quantum numbers can be calculated analytically and the results of these calculations is given in appendix C. The remaining quantum numbers $\kappa_p, \kappa_q, \nu_p, \nu_q, J, N$ and the gluon polarization $\Sigma$ all affect $J^{m\Sigma}_{pq}(z)$. The sum over these quantum numbers must be done before the integral leaving the energy as a $z$–form

$$\Delta E = \int_0^\infty dz \; \Delta E(z) \tag{4.2}$$

The variable $z$ parametrizes the divergence in the energy shift.

When this procedure is implemented on a computer the infinite sum over the quantum numbers must be truncated at some point. The truncation condition used is that the modulus of the energy of the intermediate states must be less than or equal to some maximum energy $E_{\max}$ i.e. $|\varepsilon_p|, |\varepsilon_q|, |\Omega_{m\Sigma}| \leq E_{\max}$. This condition is chosen above other conditions due to the nature of the terms in $J_{pq}^{m\Sigma}(z)$ in which each term is multiplied by $e^{-zE^2}$ where $E$ is the energy of the of an intermediate quark or gluon. The effect of this exponential in each term is to restrict the contribution of the states with high intermediate energies to only contribute significantly to the $z$–form for small values of $z$. Thus the effects of the truncation of the series will only be in the region of small $z$.

It is convenient to shift the variable of integration from $z$ to $y^2$. The reason for this shift is that $J_{pq}^{m\Sigma}(z)$ has an integrable singularity of the form $\int_0^\infty dz\ e^{-\alpha z}/\sqrt{z}$ which although the integral is finite the function of $z$ diverges near $z = 0$. This shift of variables from $z$ to $y^2$ leads to

$$\int_0^\infty dz\ \frac{e^{-\alpha z}}{\sqrt{z}} = \int_0^\infty dy\ 2e^{-\alpha y^2} \tag{4.3}$$

which makes the function of $y$ finite at $y = 0$.

It turns out that the $y$–form $\Delta E(y)$ is singular at $y = 0$, and the energy shift is also infinite, as is expected. If however one adds the contributions of the $y$–forms of the vertex correction diagram, the two self–energy diagrams and the two mass renormalization diagrams together one finds that the resultant $y$–form is finite at $y = 0$ and hence energy shift is also finite. An alternative way to do this is to add the self–energy and the corresponding mass counter–term diagrams together and then to subtract the Fourier transformed free space divergence for this diagram found in chapter 2. This procedure does not yield a unique result as one may add or subtract an arbitrary finite amount from the free space divergence depending on the choice of renormalization scheme.

## 4.2 Numerical Routines

A number of numerical routines had to be written in order to perform the calculation on the computer. These routines and some of the problems found in implementing them are discussed in this section

- *The spherical Bessel functions.* The spherical Bessel functions $j_n(x)$ can be found accurately for all values of $n$ and $x$ using reverse recursion [15]. However for this application where we do not need the Bessel functions of different orders at the same point, this technique is rather slow. Other faster techniques are used in the

regions where they converge
Forward recursion is used in the region $x \geq n$ using the formula

$$j_{n+1}(x) = \frac{2n}{x} j_n(x) - j_{n-1}(x) \tag{4.4}$$

Series expansion is used in the region $x < 2n/8 + 15$ and excluding the region where forward recursion works. The series expansion is given by

$$j_n(x) = (0.5x)^n \sum_{k=0}^{\infty} \frac{(-0.25x^2)^k}{k!\Gamma(l+k+1)} \tag{4.5}$$

and reverse recursion is used for the remaining region.

- *The error function.* The error function $\mathrm{erf}(x) = \int_0^x dt\ e^{-t^2}$ is calculated by two methods depending on its argument.
In the region $0 < x \leq \sqrt{8}$ a series expansion is used

$$\mathrm{erf}(x) = \frac{xe^{-x^2}}{2} \sum_{n=0}^{\infty} \frac{\Gamma(\frac{1}{2})}{\Gamma(\frac{3}{2}+n)} x^{2n} \tag{4.6}$$

In the region $x > \sqrt{8}$ continued fraction development is used

$$\mathrm{erf}(x) = \frac{\sqrt{\pi}}{4} - \frac{xe^{-x^2}}{2} \left( \frac{1}{x^2+} \frac{1/2}{1+} \frac{1}{x^2+} \frac{3/2}{1+} \cdots \right) \tag{4.7}$$

the relation $\mathrm{erf}(x) = -\mathrm{erf}(-x)$ is used where $x < 0$

The error function always occurs in term like $e^{-z\Omega^2}\mathrm{nerf}(\sqrt{z}A_+) + e^{-z\epsilon_q^2}\mathrm{nerf}(\sqrt{z}A_-)$. It is found that when the energy becomes large in magnitude, these expressions are prone to rounding errors as the value of these terms depends critically on the value of $\mathrm{nerf}(\sqrt{z}A_+)$ and $\mathrm{nerf}(\sqrt{z}A_-)$ which within the accuracy of the computer is one. To avoid this rounding error the above expression must be written in terms of a new but related function $\mathrm{serf}(x) = x^2 \int_x^{\infty} dt\ e^{-t^2}$ which does not tend to a constant value for large $x$. The expression in terms of the serf function is used when the modulus of the arguments of one of the error functions is greater than 2 and the sign of the arguments of the two error functions are different.

- *Integration techniques.* Gauss Legendre quadrature is used for all the numerical integrations required in the calculation. Gaussian quadrature has freedom in both the weights and abscissas which allows the integral to be calculated to an

accuracy about twice that of the Newton–Cotes formula with the same number of points. The weights and abscissas of each integral are calculated and stored at the beginning of the calculation. The radial part of the quark gluon vertex integral involves the product of three Bessel functions of the form

$$\int_0^R dr\ r^2 j_{l_p}(p_p r) j_{l_q}(p_q r) j_J(\Omega_{m\Sigma} r) \tag{4.8}$$

This integral is performed numerically as it is not known how to perform it analytically. The product of the Bessel functions becomes highly oscillatory and has approximately $\nu_p + \nu_q + N$ roots in the region $[0, R]$. In order to integrate this function accurately and not to sacrifice speed the number of integration points are allowed to vary depending on the sum $\nu_p + \nu_q + N$.

- *Eigenenergies.* The eigenenergies of the quarks and gluon modes are calculated using the secant method to find the roots of the equations. The results for all the modes are calculated and stored at the beginning of the calculation.

# Chapter 5

# Results and Conclusions

Using the numerical methods described in the previous chapter, the energy shifts of the various Feynman diagrams can be found. The numerical calculation is quite a large task and errors are quite likely to occur, so tests of the validity of the results are important. Two tests have been implemented to make sure that the numerical results are valid. The energy shift for the vertex correction diagram can be written in a form where the energy shift is split into a $z$–dependant part and a $z$–independent part as

$$\Delta E = \alpha_S \int_0^\infty dz \sum_{pqm\Sigma} g^{\Sigma\Sigma} \tilde{Q}^{m\Sigma}_{n_1 p} M_{pq} Q^{m\Sigma}_{qn_2} I^{m\Sigma}_{pq}(z) \tag{5.1}$$

The sum rule tests the correctness of the $z$–independent factors in the above expression by calculating the sum of the vertex integrals

$$4\pi \sum_{pqm\Sigma} g^{\Sigma\Sigma} \tilde{Q}^{m\Sigma}_{n_1 p} M_{pq} Q^{m\Sigma}_{qn_2} \tag{5.2}$$

analytically by using the completeness relation of the quark and gluon cavity modes. These sum rules are derived in appendix D. The sum rule result can then be compared with the sum calculated numerically. This test serves to check that the one has included enough terms in the numerical sum to approximate the infinite sum, and also checks that the computer code is correct. For $E_{\max} = 50$ one finds agreement with the sum rule to at least six digits for all the Feynman diagrams for the external quarks in the $1S_{\frac{1}{2}}$ state and for the low energy cavity modes.

The remaining part of the energy shift that needs to be tested is the spectral term $I^{m\Sigma}_{pq}(z)$ which is quite a complicated function of $z$ and the quark and gluon energies. The numerical calculation of this term requires considerable care to make sure numerical subtraction errors do not occur (see discussion under the heading *Error function* in the

previous chapter). The spectral function can be tested quite simply by integrating $I_{pq}^{m\Sigma}(z)$ over $z$ and comparing the result with the contour integrated result which, for the vertex correction diagram, is given by eq. (3.12), and comparing the result. Before the numerical integral is performed the variable of integration is shifted by $z \to y^2$ to remove the integrable singularity at $z = 0$. The resulting integral over $y$ is performed over the truncated region $[0, 2.5]$ instead of over the complete region $[0, \infty]$. Despite this truncation of the numerical integral the results of the numerical integral agree with the contour integrated result to typically 10 digits depending on the choice of quantum numbers.

## 5.1 Results

The $y$–form of the energy shift due to the vertex correction diagram diverges like $1/y$ near the origin. This divergent energy shift has to be renormalized in order to get a meaningful result. Renormalization is performed by subtracting the singularity that occurs in free space which has been Fourier transformed into cavity mode space eq. (2.74). The resulting renormalized $y$–form for the case where the external quarks have mass = 1.35 in dimensionless units and are in the $1S_{\frac{1}{2}\uparrow}$ state is given by figure (5.1). Note that this $y$–form is not calculated near the origin. This is because the truncation of the infinite sum introduces a sharp kink in the $y$–form at small values of $y$. It is found that the effect of increasing $E_{\max}$ moves this kink closer to the origin but has negligible effect for the values of $y$ that are greater than $y_{\min}$ where $y_{\min}$ is given approximately by

$$y_{\min} \sim \frac{\pi}{E_{\max}} \tag{5.3}$$

The region $[0, y_{\min}]$ has simply been left out of the $y$–form in figure (5.1). To calculate the energy shift, the integral over the whole $y$–form is performed by first extrapolating the $y$–form over the region $y = [0, y_{\min}]$ using a polynomial.

The calculation of this $y$–form for $E_{\max} = 70$ leads to a sum over 4.3 million quark modes and this $y$–form took about 30h CPU time to calculate on an Apollo DN5500 computer. Using this truncation the error in the final result is about $10^{-3}\%$. The time taken for the calculation for larger values of $E_{\max}$ becomes prohibitively long as the number of terms in the sum and hence computer time increases almost exponentially with $E_{\max}$. The calculation can be done significantly faster if one choses a smaller $E_{\max}$, but this leads to a corresponding decrease in accuracy.

The renormalized $y$–form of the energy shift due to one of the self–energy diagrams together with the corresponding mass counterterm diagram is given in figure (5.2).

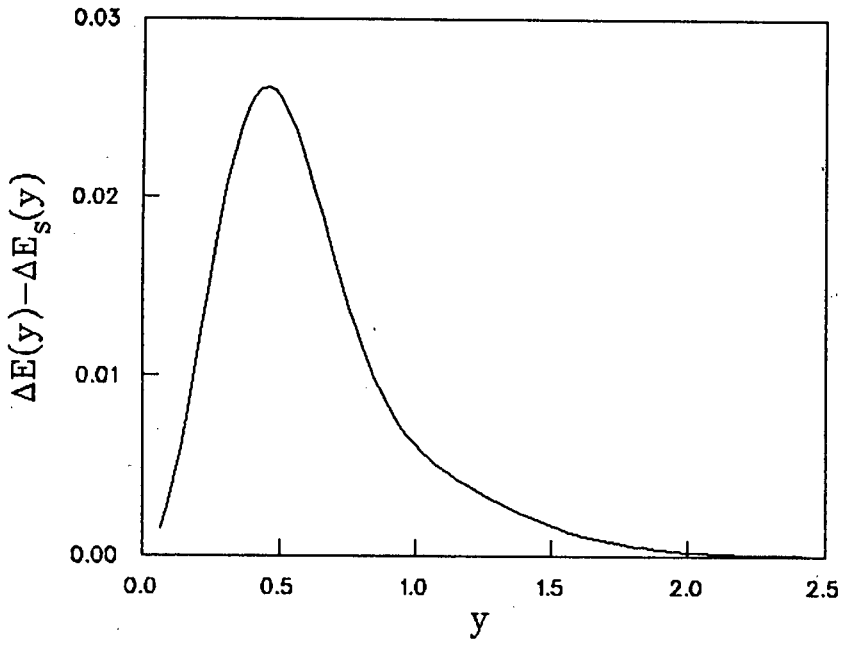


Figure 5.1: *Renormalized y–form of the energy shift in dimensionless units for the vertex correction diagram*

This $y$–form is found by adding the contribution of these two diagrams and subtracting the free space singularity that has been Fourier transformed into cavity mode space. Summing the self–energy insert and the mass counterterm diagrams removes the divergance due to mass renormalisation. The remaining divergance in these two diagrams is removed by subtracting the remainging free space divergance that has been fourier transformed into the cavity mode space. This graph is calculated with the external quark being in the $1S_{\frac{1}{2}\uparrow}$ state and having mass = 1.35 in dimensionless units.

The precise value of the energy shift due to the vertex correction diagram or the self–energy insert diagram is not known as their values depend on the renormalization scheme chosen. In free space the Ward identity relates the renormalization constants of the vertex correction and the self–energy diagram in such a way that the sum over all of these diagrams is found to be finite and renormalization scheme independent in the case of massless quarks, and depends only on the mass renormalization scheme in the case of massive quarks. It is expected that in the cavity the same thing will happen, as the main requirement for proving the Ward identity, the BRS invariance of the theory, still holds in the cavity. One can show that the Ward identity holds in cavity QCD to order $\alpha_S$ for the zeroth component of the current. This is done by simply Fourier transforming the expression for the cavity self–energy graph and the cavity vertex correction graph.

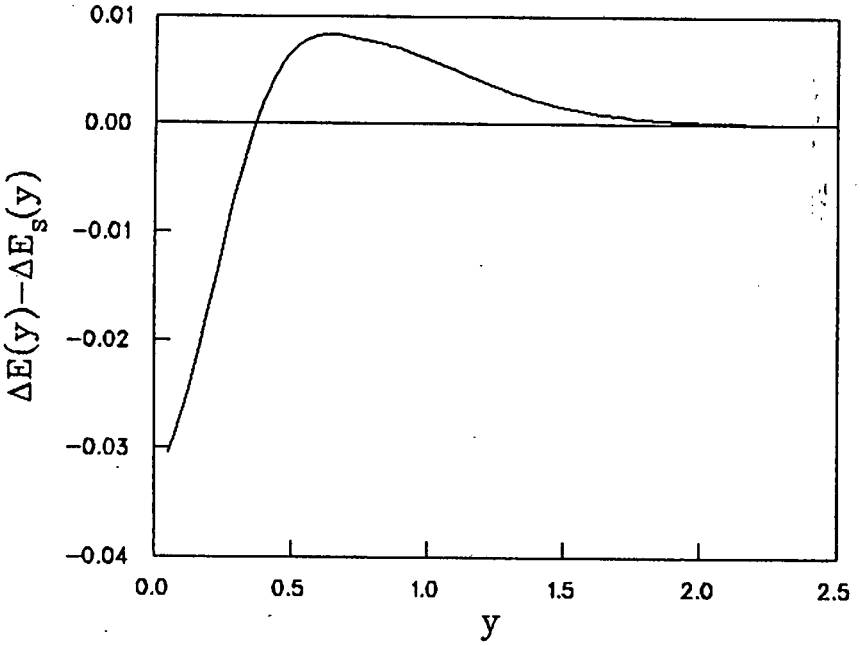


Figure 5.2: *Renormalized y–form of the energy shift in dimensionless units for the self–energy diagram*

One can show that the derivative of the self–energy with respect to the energy–like variable $\omega$ is equal to the zeroth component of the vertex correction diagram, i.e.

$$\frac{\partial \Sigma_{pp}(\omega)}{\partial \omega} = \Lambda^0_{pp}(w) \tag{5.4}$$

This is the cavity form of the Ward identity for the zeroth component of the vertex correction. What the corresponding relations for the other components are is not clear as they refer to the discrete momentum states and hence the derivative is not defined. It has however been shown that the divergence due to the vertex correction diagram and the divergence due to the two self–energy insert diagrams cancel in the case of the magnetic moment calculation which involves the space like components of the vertex correction diagram as the magnetic moment operator is given by $\vec{r} \times \vec{\gamma}$. This cancelation is guaranteed in free space due to the Ward identity holding for the space–like components.

O'Connor [7] has shown that the gauge dependant parts of the self–energy insert graphs and the vertex correction graph vanish and hence the sum of these three diagrams is gauge independent.

With these facts in mind it is only useful to talk about the sum of the vertex correction, the two self–energy insert and the two mass counterterm diagrams which are

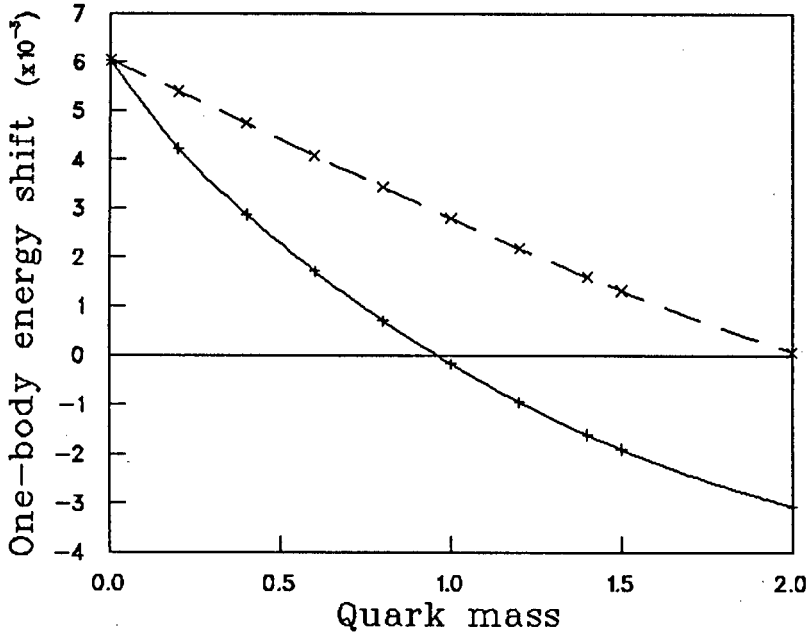


Figure 5.3: *The energy shift in dimensionless units due to the one body diagrams as a function of mass for the case where the external quarks are in the* $1S_{\frac{1}{2}\uparrow}$ *state. The dashed curve is figure in the minimal subtraction scheme where only* $1/\epsilon - \gamma$ *is subtracted while the solid line represents the free space mass shell scheme.*

collectively called the one–body diagrams due to the one–body nature of the interaction. The energy shift due to the one–body diagrams as a function of the mass of the external quark for two different possible mass renormalisation schemes is given in figure (5.3). In this graph the external quarks are assumed to be in the $1S_{\frac{1}{2}\uparrow}$ state. The contribution of the $1S_{\frac{1}{2}\downarrow}$ has the same magnitude but the opposite sign to the $1S_{\frac{1}{2}\uparrow}$ state. This can be seen by looking at the spin sums in appendix C. In figure (5.3) the energy shift of the one–body diagrams is plotted as a function of mass for two renormalisation schemes. The solid line is the free space mass shell scheme while the dashed line is in the $\overline{\text{MS}}$ scheme. One can see that there is quite a large difference depending on which scheme is chosen. The free space mass shell scheme is used in the values quoted later on as it is belived to be closest to the mass shell scheme in the cavity.

The two–body diagrams are significantly easier to calculate. The graphs on their own are convergent and gauge independent. Conservation of angular momentum restricts the sum over the intermediate quantum numbers to only a few of the possible values. The graph of the contribution of one of the two–body diagrams are given in figure (5.4a,b,c)

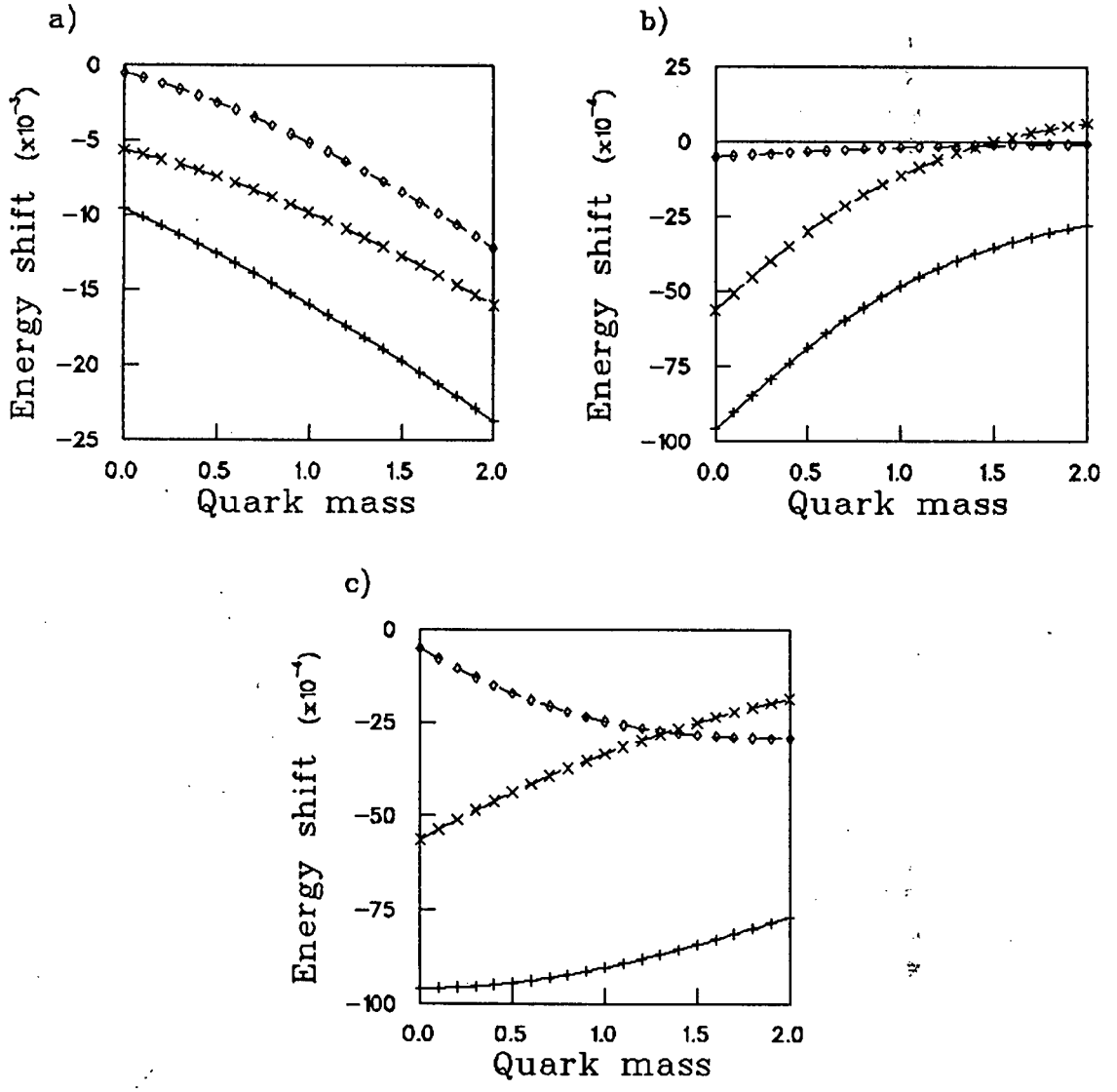


Figure 5.4: *Graphs of the two–body contributions for various mass and spin combinations. In all the graphs the + represents spin* $\uparrow\uparrow\uparrow\uparrow$, $\times$ *represents spin* $\uparrow\uparrow\downarrow\downarrow$ *while* $\diamond$ *represents spin* $\uparrow\downarrow\downarrow\uparrow$. *Graph a) represents the contribution as a function of the mass of the quark hit by the photon while the other quark is massless. Graph b) represents the contribution as a function of mass of the quark* **not** *hit by the photon while the other quark is massless. Graph c) represents the contribution as a function of the mass of the quarks where both quarks have the same mass.*

for various combinations of the spin and masses of the quarks. In this figure I have used the notation $\uparrow\downarrow\downarrow\uparrow = \delta_{\mu_1\uparrow}\delta_{\mu_2\downarrow}\delta_{\mu_3\downarrow}\delta_{\mu_4\uparrow}$

The invariant mass of the light quarks has been calculated by Dominguez *et al.* [19] [20]. The results of these calculations is given in the table below in both MeV and dimensionless units. The up and down quark masses are very small and will be

| Quark type | Mass (MeV) | Mass (dimensionless) |
|---|---|---|
| up | 8.2±1.5 | 0.042±0.008 |
| down | 14.4±1.5 | 0.073±0.008 |
| strange | 266±29 | 1.35±0.15 |

Table 5.1: *Table of the invariant masses of light quarks.*

assumed to be zero in the following calculations. The strange quark will be assumed to have mass $m_s = 1.35$ in dimensionless units.

The contribution to the energy shift of the one-body diagrams for quarks in the $1S_{\frac{1}{2}\uparrow}$ state with charge of +1 for quarks which are massless or have the strange quark mass is given in table (5.2). Quarks in the $1S_{\frac{1}{2}\downarrow}$ state give the same contribution but

| Quark mass | Zeroth order | order $\alpha_S$ |
|---|---|---|
| 0 | −0.2023 | 0.06336 |
| 1.35 | −0.1574 | −0.01104 |

Table 5.2: *Results of the energy shift due to the one body diagrams in dimensionless units.*

with the opposite sign. This information can be used together with the colour flavour matrix elements which include the charge factors of 2/3 and -1/3 associated with up, down and strange quarks to calculate the contribution of the one body diagrams.

The contribution to the energy shift of the two-body diagrams for quarks in the $1S_{\frac{1}{2}}$ state with charge 1 with various spin and mass combinations is given in table (5.3). The headings of the columns contains two letters each either O or S meaning massless and strange quark mass respectively. The second letter refers to the mass of the quark hit by the photon labelled $n_3, n_4$ while the first letter refers to the mass of the other quark involved labelled $n_1, n_2$. The zero energy scalar mode contributes significantly to these values. This data can be used together with the two-body colour flavour matrix elements which include the charge factors of 2/3 and -1/3 for the up, down and strange quarks.

The energy shifts can be converted to magnetic moments using $\Delta E = -\vec{\mu} \cdot \vec{B}$ and converted into nuclear magnetons which are defined as $\mu_N = e\hbar/2m_p$ as shown in

| Spins | Energy shift $\times 10^3$ for various masses | | | |
|---|---|---|---|---|
| $\mu_1\mu_2\mu_3\mu_4$ | O O | O S | S O | S S |
| $\uparrow\uparrow\uparrow\uparrow$ | −6.5844 | −5.4952 | −5.7831 | −4.8752 |
| $\uparrow\uparrow\downarrow\downarrow$ | −0.5020 | −3.3527 | −0.4186 | −2.7699 |
| $\uparrow\downarrow\downarrow\uparrow$ | −8.6363 | −8.3063 | −6.6245 | −6.4882 |
| $\downarrow\uparrow\uparrow\downarrow$ | 8.6363 | 8.3063 | 6.6245 | 6.4882 |
| $\downarrow\downarrow\uparrow\uparrow$ | 0.5020 | 3.3527 | 0.4186 | 2.7699 |
| $\downarrow\downarrow\downarrow\downarrow$ | 6.5844 | 5.4952 | 5.7831 | 4.8752 |

Table 5.3: *Table of the two–body energy shifts in dimensionless units for various spin and mass combinations.*

appendix G. Table (5.4) uses the above data and the colour flavour matrix elements to calculate the magnetic moment of the baryons which has been split up into its one–body and two–body parts. Note that in this table all the results are scaled by $R$ where $R$ is the cavity radius in femtometers.

| State | Zeroth | One–body | Two–body | Total | $\alpha_S$=1 | Exp |
|---|---|---|---|---|---|---|
| P | 1.924 | $-0.8034\alpha_S$ | $0.0502\alpha_S$ | $1.924-0.753\alpha_S$ | 1.170 | 2.793 |
| N | −1.283 | $0.5356\alpha_S$ | $0.0308\alpha_S$ | $-1.283+0.566\alpha_S$ | −0.716 | −1.913 |
| $\Sigma^+$ | 1.876 | $-0.6985\alpha_S$ | $0.0700\alpha_S$ | $1.876-0.629\alpha_S$ | 1.248 | 2.419 |
| $\Sigma^0$ | 0.594 | $-0.1630\alpha_S$ | $-0.0134\alpha_S$ | $0.594-0.176\alpha_S$ | 0.417 | |
| $\Sigma^-$ | −0.689 | $0.3726\alpha_S$ | $-0.0834\alpha_S$ | $-0.689+0.289\alpha_S$ | −0.400 | −1.156 |
| $\Xi^0$ | −1.093 | $0.1163\alpha_S$ | $0.0130\alpha_S$ | $-1.093+0.129\alpha_S$ | −0.964 | −1.253 |
| $\Xi^-$ | −0.452 | $-0.1515\alpha_S$ | $-0.0700\alpha_S$ | $-0.452-0.222\alpha_S$ | −0.673 | −0.675 |
| $\Lambda$ | −0.499 | $-0.0467\alpha_S$ | $0.0043\alpha_S$ | $-0.499-0.038\alpha_S$ | −0.537 | −0.613 |

Table 5.4: *Magnetic moments of the baryons.*

## 5.2 Comparison of Results

It can be seen from the data in table (5.4) that the ordr $\alpha_S$ contributions makes the ratio of the magnetic moments to the proton magnetic moment worse than the zeroth order ratios. The ratio $\mu_n/\mu_p$ is only affected by the one gluon exchange diagrams, and the ratio is worse than the zeroth order data for positive $\alpha_S$. For all the other ratios, $\mu_{\Sigma^+}/\mu_p$, $\mu_{\Xi^0}/\mu_p$ etc. one finds that if one includes only the one–body diagrams the ratio becomes worse than the corresponding zeroth order ratios. If one includes only

the two–body diagrams, one finds that the rations become closer to the experimental values for all the states except for the ratios $\mu_{\Sigma^+}/\mu_p$ and $\mu_n/\mu_p$ which becomes worse. The inclusion of the one–body terms is thus largely responsible for the poor fit of these ratios with experimental ratios.

A number of calculations of the one gluon exchange effects have been made. The most recent of which are due to Tsushima *et al.* [22] and to Høgaasen and Myhrer [23]. A brief discussion about the techniques used to calculate these quantities is in order. It has been shown that if one includes the Coulomb part of the colour field in the in the Coulomb gauge in the one gluon exchange diagrams there is an inconsistency with the boundary conditions. Two approaches have been used to overcome this problem. The first, which I will call type I is to include together with all the one gluon exchange diagrams, including those involving the Coulomb part of the interaction, a number of parts of the one–body loop diagrams which involve the Coulomb part of the quark propagator and where one of the intermediate quarks in the loop has been restricted to be in the ground state. The inclusion of these partial one–body diagrams restores the consistency with the boundary conditions.

The second method called type II is just to exclude the Coulomb part of the gluon propagator in the one gluon exchange diagrams.

I have calculated the one gluon exchange diagrams in the Feynman gauge including the Coulomb part of the propagator. There is no inconsistancy with the boundary here as the gluon propagator is constructed out of cavity modes which satisfy the boundary conditions.

Høgaasen and Myhrer [23] have calculated the contribution of the one gluon exchange diagrams in the type II scheme i.e. they have calculated the contribution of the transverse magnetic gluon (the transverse electric and longitudinal modes do not contribute anyway). There results are $\delta\mu_p^{(2)} = 0\mu_N$ for the proton and $\delta\mu_n^{(2)} = 0.133\mu_N$ for the neutron. These results are confirmed in this calculation if the scalar gluon is omitted. The scalar gluon only contributes to the magnetic moment in the same ratio as the SU(3) model model predicts i.e. $\delta\mu_n^S/\delta\mu_p^S = -2/3$.

Høgaasen and Myhrer's result is in fact a recalculation and confirmation of part of the calculations by Ushio [24] and Krivoruchenko [25]. Ushio has however also calculated the results for the type I scheme and gets very similar results to the type two scheme. This similarity of the results using the two schemes is confirmed by Tsushima et al.[22].

This calculation is done using the same formalism as O'Connor [7] who calculates the contribution of the anomalous magnetic moment for the proton and neutron assuming massless quarks. The results for the one body diagrams for massless quarks agree with those of O'Connor if I do not include the zero energy scalar mode contribution. The results for the two–body diagrams differ from those given in O'Connor, but again this

is due to the fact that O'Connor excluded the contribution of the zero energy scalar mode. The final results however do agree with those obtained by O'Connor due to the fact that the zero energy mode does not contribute to the sum of all the diagram as discussed in appendix E.

The next closest formalism to that used here is due to Maxwell and Vento [17]. These authors also have only applied there formalism to massless quarks. They have included the contribution of the vertex correction diagram, but have excluded the contribution of the two self–energy insert diagrams, so there results for the one–body diagrams are both gauge dependant and renormalization scheme dependant and hence no direct comparison can be made between the results. One can however note that Maxwell and Vento's one–body contribution has the same order of magnitude as our calculation. The contribution of there two–body diagrams are automatically gauge invariant and hence there results can be compared with ours.

| | M&V | R.L. |
|---|---|---|
| $\mu_p$ | $-0.11$ | 0.05024 |
| $\mu_n$ | 0.22 | 0.03084 |

These results differ from those obtained by Maxwell and Vento. The reason for the discrepancey has not been found.

A number of calculations of two–body contribution to the magnetic moment prior M&V's calculation had been made, but they all did not include a complete set of intermediate states and hence cannot be compared with our calculation.

## 5.3 Conclusion

It has been shown here that the order $\alpha_S$ corrections makes the magnetic moment of the baryons worse for reasonable values of $\alpha_S$. This can be seen by the values of $\alpha_S = g^2/4\pi$ and $R$ that best fit the experimental magnetic moment data which are $\alpha_S = -0.08$ and $R = 1.34$ with an average error of 4.5%. The average error does not increase very much for some different values of $\alpha_S$ and $R$ eg. for $\alpha_S = 0.4$ and $R = 1.8$ the average error is 12%.

The deviation from the zeroth order ratio $\mu_n/\mu_p$ comes about due to the one–gluon exchange diagrams. The deviation from the zeroth order ratio of the all the other states where the quarks have different masses is due to both the one–gluon exchange and the one–body diagrams. The one–body diagrams make the ratio worse for all the states calculated, except the the neutron where $\mu_n/\mu_p$ is not altered.

It is in principle possible that higher order corrections may improve these ratios. This is possible as the worsening of the ratio is due to the one–body diagrams, where

the changes in the ratio is due to small deviations of the ratio of the large one–body terms. Higer order terms may have a smaller magnitude, but the magnutude of the ratio changing terms may be larger than those of the first order corrections. Another possible explanation of the poor agreement with experimental ratios could be due to not including c.m.s. corrections, especially in the divergent one–body terms.

The relatively large value of the cavity radius $R$ and small values of $\alpha_S$ suggested by the results of this magnetic moment calculation appear to be consistent with some other calculations using the same formalism. Stoddart *et al.* [26] calculated the energy shift due to the tree diagrams in cavity QCD to order $\alpha_S^2$ in order to see if these results could fit the masses splittings of the $\eta$ and $\rho$ mesons. The results of his calculations were that the coefficient of the order $\alpha_S^2$ contribution was often larger than the coefficient of the order $\alpha_S$ contribution. It is thus appears that fairly small values of $\alpha_S$ are required to make the perturbative expansion meaningful in cavity QCD. A calculation of $g_A/g_V$ by Page, Lindebaum and Viollier [27] find that the value of $\alpha_S$ that gives the exact experimental ratio is $\alpha_S = 0.5$. This ratio is independent of the cavity radius. A recent calculation by O'Connor [28] of the proton and neutron charge squared radius which scales like $R^2$ yields close to experimental values for small $\alpha_S$ and large $R \sim 2fm$. This is important in that it shows that the large cavity still leads to the correct measured radius of the nucleons.

In this thesis a successful way of calculating the divergent vertex corrections and self–energy insert diagrams has been found for massive quarks. The results depend only on the mass renormalization scheme as the diagrams included in the calculation turn out to be gauge independent and the other divergences in the diagrams cancel when the sum of the one–body diagrams is taken. The main benefit of the formalism used in this calculation is the way that it easily generates all the Feynman diagrams involved and the corresponding energy denominators. The dangers of not including all of the correct diagrams is discussed by Maxwell and Vento [17].

Further work in this field could be done by trying to find a reliable method of calculating the c.m.s. correction. Higher order calculations may be attempted as methods exist to calculate all the order $\alpha_S$ diagrams. Higher order diagrams would be interesting to calculate as they would start to bring in the non–Abealian nature of QCD which does not surface in the order $\alpha_S$ calculations. These calculations will be time consuming due to the comlexity and the number of diagrams that have to be calculated.

## 5.4 Acknowledgements

I am grateful to the Foundation for Research and Development for its financial support in the form of an FRD bursary.

My thanks goes to my supervisor, Prof R. D. Viollier for his support during this project and for providing the computer systems needed for these calculations.

I thank the staff and students of the Institute of Theoretical Physics who brought me to a stage where attempting this thesis was possible. I thank Philip Page and the many useful discussions we had during this project. I also thank Dr. Mike O'Connor for many helpful discussions, for checking the preliminary version of this thesis and for his excellent maintenance of the computer centre.

# Appendix A

# Cavity Modes

The quark and gluon cavity modes will be discussed in this chapter for easy reference. Most of this section comes from Buser [3]

## A.1 Quark Cavity Modes

The quark cavity modes are explicit solutions of the time independent Dirac equation (A.1) subject to the M.I.T. bag boundary conditions.

$$\left(i\vec{\gamma}\cdot\vec{\nabla}+m_f\right)u_n(\vec{r})=\varepsilon_n\gamma^0 u_n(\vec{r}) \tag{A.1}$$

where $\varepsilon_n$ is the energy and $m_f$ is the mass of the quark with flavour $f$. The solutions of the Dirac equation are Dirac spinors which are labelled by the quantum numbers $n=\{f,\nu,\kappa,\mu\}$ which are the flavour, radial, Dirac and magnetic quantum numbers respectively. The solutions can be written as

$$u_n(\vec{r})=\begin{pmatrix} g_n(r)\chi^\mu_\kappa(\hat{r}) \\ if_n(r)\chi^\mu_{-\kappa}(\hat{r}) \end{pmatrix} \tag{A.2}$$

where $\chi^\mu_\kappa(\hat{r})$ are the usual two component spherical spinors. The radial functions $g_n(r)$ and $f_n(r)$ are given in terms of spherical Bessel functions by

$$g_n(r) = \frac{\mathcal{N}_n}{R^{3/2}}j_l(p_n r) \tag{A.3}$$

$$f_n(r) = \frac{\mathcal{N}_n p_n \operatorname{sgn}\kappa}{R^{3/2}(\varepsilon_n+m_f)}j_{\bar{l}}(p_n r) \tag{A.4}$$

where $R$ is the radius of the cavity. The angular momenta $j, l$ and $\bar{l}$ are defined in terms of the Dirac quantum number $\kappa$ by

$$j(\kappa) = |\kappa| - \frac{1}{2} \tag{A.5}$$

$$l(\kappa) = j(\kappa) + \frac{1}{2}\mathrm{sgn}\,\kappa \tag{A.6}$$

$$\bar{l}(\kappa) = j(\kappa) - \frac{1}{2}\mathrm{sgn}\,\kappa \tag{A.7}$$

The energy $\varepsilon_n$ satisfies the symmetry relation $\varepsilon_{\kappa,\nu} = -\varepsilon_{-\kappa,-\nu}$ and the sign of the energy is the same as the sign of $\nu$. In other parts of this thesis I have labelled the energy with the quantum number $n = \{\nu, \kappa, \mu\}$ and have left it implicit the flavour quantum number. This does not introduce any ambigueties as it is quite clear to which quark's flavour we are refering.

The quark momenta $p_n$ are determined by the linear boundary condition of the M.I.T. bag model (1.48) which reduces to

$$j_l(p_n R) + \frac{p_n R\,\mathrm{sgn}\,\kappa}{\varepsilon_n R + m_f R} j_{\bar{l}}(p_n R) = 0 \tag{A.8}$$

when the cavity modes (A.2) are substituted in eq. (1.48). It is useful to introduce dimensionless momentum, mass and energy parameters defined by

$$x_n = p_n R \tag{A.9}$$

$$\eta_f = m_f R \tag{A.10}$$

$$\omega_n = \varepsilon_n R = \mathrm{sgn}\,\nu \sqrt{x_n^2 + \eta_f^2} \tag{A.11}$$

The normalisation constants $\mathcal{N}_n$ are given by

$$\mathcal{N}_n^2 = \frac{1}{2\omega_n(\omega_n + \kappa) + \eta_f} \left( \frac{x_n}{j_l(x_n)} \right)^2 \tag{A.12}$$

These solutions of the Dirac equation subject to the M.I.T. boundary condition form a complete and orthonormal set of Dirac spinors in the cavity i.e.

$$\sum_n u_n(\vec{r}) u_n^\dagger(\vec{r}') = I\delta^{(3)}(\vec{r}, \vec{r}') \tag{A.13}$$

$$\int d^3r\; u_n^\dagger(\vec{r}) u_{n'}(\vec{r}) = \delta_{nn'} \tag{A.14}$$

where $I$ is the unit 4×4 matrix.

## A.2 Gluon Cavity Modes

In the Feynman gauge ($\lambda = 1$) the gluon cavity modes are solutions of the time independent Dirac equation (A.15) subject to the M.I.T. bag model boundary conditions (1.48)

$$\left(\nabla^2 + \Omega_{m\Sigma}^2\right) a_{m\Sigma}(\vec{r}) = 0 \tag{A.15}$$

where the solutions to the equation have been labelled according to its polarisation $\Sigma$ where $\Sigma = \mathcal{S}, \mathcal{L}, \mathcal{M}, \mathcal{E}$ which corresponds to the scalar, longitudinal, transverse magnetic and transverse electric polarisations respectively, and $m = \{N, J, M\}$ denote the radial, total angular momentum and magnetic quantum numbers respectively. The scalar mode is the zeroth component of the gluon field. The cavity modes can be expressed in terms of spherical Bessel functions and vector spherical harmonics as

$$a^0_{m\mathcal{S}} = \frac{\mathcal{N}_{m\mathcal{S}}}{R^{3/2}} i j_J(\Omega_{m\mathcal{S}} r) Y_{JM}(\hat{r}) \tag{A.16}$$

$$\vec{a}_{m\mathcal{L}}(\vec{r}) = \frac{\mathcal{N}_{m\mathcal{L}}}{\sqrt{R^3(2J+1)}} \left[\sqrt{J} j_{J-1}(\Omega_{m\mathcal{L}} r) \vec{Y}^{J-1}_{JM}(\hat{r}) + \sqrt{J+1} j_{J+1}(\Omega_{m\mathcal{L}} r) \vec{Y}^{J+1}_{JM}(\hat{r})\right] \tag{A.17}$$

$$\vec{a}_{m\mathcal{M}}(\vec{r}) = \frac{\mathcal{N}_{m\mathcal{M}}}{R^{3/2}} j_J(\Omega_{m\mathcal{M}} r) \vec{Y}^J_{JM}(\hat{r}) \tag{A.18}$$

$$\vec{a}_{m\mathcal{E}}(\vec{r}) = \frac{\mathcal{N}_{m\mathcal{E}}}{\sqrt{R^3(2J+1)}} \left[\sqrt{J+1} j_{J-1}(\Omega_{m\mathcal{E}} r) \vec{Y}^{J-1}_{JM}(\hat{r}) - \sqrt{J} j_{J+1}(\Omega_{m\mathcal{E}} r) \vec{Y}^{J+1}_{JM}(\hat{r})\right] \tag{A.19}$$

The total angular momentum J is integral and can take on values $J \geq 0$ for $\Sigma = \mathcal{S}, \mathcal{L}$ and $J \geq 1$ for $\Sigma = \mathcal{M}, \mathcal{E}$. The M.I.T. bag model boundary conditions determine the gluon energy via the eigenvalue equation

$$J j_J(\Omega_{m\Sigma} R) - \Omega_{m\Sigma} R j_{J+1}(\Omega_{m\Sigma} R) = 0 \qquad \Sigma = \mathcal{S}, \mathcal{L} \tag{A.20}$$

$$(J+1) j_J(\Omega_{m\mathcal{M}} R) - \Omega_{m\mathcal{M}} R j_{J+1}(\Omega_{m\mathcal{M}} R) = 0 \tag{A.21}$$

$$j_J(\Omega_{m\mathcal{E}} R) = 0 \tag{A.22}$$

The scalar and longitudinal modes satisfy the same eigenvalue equation and thus have the same energy spectrum, except that there is a zero energy scalar mode and no corresponding longitudinal mode. The gluon normalisation constants are

$$\mathcal{N}^{-2}_{m\mathcal{S}} = \mathcal{N}^{-2}_{m\mathcal{L}} = \frac{1}{2} j^2_J(\Omega_{m\mathcal{S}} R) \left(1 - \frac{J(J+1)}{(\Omega_{m\mathcal{S}} R)^2}\right) \tag{A.23}$$

$$\mathcal{N}_{m\mathcal{M}}^{-2} = \frac{1}{2} j_J^2(\Omega_{m\mathcal{M}} R) \left(1 - \frac{J(J+1)}{(\Omega_{m\mathcal{M}} R)^2}\right) \tag{A.24}$$

$$\mathcal{N}_{m\mathcal{E}}^{-2} = \frac{1}{2} j_{J+1}^2(\Omega_{m\mathcal{E}} R) \tag{A.25}$$

for all the gluon modes except for the zero energy scalar mode which has the following normalisation

$$\mathcal{N}_{0\mathcal{S}}^{-2} = \frac{1}{3} \tag{A.26}$$

The zero energy scalar mode has quantum numbers $m_0 = \{0, 0, 0\}$ and hence is just a constant

$$a_{m_0 \mathcal{S}} = i\sqrt{\frac{3}{4\pi}} \tag{A.27}$$

This set of gluon modes are complete and orthonormal in the cavity i.e.

$$\sum_{m\Sigma} g^{\Sigma\Sigma} a^{\mu}_{m\Sigma}(\vec{r}) a^{\nu *}_{m\Sigma}(\vec{r}') = g^{\mu\nu} \delta^{(3)}(\vec{r}, \vec{r}') \tag{A.28}$$

$$\int d^3 r \; g_{\mu\nu} a^{\mu}_{m\Sigma} a^{\nu *}_{m'\Sigma'}(\vec{r}) = g^{\Sigma\Sigma'} \delta_{mm'} \tag{A.29}$$

where $g^{\Sigma\Sigma'}$ is the diagonal metric tensor in polarisation space which is given by

$$g^{\mathcal{S}\mathcal{S}} = -g^{\mathcal{L}\mathcal{L}} = -g^{\mathcal{M}\mathcal{M}} = -g^{\mathcal{E}\mathcal{E}} = 1 \qquad g^{\Sigma\Sigma'} = 0 \qquad \Sigma \neq \Sigma' \tag{A.30}$$

The completeness relation only holds if one includes the zero scalar mode [13]. Under complex conjugation the gluon cavity modes transform according to

$$a^{\mu *}_{m\Sigma}(\vec{r}) = \zeta_\Sigma (-1)^M a^{\mu}_{m^* \Sigma}(\vec{r}) \tag{A.31}$$

where the set of quantum numbers $m^*$ is defined as

$$m^* = \{N, J, -M\} \tag{A.32}$$

and the phase $\zeta_\Sigma$ is

$$\zeta_\Sigma = \begin{cases} +1 & \text{for } \Sigma = \mathcal{L}, \mathcal{E} \\ -1 & \text{for } \Sigma = \mathcal{S}, \mathcal{M} \end{cases} \tag{A.33}$$

# Appendix B

# Vertex Integrals

The integrals associated with the quark–quark–gluon vertex and two quark external photon vertex will be evaluated in this appendix. Most of this work is well known but is put here for completeness.

## B.1 Quark Gluon Vertex Integral

Whenever there is an interaction between a quark and a gluon the Gell– Mann and Low theorem leads to an integral over the two quark and one gluon fields

$$Q^{m\Sigma}_{nn'} = i \int d^3r \; \bar{u}_n(\vec{r})\gamma_\mu u_{n'}(\vec{r}) a^\mu_{m\Sigma}(\vec{r}) \tag{B.1}$$

or alternatively an integral in which the gluon filed is replaced by its complex conjugate

$$\tilde{Q}^{m\Sigma}_{nn'} = i \int d^3r \; \bar{u}_n(\vec{r})\gamma_\mu u_{n'}(\vec{r}) a^{\mu *}_{m\Sigma} \tag{B.2}$$

There is a simple relationship between (B.1) and (B.2) which can be found using (A.31)

$$\tilde{Q}^{m\Sigma}_{nn'} = (-1)^M \zeta^\Sigma Q^{m^*\Sigma}_{nn'} = -Q^{m\Sigma}_{n'n} \tag{B.3}$$

The vertex integral involving the scalar and longitudinal modes are related by current conservation

$$Q^{m\mathcal{L}}_{nn'} = \frac{\varepsilon_{n'} - \varepsilon_n}{\Omega_{m\mathcal{S}}} Q^{m\mathcal{S}}_{nn'} \tag{B.4}$$

which is valid for all quantum numbers except the zero energy scalar mode.

Following Viollier [11] the integral can be separated into its radial and angular part as

$$\begin{aligned} Q^{m\Sigma}_{nn'} &= R^{-3/2} R^{m\Sigma}_{nn'} \int d\Omega\ \chi^{\mu\dagger}_{\kappa}(\hat{r}) Y_{JM}(\hat{r}) \chi^{\mu'}_{\kappa'}(\hat{r}) \quad \Sigma = \mathcal{S}, \mathcal{L}, \mathcal{E} \\ Q^{m\mathcal{M}}_{nn'} &= R^{-3/2} R^{m\Sigma}_{nn'} \int d\Omega\ \chi^{\mu\dagger}_{\kappa}(\hat{r}) Y_{JM}(\hat{r}) \chi^{\mu'}_{-\kappa'}(\hat{r}) \quad \Sigma = \mathcal{M} \end{aligned} \tag{B.5}$$

The integral over the angular variables can be easily performed by expanding the spinor spherical harmonics in a Clebsch–Gordan series. One finds

$$\begin{aligned} \int d\Omega\ \chi^{\mu\dagger}_{\kappa}(\hat{r}) Y_{JM}(\hat{r}) \chi^{\mu'}_{\kappa'}(\hat{r}) &= \frac{(-1)^{\mu+1/2}}{\sqrt{4\pi}} \frac{\left(1+(-1)^{l+J+l'}\right)}{2} \hat{j}\hat{J}\hat{j}' \begin{pmatrix} j & J & j' \\ \frac{1}{2} & 0 & -\frac{1}{2} \end{pmatrix} \\ &\quad \times \begin{pmatrix} j & J & j' \\ -\mu & M & \mu' \end{pmatrix} \end{aligned} \tag{B.6}$$

where we have used the abbreviation $\hat{j} = \sqrt{2j+1}$. The 3j–symbols use the notation of Varshalovich [10], and is consistent with the notation of Edmonds [9]. The radial integrals are

$$R^{m\mathcal{S}}_{nn'} = -\mathcal{N}_{m\mathcal{S}} \int_0^R dr\ r^2 j_J(\Omega_{m\mathcal{S}} r) S_{nn'}(r) \tag{B.7}$$

$$R^{m\mathcal{L}}_{nn'} = \frac{\varepsilon_{n'} - \varepsilon_n}{\Omega_{m\mathcal{S}}} R^{m\mathcal{S}}_{nn'} \tag{B.8}$$

$$R^{m\mathcal{M}}_{nn'} = -\frac{\mathcal{N}_{m\mathcal{M}}(\kappa+\kappa')}{\sqrt{J(J+1)}} \int_0^R dr\ r^2 j_J(\Omega_{m\mathcal{M}} r) T_{nn'}(r) \tag{B.9}$$

$$\begin{aligned} R^{m\mathcal{E}}_{nn'} &= -\frac{\mathcal{N}_{m\mathcal{M}}}{\Omega_{m\mathcal{E}}\sqrt{J(J+1)}} \int_0^R dr\ r \left( J(J+1) j_J(\Omega_{m\mathcal{E}} r) U_{nn'}(r) \right. \\ &\quad \left. + (\kappa - \kappa') \left[ J j_J(\Omega_{m\mathcal{E}} r) - \Omega_{m\mathcal{E}} r j_{J-1}(\Omega_{m\mathcal{E}} r) \right] T_{nn'}(r) \right) \end{aligned} \tag{B.10}$$

where the functions $S_{nn'}$, $T_{nn'}$ and $U_{nn'}$ are defined in terms of the radial parts of the quark wave functions as

$$S_{nn'} = g_n g_{n'} + f_n f_{n'} \tag{B.11}$$

$$T_{nn'} = g_n f_{n'} + f_n g_{n'} \tag{B.12}$$

$$U_{nn'} = g_n f_{n'} - f_n g_{n'} \tag{B.13}$$

It is useful to include the parity selection rule in the radial part of the wave function. This is done by defining

$$S^{m\Sigma}_{nn'} = \frac{\left(1 + \zeta_\Sigma g^{\Sigma\Sigma} (-1)^{l+J+l'}\right)}{2} R^{m\Sigma}_{nn'} \tag{B.14}$$

The parity factor can now just be dropped from the result of the angular integral when $S_{nn'}^{m\Sigma}$ is used for the radial part.

## B.2 Quark–External Photon Vertex

Whenever an interaction between a quark and an external photon occurs the Gell–Mann and Low theorem gives rise to the quark photon vertex integral

$$M_{nn'} = \int d^3r \; \bar{u}_n(\vec{r})\gamma_\mu u_{n'}(\vec{r})A^\mu_{\text{ext}} \tag{B.15}$$

For our case we wish the external field to be a static magnetic field directed along the $z$–axis. Thus the external field can be written as

$$\vec{A}_{\text{ext}}(\vec{r}) = -\frac{1}{2}(\vec{r}\times\vec{B}) = -\frac{1}{2}(y,-x,0) \tag{B.16}$$

where we have set the magnetic field strength to be unity. This can be done as the magnetic field strength is cancelled in the calculation of the magnetic moment.

Following O'Connor [7] the integral may be performed by writing $\vec{A}_{\text{ext}}(\vec{r})$ in terms of the angular momentum operator as

$$\vec{A}_{\text{ext}}(\vec{r}) = -i\sqrt{\frac{\pi}{3}}\vec{L}rY_{10}(\hat{r}) \tag{B.17}$$

The vertex integral can now be written as

$$M_{nn'} = \sqrt{\frac{\pi}{3}}\int d^3r \; \left(g_n f_{n'}\chi^{\mu\,\dagger}_{\kappa}(\vec{\sigma}\cdot\vec{L}rY_{10})\chi^{\mu'}_{-\kappa'} - f_n g_{n'}\chi^{\mu}_{-\kappa}{}^{\dagger}(\vec{\sigma}\cdot\vec{L}rY_{10})\chi^{\mu'}_{\kappa'}\right) \tag{B.18}$$

where the $\vec{\sigma}$'s are the Pauli matrices. Using the shorthand notation $\sigma_r = \hat{r}\cdot\vec{\sigma}$, the angular part of the second term in (B.18) can be put into the same form as the angular part of the first term by inserting $\sigma_r^2 = 1$ on either side of the hermitian operator $\vec{\sigma}\cdot\vec{L}$ in the second term. Noting that

$$\sigma_r(\vec{\sigma}\cdot\vec{L})\sigma_r = -\vec{\sigma}\cdot\vec{L} \tag{B.19}$$

and $\sigma_r\chi^{\mu}_{-\kappa} = -\chi^{\mu}_{\kappa}$ equation (B.18) can be written as

$$M_{nn'} = \sqrt{\frac{\pi}{3}}\int d^3r \; r^3\,(g_n f_{n'} + f_n g_{n'})\int d\Omega \; \chi^{\mu\,\dagger}_{\kappa}(\hat{r})\left(\vec{\sigma}\cdot\vec{L}Y_{10}(\hat{r})\right)\chi^{\mu'}_{-\kappa'}(\hat{r}) \tag{B.20}$$

In this equation $\vec{\sigma}\cdot\vec{L}$ acts only on $Y_{10}$, but one can write

$$\chi_\kappa^{\mu\dagger}\left(\vec{\sigma}\cdot\vec{L}Y_{10}\right)\chi_{-\kappa'}^{\mu'} = \chi_\kappa^{\mu\dagger}\left(\vec{\sigma}\cdot\vec{L}Y_{10}\chi_{-\kappa'}^{\mu'}\right) - \chi_\kappa^{\mu\dagger}Y_{10}\left(\vec{\sigma}\cdot\vec{L}\chi_{-\kappa'}^{\mu'}\right) \tag{B.21}$$

Noting that $\vec{\sigma}\cdot\vec{L}\chi_\kappa^\mu(\hat{r}) = -(\kappa+1)\chi_\kappa^\mu(\hat{r})$ and exploiting the Hermitian nature of the operator $\vec{\sigma}\cdot\vec{L}$ one can write

$$\chi_\kappa^{\mu\dagger}\left(\vec{\sigma}\cdot\vec{L}Y_{10}\right)\chi_{-\kappa'}^{\mu'} = -(\kappa+\kappa')\chi_\kappa^{\mu\dagger}Y_{10}\chi_{-\kappa'}^{\mu'} \tag{B.22}$$

Thus

$$M_{nn'} = -\sqrt{\frac{\pi}{3}}(\kappa+\kappa')\int d^3r\; r^3\left(g_n f_{n'} + f_n g_{n'}\right)\int d\Omega\;\chi_\kappa^{\mu\dagger}(\hat{r})Y_{10}(\hat{r})\chi_{-\kappa'}^{\mu'}(\hat{r}) \tag{B.23}$$

The angular part of this integral may be written as

$$A_{\kappa\kappa'} = -\sqrt{\frac{\pi}{3}}(\kappa+\kappa')\int d\Omega\;\chi_\kappa^{\mu\dagger}(\hat{r})Y_{10}(\hat{r})\chi_{\kappa'}^{\mu'}(\hat{r}) \tag{B.24}$$

Note that this integral is just a special case of eq. (B.6) The angular momentum of the external field is $J=1$ and hence the difference between the total angular momentum between the final and initial quark state is either 0 or 1. This restriction and the parity term in eq. (B.6) restricts the values of $\kappa$ and $\kappa'$ such that $\kappa=\kappa'$, $\kappa=-\kappa'\pm1$. The angular integrals can thus be evaluated and one finds

$$A_{\kappa\kappa'} = \begin{cases} \dfrac{2\kappa\mu}{4\kappa^2-1} & \text{if } \kappa=\kappa' \\ \dfrac{\text{sgn }\kappa}{4|\kappa|+2}\sqrt{\left(|\kappa|+\frac{1}{2}\right)^2-\mu^2} & \text{if } \kappa'=-\kappa\pm1 \end{cases} \tag{B.25}$$

This angular integral is symmetric as $A_{\kappa\kappa'} = A_{\kappa'\kappa}$ if $\kappa=-\kappa'\pm1$ or $\kappa=\kappa'$. The radial matrix elements are defined as

$$R_{\kappa\kappa'}^{\nu\nu'} = \int_0^R dr\; r^3\left(g_n f_{n'} + f_n g_{n'}\right) \tag{B.26}$$

The radial matrix elements may be derived using the recursion relations of spherical Bessel functions [7] and a lot of algebra. Using dimensionless variables and the short hand notation $\omega' = \omega_{n'}$ etc. the results fall into three possible categories

$$R_{\kappa\kappa}^{\nu\nu} = \frac{R}{2}\frac{4\omega\kappa - 2\eta_f + 4\kappa^2 - 1}{2\omega(\omega+\kappa)+\eta_f} \tag{B.27}$$

$$R_{\kappa\kappa}^{\nu\nu'} = \frac{-2xx'R}{(\omega+\omega')^2\sqrt{\left(2\omega(\omega+\kappa)+\eta_f\right)\left(2\omega'(\omega'+\kappa)+\eta_f\right)}}\times\phi \tag{B.28}$$

$$R_{\kappa\kappa'}^{\nu\nu'} = \frac{-2xx'R\left(\omega-\omega'+\kappa-\kappa'\right)}{(\omega+\omega')(x^2-x'^2)\sqrt{\left(2\omega(\omega+\kappa)+\eta_f\right)\left(2\omega'(\omega'+\kappa')+\eta_f\right)}}\times\phi \tag{B.29}$$

In the last equation (B.29) $\kappa = -\kappa' \pm 1$ or $\kappa' = -\kappa \pm 1$. The phase factor $\phi$ in eq. (B.28) and (B.29) is given by

$$\phi = (-1)^{\rho+\rho'} \qquad \text{where } \rho = \begin{cases} |\mu| + 1 & \kappa < 0, \nu < 0 \\ |\mu| & \text{otherwise} \end{cases} \tag{B.30}$$

Thus the total integral describing the quark external photon vertex can be written as the product of the radial and angular parts as

$$M_{nn'} = R^{\nu\nu'}_{\kappa\kappa'} A_{\kappa\kappa'} \tag{B.31}$$

These results differ from those found on O'Conner [7] which contain a number of typographical errors.

# Appendix C

# Spin Sums

The sum over the spins of the intermediate particles in the vertex correction diagram, the self–energy diagrams and the one gluon exchange diagrams are given in this appendix.

## C.1 Vertex Correction Spin Sum

The sum over the spins of the intermediate particles in then vertex correction diagram is given by

$$
\begin{aligned}
4\pi \sum_{\mu_p \mu_q M} \tilde{Q}^{m\Sigma}_{n_1 p} M_{pq} Q^{m\Sigma}_{q n_2} \;=\; & S^{m\Sigma}_{p n_1} R^{\nu_p \nu_q}_{\kappa_p \kappa_q} S^{m\Sigma}_{q n_2} \frac{(\kappa_p + \kappa_q)}{2} (-1)^{j_1 + j_2 - J - \mu_1 + \frac{1}{2}} \hat{j}_1 \hat{j}_2 \hat{j_P}^2 \hat{j_q}^2 \hat{J}^2 \\
& \begin{pmatrix} j_1 & J & j_p \\ \frac{1}{2} & 0 & -\frac{1}{2} \end{pmatrix} \begin{pmatrix} j_q & J & j_2 \\ \frac{1}{2} & 0 & -\frac{1}{2} \end{pmatrix} \begin{pmatrix} j_p & 1 & j_q \\ \frac{1}{2} & 0 & -\frac{1}{2} \end{pmatrix} \\
& \begin{pmatrix} j_1 & 1 & j_2 \\ \mu_1 & 0 & -\mu_2 \end{pmatrix} \begin{Bmatrix} j_p & J & j_1 \\ j_2 & 1 & j_q \end{Bmatrix}
\end{aligned} \tag{C.1}
$$

where the definitions of $Q^{m\Sigma}_{nn'}, M_{nn'}, S^{m\Sigma}_{nn'}$ and $R^{\nu\nu'}_{\kappa\kappa'}$ are found in appendix B

## C.2 Self–Energy Insert Spin Sum

The self energy spin sum yields

$$4\pi \sum_{\mu_p \mu_q M} M_{n_1 q} \tilde{Q}^{m\Sigma}_{qp} Q^{m\Sigma}_{pn_2} = R^{\nu_1 \nu_q}_{\kappa_1 \kappa_q} S^{m\Sigma}_{pq} S^{m\Sigma}_{pn_2} \frac{(\kappa_1 + \kappa_q)}{2} (-1)^{\mu_1 + \frac{1}{2}} \hat{j}_1 \hat{j}_2 \hat{j}_p{}^2 \hat{J}^2 \delta_{j_q j_2} \quad \text{(C.2)}$$
$$\begin{pmatrix} j_p & J & j_2 \\ \frac{1}{2} & 0 & -\frac{1}{2} \end{pmatrix}^2 \begin{pmatrix} j_1 & 1 & j_2 \\ -\mu_1 & 0 & \mu_2 \end{pmatrix} \begin{pmatrix} j_1 & 1 & j_2 \\ \frac{1}{2} & 0 & -\frac{1}{2} \end{pmatrix}$$

## C.3 One Gluon Exchange Spin Sum

For the one gluon exchange only the sum over the intermediate quark spins can be done analytically while the sum over the gluon spin must be done numerically

$$4\pi \sum_{\mu_p M} \tilde{Q}^{m\Sigma}_{n_1 n_2} Q^{m\Sigma}_{n_3 p} M_{pn_4} = S^{m\Sigma}_{n_2 n_1} S^{m\Sigma}_{n_3 p} R^{\nu_p \nu_4}_{\kappa_p \kappa_4} \frac{(\kappa_p + \kappa_4)}{2} (-1)^{\mu_1 + \mu_3 + \mu_4 + \frac{3}{2}}$$
$$\hat{j}_1 \hat{j}_2 \hat{j}_3 \hat{j}_4 \hat{j}_p{}^2 \hat{J}^2 \begin{pmatrix} j_1 & J & j_2 \\ \frac{1}{2} & 0 & -\frac{1}{2} \end{pmatrix} \begin{pmatrix} j_3 & J & j_p \\ \frac{1}{2} & 0 & -\frac{1}{2} \end{pmatrix}$$
$$\begin{pmatrix} j_p & 1 & j_4 \\ \frac{1}{2} & 0 & -\frac{1}{2} \end{pmatrix} \begin{pmatrix} j_p & 1 & j_4 \\ -\mu_4 & 0 & \mu_4 \end{pmatrix}$$
$$\sum_M (-1)^M \begin{pmatrix} j_1 & J & j_2 \\ -\mu_1 & -M & \mu_2 \end{pmatrix} \begin{pmatrix} j_3 & J & j_p \\ -\mu_3 & M & \mu_4 \end{pmatrix} \quad \text{(C.3)}$$

One can see by the last two $3-j$ symbols that $M = \mu_2 - \mu_1 = mu_3 - \mu_4$ which restricts the allowed spins of the incoming and outgoing quarks such that the sum of the initial spin is equal to the sum of the final spins.

# Appendix D

# Sum Rules

In cavity QCD one often will have a sum over complete sets of states of a product of a number of vertex integrals multiplied by some function of the energy. Computing the vertex integrals is quite a large computational task and is prone to errors. One way of checking the computer code and of checking to see if the truncation technique is adequate is to derive a sum rule which is obtained by analytically summing the product of vertex integrals over the intermediate quark and gluon states by using their completeness relations. This allows you to compare the sum of the product of vertex integrals obtained while calculating the energy shift contributing to the magnetic moment with the analytic sum rule which will serve as both a check of the computer code and whether the limits of the truncation are suitable. Most of the work is taken from O'Connor [7] and hence the details of the calculations will be left out.

## D.1 Vertex Correction Sum Rule

The energy shift contributing to the magnetic moment due to the vertex correction diagram is

$$\Delta E = g^2 \int_0^\infty dz \sum_{pqm\Sigma} g^{\Sigma\Sigma} \tilde{Q}^{m\Sigma}_{n_1 p} M_{pq} Q^{m\Sigma}_{qn_2} I^{m\Sigma}_{pq}(z) \tag{D.1}$$

The sum rule is derived by taking only the terms in eq. (D.1) that are the vertex integrals, thus the sum rule is

$$V^{m\Sigma}_{nn'} = 4\pi g^{\Sigma\Sigma} \sum_{pqM} \tilde{Q}^{m\Sigma}_{np} M_{pq} Q^{m\Sigma}_{qn'} \tag{D.2}$$

In eq. (D.2) the sum does not include all the gluon quantum numbers, since if we sum over all intermediate states the result is an inconvenient delta function. The choice over

which quantum numbers to sum over completely and which one to only sum partially is not important and different sum rules could be derived depending on this choice. Writing eq. (D.2) in full and using the completeness relations to sum over the complete set of quark states and after some Dirac algebra one finds

$$V_{nn'}^{m\Sigma} = -4\pi g^{\Sigma\Sigma} \sum_{M} \int d^3r \; \bar{u}_n(\vec{r}) \left( \not{A}_{\rm ext}(\vec{r}) |a_{m\Sigma}(\vec{r})|^2 + 2\vec{a}_{m\Sigma}(\vec{r}) \cdot \vec{A}_{\rm ext}(\vec{r}) \not{a}^*_{m\Sigma}(\vec{r}) \right) u_{n'}(\vec{r}) \tag{D.3}$$

This can be evaluated to give

$$V_{nn'}^{m\Sigma} = -A_{\kappa\kappa'} \int dr \; r^3 \left( f_n(r) g_{n'}(r) + g_n(r) f_{n'}(r) \right) \Phi_{m\Sigma}(r) \tag{D.4}$$

where $A_{\kappa\kappa'}$ is defined in appendix B and $\Phi_{m\Sigma}(r)$ is given by

$$\Phi_{m\mathcal{S}}(r) = \mathcal{N}_{m\mathcal{S}}^2 (2J+1) {j_J}^2(\Omega r) \tag{D.5}$$

$$\Phi_{m\mathcal{L}}(r) = \frac{\mathcal{N}_{m\mathcal{L}}^2}{2J+1} \left( (J+1) j_{J+1}(\Omega R) - J j_{J-1}(\Omega r) \right)^2 \tag{D.6}$$

$$\Phi_{m\mathcal{M}}(r) = 0 \tag{D.7}$$

$$\Phi_{m\mathcal{E}}(r) = \frac{\mathcal{N}_{m\mathcal{E}}^2}{2J+1} J(J+1) \left( j_{J+1}(\Omega R) - j_{J-1}(\Omega r) \right)^2 \tag{D.8}$$

The radial integral may be evaluated numerically once the quantum numbers of the initial and final quarks $n$ and $n'$, and the intermediate gluon quantum numbers $J, N, \Sigma$ are chosen.

## D.2 Self–Energy Insert Sum Rule

The energy shift due to the self energy insert diagram is given by

$$\Delta E = g^2 \int_0^\infty dz \; \sum_{pm\Sigma} g^{\Sigma\Sigma} M_{n_1 q} \tilde{Q}_{qp}^{m\Sigma} Q_{pn_2}^{m\Sigma} J_{pq}^{m\Sigma}(z) \tag{D.9}$$

The sum rule is defined by taking the sum over the vertex integrals appearing in eq. (D.9) and is

$$U_{nn'}^{m\Sigma} = 4\pi g^{\Sigma\Sigma} \sum_{pqM} \tilde{Q}_{np}^{m\Sigma} Q_{pq}^{m\Sigma} M_{qn'} \tag{D.10}$$

where again where again we only sum over the intermediate quark states and the gluon magnetic quantum number. This can be evaluated using the same techniques as for the vertex correction sum rule and one finds

$$U_{nn'}^{m\Sigma} = -(2J+1) A_{\kappa\kappa'} \int dr \; r^3 \left( f_n(r) g_{n'}(r) + g_n(r) f_{n'}(r) \right) \Phi'_{m\Sigma} \tag{D.11}$$

where $\Phi'_{m\Sigma}(r)$ is defined as

$$\Phi'_{m\mathcal{S}}(r) = \mathcal{N}^2_{m\mathcal{S}} {j_J}^2(\Omega r) \tag{D.12}$$

$$\Phi'_{m\mathcal{L}}(r) = -\frac{\mathcal{N}^2_{m\mathcal{L}}}{2J+1}\left((J+1){j_{J+1}}^2(\Omega R) - J{j_{J-1}}^2(\Omega r)\right) \tag{D.13}$$

$$\Phi'_{m\mathcal{M}}(r) = -\mathcal{N}^2_{m\mathcal{M}} {j_J}^2(\Omega r) \tag{D.14}$$

$$\Phi'_{m\mathcal{E}}(r) = -\frac{\mathcal{N}^2_{m\mathcal{E}}}{2J+1}\left(J{j_{J+1}}^2(\Omega R) - J + 1{j_{J-1}}^2(\Omega r)\right) \tag{D.15}$$

## D.3 One–Gluon Exchange Sum Rule

The energy shift due to the one–gluon exchange diagrams is

$$\Delta E = g^2 \sum_{pm\Sigma} g^{\Sigma\Sigma} \tilde{Q}^{m\Sigma}_{n_1 n_2} Q^{m\Sigma}_{n_3 p} M_{pn_4} \frac{1}{(\varepsilon_4 - \varepsilon_p)\left((\varepsilon_1 - \varepsilon_2)^2 - \Omega^2\right)} \tag{D.16}$$

The sum rule is defined as

$$W^{n_1 n_2}_{n_3 n_4} = 4\pi \sum pm\Sigma g^{\Sigma\Sigma} \tilde{Q}^{m\Sigma}_{n_1 n_2} Q^{m\Sigma}_{n_3 p} M_{pn_4} \tag{D.17}$$

This can be evaluated to give

$$\begin{aligned} W^{n_1 n_2}_{n_3 n_4} = \int dr\ r^2 \left(g_{n_1} f_{n_2} + f_{n_1} g_{n_2}\right)\left(g_{n_3} g_{n_4} + f_{n_3} f_{n_4}\right) \\ \times \left(C^{\mu_1\mu_2\mu_3\mu_4}_{\kappa_1\kappa_2\kappa_3\kappa_4} - C^{\mu_3\mu_4\mu_1\mu_2}_{\kappa_3-\kappa_4\kappa_1-\kappa_2} + D^{\mu_3\mu_4\mu_1\mu_2}_{\kappa_3\kappa_4\kappa_1-\kappa_2}\right) \\ + \int dr\ r^3 \left(2 f_{n_1} g_{n_2} g_{n_3} g_{n_4} + 2 g_{n_1} f_{n_2} f_{n_3} f_{n_4} + \left(g_{n_1} g_{n_2} + f_{n_1} f_{n_2}\right)\left(g_{n_3} f_{n_4} + f_{n_3} g_{n_4}\right)\right) \\ \times D^{\mu_1\mu_2\mu_3\mu_4}_{\kappa_1\kappa_2\kappa_3-\kappa_4} \end{aligned} \tag{D.18}$$

where the angular integrals are given by the terms $C^{\mu_1\mu_2\mu_3\mu_4}_{\kappa_1\kappa_2\kappa_3\kappa_4}$ and $D^{\mu_1\mu_2\mu_3\mu_4}_{\kappa_1\kappa_2\kappa_3\kappa_4}$ which are given below.

$$C^{\mu_1\mu_2\mu_3\mu_4}_{\kappa_1\kappa_2\kappa_3\kappa_4} = 2\pi \int d\Omega\ \chi^{\mu_1}_{\kappa_1}{}^{\dagger}\sigma_z\chi^{\mu_2}_{\kappa_2}\chi^{\mu_3}_{\kappa_3}{}^{\dagger}\chi^{\mu_4}_{\kappa_4} = (-1)^{\mu_1+\mu_3}\sum_{mL}(-1)^{L}\hat{j}_1\hat{j}_2\hat{j}_3\hat{j}_4\hat{l}_1\hat{l}_2\hat{L}^2$$
$$\frac{1+(-1)^{l_3+L+l_4}}{4}\begin{pmatrix} l_1 & \frac{1}{2} & j_1 \\ \mu_1-m & m & -\mu_1\end{pmatrix}\begin{pmatrix} l_2 & \frac{1}{2} & j_2 \\ \mu_2-m & m & -\mu_2\end{pmatrix}\begin{pmatrix} j_3 & L & j_4 \\ \frac{1}{2} & 0 & -\frac{1}{2}\end{pmatrix}$$
$$\begin{pmatrix} j_3 & L & j_4 \\ -\mu_3 & \mu_2-\mu_1 & \mu_4\end{pmatrix}\begin{pmatrix} l_1 & l_2 & L \\ 0 & 0 & 0\end{pmatrix}\begin{pmatrix} l_1 & L & l_2 \\ m-\mu_1 & \mu_1-\mu_2 & \mu_2-m\end{pmatrix} \qquad \text{(D.19)}$$

The other angular integral is

$$D^{\mu_1\mu_2\mu_3\mu_4}_{\kappa_1\kappa_2\kappa_3\kappa_4} = \frac{i4\pi}{r}\int d\Omega\ \chi^{\mu_1}_{\kappa_1}{}^{\dagger}\chi^{\mu_2}_{\kappa_2}\chi^{\mu_3}_{\kappa_3}{}^{\dagger}\left(\vec{\sigma}\cdot\vec{A}_{\rm ext}\right)\chi^{\mu_4}_{\kappa_4} = \frac{(-1)^{\mu_2+\mu_4}}{\sqrt{2}}$$
$$\hat{j}_1\hat{j}_2\hat{j}_3\hat{j}_4\hat{l}_1\hat{l}_2\hat{l}_3\hat{l}_4\sum_{mm'LL'}(-1)^{L+L'-m-m'}\hat{L}^2\hat{L}'^2\begin{pmatrix} l_1 & \frac{1}{2} & j_1 \\ \mu_1-m & m & -\mu_1\end{pmatrix}$$
$$\begin{pmatrix} l_2 & \frac{1}{2} & j_2 \\ \mu_2-m & m & -\mu_2\end{pmatrix}\begin{pmatrix} l_3 & \frac{1}{2} & j_3 \\ \mu_3+m' & -m' & -\mu_3\end{pmatrix}\begin{pmatrix} l_4 & \frac{1}{2} & j_4 \\ \mu_4-m' & -m' & -\mu_4\end{pmatrix}$$
$$\begin{pmatrix} l_1 & L & l_2 \\ m-\mu_1 & \mu_4-\mu_3 & \mu_2-m\end{pmatrix}\begin{pmatrix} l_3 & L' & l_4 \\ -\mu_3-m' & \mu_3-\mu_4+2m' & \mu_4-m'\end{pmatrix}$$
$$\begin{pmatrix} L' & 1 & L \\ \mu_4-\mu_3-2m' & 2m' & \mu_3-\mu_4\end{pmatrix}\begin{pmatrix} l_1 & l_2 & L \\ 0 & 0 & 0\end{pmatrix}\begin{pmatrix} l_3 & l_4 & L' \\ 0 & 0 & 0\end{pmatrix}$$
$$\begin{pmatrix} l_1 & l_2 & L \\ 0 & 0 & 0\end{pmatrix} \qquad \text{(D.20)}$$

The one–gluon exchange sum rule has a sum over the complete set of gluon quantum numbers including the zero energy scalar mode with the quantum numbers $m_0 = \{0,0,0\}$. The contribution of the zero energy scalar mode has to be calculated differently from the other modes and is calculated separately in appendix E. It is useful to calculate the sum rule for the sum over all modes except the zero energy mode. This is done by computing the contribution of this mode to the sum rule and simply subtracting it from the sum rule calculated above. The contribution of this mode to the sum rule is

$$4\pi g^{SS}\sum_{p}\tilde{Q}^{m_0S}_{n_1n_2}Q^{m_0S}_{n_3p}M_{pn_4} = -3\delta_{n_1n_2}M_{n_3n_4} \qquad \text{(D.21)}$$

and it may be subtracted from the sum rule depending on whether the zero energy mode is included in the numerical sum.

# Appendix E

# The Zero Energy Scalar Mode

The solution of the wave equation for massless vector fields subject to the M.I.T. boundary conditions includes a zero energy scalar mode. Explicitly this cavity mode is

$$a_{m_0 \mathcal{S}} = \frac{i\mathcal{N}_{m_0 \mathcal{S}}}{R^{3/2}} j_0(\Omega_{m_0 \mathcal{S}} r) Y_{00}(\hat{r}) = i\sqrt{3} Y_{00}(\hat{r}) = i\sqrt{\frac{3}{4\pi}} \tag{E.1}$$

where $m_0 = \{0, 0, 0\}$ is the set of quantum numbers describing this mode. This mode is just a constant and makes the derivative operator non–invertible.

Calculating the contribution of this mode is problematic in that at first it appears that all the Feynman diagrams diverge as the limit $\Omega \to 0$ is taken. If however proper care is taken one can show that the divergent pieces cancel to leave a finite contribution. The idea behind the method used to calculate the contribution of this mode is to consider the contribution of a new mode with the same quantum numbers but with a small but non–zero energy. The calculation is performed assuming that $\Omega$ is small and the contribution of the zero energy mode is found by taking the limit $\Omega \to 0$ of this result.

Consider a mode similar to the zero energy scalar mode which has a small but non–zero energy

$$\tilde{a}_{m_0 \mathcal{S}} = \frac{i\mathcal{N}_{m_0 \mathcal{S}}}{R^{3/2}} j_0(\Omega r) Y_{00}(\hat{r}) \tag{E.2}$$

Performing a Taylor expansion of this mode around $\Omega = 0$ one finds

$$\tilde{a}_{m_0 \mathcal{S}} = \frac{i\mathcal{N}_{m_0 \mathcal{S}}}{R^{3/2}} \left(1 - \frac{\Omega^2 r^2}{6}\right) \frac{1}{\sqrt{4\pi}} \tag{E.3}$$

The normalisation constant turns out to be

$$\mathcal{N}^{-2}_{m_0 \mathcal{S}} = \frac{1}{3}\left(1 - \frac{\Omega^2 R^2}{5}\right) \tag{E.4}$$

Using this mode one may proceed as usual to calculate the energy shift due to this mode. For example for the energy shift due to the one gluon exchange diagram is given by

$$\begin{aligned}\Delta E &= \lim_{\epsilon\to 0}\frac{3\epsilon}{2}g^2\sum_p \tilde{Q}^{0S}_{n_1n_2}Q^{0S}_{n_3p}M_{pn_4}\int dt_1\,dt_2\,dt_3 \\ &\int_{-\infty}^{\infty}\frac{d\omega}{2\pi}\frac{d\omega'}{2\pi}\,\frac{e^{-\epsilon(|t_1|+|t_2|+|t_3|)}e^{it_1(\varepsilon_1-\varepsilon_2+\omega)}e^{it_2(\varepsilon_3-\omega-\omega')}e^{it_3(\omega'-\varepsilon_4)}}{(\omega'-\varepsilon_p)(\omega^2-\Omega^2)}\end{aligned} \tag{E.5}$$

where the colour flavour matrix element has been left out. The integrals over time and $\omega$ variables may be performed in the usual way and one obtains

$$\Delta E = g^2\sum_{p\neq n_4}\tilde{Q}^{0S}_{n_1n_2}Q^{0S}_{n_3p}M_{pn_4}\frac{\delta(\varepsilon_1+\varepsilon_3,\varepsilon_2+\varepsilon_4)}{(\varepsilon_4-\varepsilon_p)\left((\varepsilon_1-\varepsilon_2)^2-\Omega^2\right)} \tag{E.6}$$

Using the definition of $\tilde{Q}^{0S}_{n_1n_2}$ and $Q^{0S}_{n_1n_2}$ and substituting the gluon mode (E.3) and the normalisation constant (E.4) one finds

$$\begin{aligned}\Delta E &= -\frac{g^2}{4\pi}\frac{3}{R^3}\left(1+\frac{\Omega^2R^2}{5}\right)\sum_{p\neq n_4}\int d^3x\; u^\dagger_{n_1}(\vec{x})u_{n_2}(\vec{x})\left(1-\frac{\Omega^2r_x^2}{6}\right) \\ &\int d^3y\; u^\dagger_{n_3}(\vec{y})u_p(\vec{y})\left(1-\frac{\Omega^2r_y^2}{6}\right)M_{pn_4}\frac{\delta(\varepsilon_1+\varepsilon_3,\varepsilon_2+\varepsilon_4)}{(\varepsilon_4-\varepsilon_p)\left((\varepsilon_1-\varepsilon_2)^2-\Omega^2\right)}\end{aligned} \tag{E.7}$$

Using the quark orthonormality relation $\int d^3x\; u^\dagger_n(\vec{x})u_{n'}(\vec{x}) = \delta_{nn'}$ and keeping only terms up to $O(\Omega^2)$ this can be written as

$$\begin{aligned}\Delta E &= \alpha_S\frac{-3}{R^3}\left(1+\frac{\Omega^2R^2}{5}\right)\sum_{p\neq n_4}\left[\delta_{n_1n_2}\delta_{n_3p}-\frac{\Omega^2}{6}\delta_{n_1n_2}P_{n_3p}-\frac{\Omega^2}{6}\delta_{n_3p}P_{n_1n_2}\right] \\ &M_{pn_4}\frac{\delta(\varepsilon_1+\varepsilon_3,\varepsilon_2+\varepsilon_4)}{(\varepsilon_4-\varepsilon_p)\left((\varepsilon_1-\varepsilon_2)^2-\Omega^2\right)}\end{aligned} \tag{E.8}$$

where $P_{nn'}$ is defined as

$$\begin{aligned}P_{nn'} &= \int d^3r\; r^2u^\dagger_n(\vec{r})u_{n'}(\vec{r}) \\ &= \int_0^R dr\; r^4(g_ng_{n'}+f_nf_{n'})\delta_{\kappa\kappa'}\delta_{\mu\mu'}\end{aligned} \tag{E.9}$$

The first term in eq. (E.8) can be dropped as this term forces $p = n_4$ which is excluded from the sum. The third term tends to zero in the limit $\Omega \to 0$, leaving only the second term which in the limit $\Omega \to 0$ is

$$\Delta E = \alpha_S \sum_{p \neq n_4} \frac{M_{pn_4} P_{n_3 p} \delta_{n_1 n_2}}{2R^3(\varepsilon_p - \varepsilon_4)} \tag{E.10}$$

There are two one gluon exchange diagrams so this result must be multiplied by 2 to get the two–body contribution. Note that there is a delta function forcing $n_1 = n_2$ which includes the magnetic quantum number. This differs from all the previous results which had a delta function of the energies which does not restrict the magnetic quantum numbers. The calculation of the contribution of the zero energy mode to the vertex correction diagram proceeds in the same way as for the one–gluon exchange diagram. The contribution of this mode to this graph is

$$\Delta E = \frac{3\alpha_S M_{n_1 n_2}}{2\Omega^3 R^3}\left(1 + \frac{\Omega^2 R^2}{5}\right) - \frac{\alpha_S P_{n_1 n_2} M_{n_2 n_2}}{2\Omega R^3} + \frac{\alpha_S}{R^3} \sum_{p \neq n_2} M_{n_1 p} P_{p n_1} \frac{\text{sgn } \varepsilon_{n_1}}{2(\varepsilon_{n_1} - \varepsilon_p)} \tag{E.11}$$

which is infinite in the limit $\Omega \to 0$. This is not a problem as the divergent part here is exactly by the corresponding divergant part of the two self–energy insert diagrams. The zero energy scalar mode to the self–energy insert diagram is given by

$$\Delta E = \frac{-3\alpha_S M_{n_1 n_2}}{4\Omega^3 R^3}\left(1 + \frac{\Omega^2 R^2}{5}\right) + \frac{\alpha_S P_{n_1 n_2} M_{n_2 n_2}}{4\Omega R^3} + \frac{\alpha_S}{R^3} \sum_{p \neq n_2} M_{n_1 p} P_{p n_1} \frac{\text{sgn } \varepsilon_{n_1}}{4(\varepsilon_{n_1} - \varepsilon_p)} \tag{E.12}$$

Since there are two self–energy insert diagrams the sum of the one–body corrections is given by

$$\Delta E = \frac{-\alpha_S}{R^3} \sum_{p \neq n_2} M_{n_1 p} P_{p n_1} \frac{\text{sgn } \varepsilon_{n_1}}{(\varepsilon_p - \varepsilon_{n_1})} \tag{E.13}$$

which has the same magnitude as the zero energy scalar mode for the two one gluon exchange diagrams, but the opposite sign.

It should be noted that the zero energy scalar mode has no net effect on the final results. This is because the scalar modes in the one gluon exchange diagrams depend only on the quark which is hit by the photon and not the other quark which is hit by the gluon. This leads to the two–body colour flavour matrix element reducing to the one body colour flavour matrix element for this state. Due to the fact that the one–body contributions have equal magnitude but opposite sign to the two–body contribution the sum of the diagrams involving the zero energy scalar mode vanish. It is however important to include these modes in the results if one wishes to compare the results of

the one–body and two–body diagrams seperately, especially with calculations in other guages.

# Appendix F

# Colour Flavour Matrix Elements

The colour flavour matrix elements are the matrix elements of the quark creation and annihilation operators between the various baryon states. There are two types of colour flavour matrix elements used in this work, the one–body and the two–body matrix elements. The introduction of massive quarks makes these matrix elements somewhat longer than if it is assumed that all quarks are massless as one has to keep track of the flavour of the quark states as well. This is especially true for the two–body matrix elements.

## F.1 One–Body Matrix Elements

The one body colour flavour matrix elements are given by

$$\langle X| \sum_{\substack{cfn_1 \\ c'f'n_2}} a^\dagger_{c'f'n_1} \left(\frac{\lambda^a}{2}\right)_{c'd} \left(\frac{\lambda^a}{2}\right)_{dc} Q a_{cfn_2} |X\rangle \tag{F.1}$$

where $Q$ is the electromagnetic charge operator which returns the electromagnetic charge of a quark with flavour $f$. The $\lambda^a$'s refer to the Gell–Mann matrices and the states $|X\rangle$ refer to the non interacting quark wave function of one of the baryons. The wavefunctions of the baryons can be written in second quantised form, for example

$$|\Sigma^+\rangle = \frac{\varepsilon^{abc}}{\sqrt{18}} \left(a^\dagger_{aun\uparrow} a^\dagger_{bsn\downarrow} - a^\dagger_{aun\downarrow} a^\dagger_{bsn\uparrow}\right) a^\dagger_{cun\uparrow} |0\rangle \tag{F.2}$$

where the quantum numbers $n\uparrow$ ($n\downarrow$) refer to the $1S_{\frac{1}{2}}$ state with spin up (down). $\varepsilon^{abc}$ is the totally antisymmetric tensor of rank 3. Since the external photon is colourless

and flavourless, quarks on either side of the quark–photon vertex have the same colour and flavour. The gluons are flavourless and the effect of the gluons on the colour of the quark is all in the Gell–Mann matrices which via the standard relation

$$\sum_d \left(\frac{\lambda^a}{2}\right)_{c'd} \left(\frac{\lambda^a}{2}\right)_{dc} = \frac{4}{3}\delta_{c'c} \tag{F.3}$$

show that the colour of the quarks on either side of the matrix element must be the same. Energy and angular momentum are conserved in the cavity due to time translational invariance and spatial rotational invariance of the cavity. Since the external photon carries no energy, the energy of the quark before and after the interaction is the same. Due to the discrete nature of the energy states in the cavity this means that the radial and angular quantum numbers are the same. The spin of the quarks is also the same due to the fact that the photon carries no angular momentum in the $z$–direction. Thus the colour flavour matrix elements can be written as

$$\frac{4}{3}\langle X|a^\dagger_{cfn} Q a_{cfn}|X\rangle \tag{F.4}$$

where there is an implicit sum over the quantum numbers $c, f$ and $n$. Using the anti-commutation relation between the quark creation and annihilation operators

$$\left\{a_{cfn}, a^\dagger_{c'f'n'}\right\} = \delta_{cc'}\delta_{ff'}\delta_{nn'} \tag{F.5}$$

the quark creation operators can be anti–commuted to the left and the annihilation operators anti–commuted to the right until the vacuum state is reached where the relations $a_{cfn}|0\rangle = 0$ and $\langle 0|a^\dagger_{cfn} = 0$ are used. These anti–commutations can be done analytically using a symbolic manipulation package REDUCE 3.3. The results of the one body colour flavour matrix elements as given in eq. (F.4) between the following states are

$$|P\rangle \rightsquigarrow -\frac{4}{27}\Big(\delta_{f,d}\left[2\delta_{\mu,\downarrow} + \delta_{\mu,\uparrow}\right] - \delta_{f,u}\left[2\delta_{\mu,\downarrow} + 10\delta_{\mu,\uparrow}\right]\Big) \tag{F.6}$$

$$|N\rangle \rightsquigarrow -\frac{4}{27}\Big(\delta_{f,d}\left[\delta_{\mu,\downarrow} + 5\delta_{\mu,\uparrow}\right] - \delta_{f,u}\left[4\delta_{\mu,\downarrow} + 2\delta_{\mu,\uparrow}\right]\Big) \tag{F.7}$$

$$|\Sigma^+\rangle \rightsquigarrow -\frac{4}{27}\Big(\delta_{f,s}\left[2\delta_{\mu,\downarrow} + \delta_{\mu,\uparrow}\right] - \delta_{f,u}\left[2\delta_{\mu,\downarrow} + 10\delta_{\mu,\uparrow}\right]\Big) \tag{F.8}$$

$$|\Sigma^0\rangle \rightsquigarrow -\frac{2}{27}\Big(\delta_{f,s}\left[4\delta_{\mu,\downarrow} + 2\delta_{\mu,\uparrow}\right] + \delta_{f,d}\left[\delta_{\mu,\downarrow} + 5\delta_{\mu,\uparrow}\right] - \delta_{f,u}\left[2\delta_{\mu,\downarrow} + 10\delta_{\mu,\uparrow}\right]\Big) \tag{F.9}$$

$$|\Sigma^-\rangle \rightsquigarrow -\frac{4}{27}\Big(\delta_{f,s}\left[2\delta_{\mu,\downarrow} + \delta_{\mu,\uparrow}\right] - \delta_{f,d}\left[\delta_{\mu,\downarrow} + 5\delta_{\mu,\uparrow}\right]\Big) \tag{F.10}$$

$$|\Lambda^0\rangle \rightsquigarrow \frac{4}{9}\Big(\delta_{f,s}\delta_{\mu,\uparrow} + \delta_{f,u}\left[\delta_{\mu,\downarrow} + \delta_{\mu,\uparrow}\right]\Big) \tag{F.11}$$

$$|\Xi^-\rangle \rightsquigarrow -\frac{4}{27}\Big(\delta_{f,d}\left[2\delta_{\mu,\downarrow} + \delta_{\mu,\uparrow}\right] + \delta_{f,s}\left[\delta_{\mu,\downarrow} + 5\delta_{\mu,\uparrow}\right]\Big) \tag{F.12}$$

$$|\Xi^0\rangle \rightsquigarrow -\frac{4}{27}\Big(\delta_{f,s}\left[\delta_{\mu,\downarrow} + 5\delta_{\mu,\uparrow}\right] - \delta_{f,u}\left[4\delta_{\mu,\downarrow} - 2\delta_{\mu,\uparrow}\right]\Big) \tag{F.13}$$

## F.2 Two–Body Matrix Elements

The two body colour flavour matrix elements are found in the one–gluon exchange diagrams and they are defined as follows

$$\langle X| \sum_{\substack{cdc'd'fgf'g' \\ n_1n_2n_3n_4}} a^\dagger_{c'f'n_1} a^\dagger_{d'g'n_3} \left(\frac{\lambda^a}{2}\right)_{c'c} \left(\frac{\lambda^a}{2}\right)_{d'd} Q a_{cfn_2} a_{dgn_4} |X\rangle \tag{F.14}$$

where the operator $Q$ returns the electromagnetic charge of a quark with flavour $g$. As there are no flavour changing interactions occurring the quark flavour along the quark lines $n_1n_2$ and $n_3n_4$ must remain the same. The colour factor

$$\left(\frac{\lambda^a}{2}\right)_{c'c} \left(\frac{\lambda^a}{2}\right)_{d'd} = \frac{1}{2}\left(\delta_{c'd}\delta_{cd'}\right) - \frac{1}{3}\delta_{cc'}\delta_{d'd} \tag{F.15}$$

restricts the change of colour along the quark lines. The colour flavour matrix elements may thus be written as

$$\langle X| a^\dagger_{c'fn_1} a^\dagger_{d'gn_3} \left(\frac{\lambda^a}{2}\right)_{c'c} \left(\frac{\lambda^a}{2}\right)_{d'd} Q a_{cfn_2} a_{dgn_4} |X\rangle \tag{F.16}$$

Using the same techniques as for the one–body colour flavour matrix elements one finds the following results when the two–body colour flavour matrix element is taken between the states $|X\rangle$ :

$$\begin{aligned} |P\rangle \rightsquigarrow \frac{2}{27}\Big[ & \delta_{f,d}\delta_{g,u}\left(8\delta_{\downarrow\downarrow\uparrow\uparrow} - 4\delta_{\downarrow\uparrow\uparrow\downarrow} - 4\delta_{\uparrow\downarrow\downarrow\uparrow} + 2\delta_{\uparrow\uparrow\downarrow\downarrow} + 2\delta_{\uparrow\uparrow\uparrow\uparrow}\right) \\ & + \delta_{f,u}\delta_{g,d}\left(-\delta_{\downarrow\downarrow\uparrow\uparrow} + 2\delta_{\downarrow\uparrow\uparrow\downarrow} + 2\delta_{\uparrow\downarrow\downarrow\uparrow} - 4\delta_{\uparrow\uparrow\downarrow\downarrow} - \delta_{\uparrow\uparrow\uparrow\uparrow}\right) \\ & + \delta_{f,u}\delta_{g,u}\left(2\delta_{\downarrow\downarrow\uparrow\uparrow} + 2\delta_{\downarrow\uparrow\uparrow\downarrow} + 2\delta_{\uparrow\downarrow\downarrow\uparrow} + 2\delta_{\uparrow\uparrow\downarrow\downarrow} + 8\delta_{\uparrow\uparrow\uparrow\uparrow}\right)\Big] \end{aligned} \tag{F.17}$$

$$|N\rangle \rightsquigarrow -\frac{2}{27}\Big[\delta_{f,d}\delta_{g,d}\left(\delta_{\downarrow\uparrow\uparrow\uparrow}+\delta_{\downarrow\uparrow\uparrow\downarrow}+\delta_{\uparrow\downarrow\uparrow\uparrow}+\delta_{\uparrow\uparrow\downarrow\uparrow}+4\delta_{\uparrow\uparrow\uparrow\uparrow}\right) \tag{F.18}$$
$$+\delta_{f,d}\delta_{g,u}\left(-2\delta_{\downarrow\uparrow\uparrow\uparrow}+4\delta_{\downarrow\uparrow\uparrow\downarrow}+4\delta_{\uparrow\downarrow\uparrow\uparrow}-8\delta_{\uparrow\uparrow\downarrow\uparrow}-2\delta_{\uparrow\uparrow\uparrow\uparrow}\right)$$
$$+\delta_{f,u}\delta_{g,d}\left(4\delta_{\downarrow\uparrow\uparrow\uparrow}-2\delta_{\downarrow\uparrow\uparrow\downarrow}-2\delta_{\uparrow\downarrow\uparrow\uparrow}+\delta_{\uparrow\uparrow\downarrow\uparrow}+\delta_{\uparrow\uparrow\uparrow\uparrow}\right)\Big]$$

$$|\Sigma^+\rangle \rightsquigarrow \frac{2}{27}\Big[\delta_{f,s}\delta_{g,u}\left(8\delta_{\downarrow\uparrow\uparrow\uparrow}-4\delta_{\downarrow\uparrow\uparrow\downarrow}-4\delta_{\uparrow\downarrow\uparrow\uparrow}+2\delta_{\uparrow\uparrow\downarrow\uparrow}+2\delta_{\uparrow\uparrow\uparrow\uparrow}\right) \tag{F.19}$$
$$+\delta_{f,u}\delta_{g,s}\left(-\delta_{\downarrow\uparrow\uparrow\uparrow}+2\delta_{\downarrow\uparrow\uparrow\downarrow}+2\delta_{\uparrow\downarrow\uparrow\uparrow}-4\delta_{\uparrow\uparrow\downarrow\uparrow}-\delta_{\uparrow\uparrow\uparrow\uparrow}\right)$$
$$+\delta_{f,u}\delta_{g,u}\left(2\delta_{\downarrow\uparrow\uparrow\uparrow}+2\delta_{\downarrow\uparrow\uparrow\downarrow}+2\delta_{\uparrow\downarrow\uparrow\uparrow}+2\delta_{\uparrow\uparrow\downarrow\uparrow}+8\delta_{\uparrow\uparrow\uparrow\uparrow}\right)\Big]$$

$$|\Sigma^0\rangle \rightsquigarrow -\frac{2}{27}\Big[\delta_{f,s}\delta_{g,d}\left(4\delta_{\downarrow\uparrow\uparrow\uparrow}-2\delta_{\downarrow\uparrow\uparrow\downarrow}-2\delta_{\uparrow\downarrow\uparrow\uparrow}+\delta_{\uparrow\uparrow\downarrow\uparrow}+\delta_{\uparrow\uparrow\uparrow\uparrow}\right) \tag{F.20}$$
$$+\delta_{f,s}\delta_{g,u}\left(-8\delta_{\downarrow\uparrow\uparrow\uparrow}+4\delta_{\downarrow\uparrow\uparrow\downarrow}+4\delta_{\uparrow\downarrow\uparrow\uparrow}-2\delta_{\uparrow\uparrow\downarrow\uparrow}-2\delta_{\uparrow\uparrow\uparrow\uparrow}\right)$$
$$+\delta_{f,d}\delta_{g,s}\left(\delta_{\downarrow\uparrow\uparrow\uparrow}-2\delta_{\downarrow\uparrow\uparrow\downarrow}-2\delta_{\uparrow\downarrow\uparrow\uparrow}+4\delta_{\uparrow\uparrow\downarrow\uparrow}+\delta_{\uparrow\uparrow\uparrow\uparrow}\right)$$
$$+\delta_{f,d}\delta_{g,u}\left(-2\delta_{\downarrow\uparrow\uparrow\uparrow}-2\delta_{\downarrow\uparrow\uparrow\downarrow}-2\delta_{\uparrow\downarrow\uparrow\uparrow}-2\delta_{\uparrow\uparrow\downarrow\uparrow}-8\delta_{\uparrow\uparrow\uparrow\uparrow}\right)$$
$$+\delta_{f,u}\delta_{g,s}\left(\delta_{\downarrow\uparrow\uparrow\uparrow}-2\delta_{\downarrow\uparrow\uparrow\downarrow}-2\delta_{\uparrow\downarrow\uparrow\uparrow}+4\delta_{\uparrow\uparrow\downarrow\uparrow}+\delta_{\uparrow\uparrow\uparrow\uparrow}\right)$$
$$+\delta_{f,u}\delta_{g,d}\left(\delta_{\downarrow\uparrow\uparrow\uparrow}+\delta_{\downarrow\uparrow\uparrow\downarrow}+\delta_{\uparrow\downarrow\uparrow\uparrow}+\delta_{\uparrow\uparrow\downarrow\uparrow}+4\delta_{\uparrow\uparrow\uparrow\uparrow}\right)\Big]$$

$$|\Sigma^-\rangle \rightsquigarrow -\frac{2}{27}\Big[\delta_{f,s}\delta_{g,d}\left(4\delta_{\downarrow\uparrow\uparrow\uparrow}-2\delta_{\downarrow\uparrow\uparrow\downarrow}-2\delta_{\uparrow\downarrow\uparrow\uparrow}+\delta_{\uparrow\uparrow\downarrow\uparrow}+\delta_{\uparrow\uparrow\uparrow\uparrow}\right) \tag{F.21}$$
$$+\delta_{f,d}\delta_{g,s}\left(\delta_{\downarrow\uparrow\uparrow\uparrow}-2\delta_{\downarrow\uparrow\uparrow\downarrow}-2\delta_{\uparrow\downarrow\uparrow\uparrow}+4\delta_{\uparrow\uparrow\downarrow\uparrow}+\delta_{\uparrow\uparrow\uparrow\uparrow}\right)$$
$$+\delta_{f,d}\delta_{g,d}\left(\delta_{\downarrow\uparrow\uparrow\uparrow}+\delta_{\downarrow\uparrow\uparrow\downarrow}+\delta_{\uparrow\downarrow\uparrow\uparrow}+\delta_{\uparrow\uparrow\downarrow\uparrow}+4\delta_{\uparrow\uparrow\uparrow\uparrow}\right)\Big]$$

$$|\Lambda^0\rangle \rightsquigarrow \frac{2}{27}\Big[ + \delta_{f,d}\delta_{g,u}\,(-2\delta_{\downarrow\uparrow\uparrow\uparrow} + 2\delta_{\downarrow\uparrow\uparrow\downarrow} + 2\delta_{\uparrow\downarrow\uparrow\uparrow} - 2\delta_{\uparrow\uparrow\downarrow\downarrow}) \tag{F.22}$$

$$+ \delta_{f,s}\delta_{g,d}\,(+\delta_{\uparrow\uparrow\downarrow\downarrow} + \delta_{\uparrow\uparrow\uparrow\uparrow}) + \delta_{f,s}\delta_{g,u}\,(-2\delta_{\uparrow\uparrow\downarrow\downarrow} - 2\delta_{\uparrow\uparrow\uparrow\uparrow})$$

$$+ \delta_{f,u}\delta_{g,s}\,(\delta_{\downarrow\uparrow\uparrow\uparrow} - \delta_{\uparrow\uparrow\uparrow\uparrow}) + \delta_{f,d}\delta_{g,s}\,(\delta_{\downarrow\uparrow\uparrow\uparrow} + \delta_{\uparrow\uparrow\uparrow\uparrow})$$

$$+ \delta_{f,u}\delta_{g,d}\,(\delta_{\downarrow\uparrow\uparrow\uparrow} - \delta_{\downarrow\uparrow\uparrow\downarrow} - \delta_{\uparrow\downarrow\uparrow\uparrow} + \delta_{\uparrow\uparrow\downarrow\downarrow})\Big]$$

$$|\Xi^-\rangle \rightsquigarrow \frac{2}{27}\Big[\delta_{f,s}\delta_{g,d}\,(4\delta_{\downarrow\uparrow\uparrow\uparrow} - 2\delta_{\downarrow\uparrow\uparrow\downarrow} - 2\delta_{\uparrow\downarrow\uparrow\uparrow} + \delta_{\uparrow\uparrow\downarrow\downarrow} + \delta_{\uparrow\uparrow\uparrow\uparrow}) \tag{F.23}$$

$$+ \delta_{f,d}\delta_{g,s}\,(\delta_{\downarrow\uparrow\uparrow\uparrow} - 2\delta_{\downarrow\uparrow\uparrow\downarrow} - 2\delta_{\uparrow\downarrow\uparrow\uparrow} + 4\delta_{\uparrow\uparrow\downarrow\downarrow} + \delta_{\uparrow\uparrow\uparrow\uparrow})$$

$$+ \delta_{f,d}\delta_{g,d}\,(\delta_{\downarrow\uparrow\uparrow\uparrow} + \delta_{\downarrow\uparrow\uparrow\downarrow} + \delta_{\uparrow\downarrow\uparrow\uparrow} + \delta_{\uparrow\uparrow\downarrow\downarrow} + 4\delta_{\uparrow\uparrow\uparrow\uparrow})\Big]$$

$$|\Xi^0\rangle \rightsquigarrow -\frac{2}{27}\Big[\delta_{f,d}\delta_{g,d}\,(\delta_{\downarrow\uparrow\uparrow\uparrow} + \delta_{\downarrow\uparrow\uparrow\downarrow} + \delta_{\uparrow\downarrow\uparrow\uparrow} + \delta_{\uparrow\uparrow\downarrow\downarrow} + 4\delta_{\uparrow\uparrow\uparrow\uparrow}) \tag{F.24}$$

$$+ \delta_{f,d}\delta_{g,u}\,(-2\delta_{\downarrow\uparrow\uparrow\uparrow} + 4\delta_{\downarrow\uparrow\uparrow\downarrow} + 4\delta_{\uparrow\downarrow\uparrow\uparrow} - 8\delta_{\uparrow\uparrow\downarrow\downarrow} - 2\delta_{\uparrow\uparrow\uparrow\uparrow})$$

$$+ \delta_{f,u}\delta_{g,d}\,(4\delta_{\downarrow\uparrow\uparrow\uparrow} - 2\delta_{\downarrow\uparrow\uparrow\downarrow} - 2\delta_{\uparrow\downarrow\uparrow\uparrow} + \delta_{\uparrow\uparrow\downarrow\downarrow} + \delta_{\uparrow\uparrow\uparrow\uparrow})\Big]$$

where the shorthand $\delta_{\uparrow\downarrow\uparrow\downarrow} = \delta_{\mu_1,\uparrow}\delta_{\mu_2,\downarrow}\delta_{\mu_3,\uparrow}\delta_{\mu_4,\downarrow}$ and all of the quarks above are restricted to be in the $1S_{\frac{1}{2}}$ state.

# Appendix G

# Units and Conventions

Throughout this thesis natural units $\hbar = c = 1$ have been used. These factors may be restored in the final results of the calculation using simple dimensional analysis. The numerical values of $\hbar c$ and the proton mass used are

$$\begin{aligned} \hbar c &= 197,327053 \quad \text{MeVfm} \\ m_p &= 938,272 \quad \text{MeV/c}^2 \end{aligned}$$

The cavity radius has been set to 1 fm and is the natural unit of length in the cavity. This unit of length must also be restored if M.K.S. units are needed. For example the mass is related to the dimensionless mass by

$$m_f = \frac{\eta_f \hbar}{Rc} \tag{G.1}$$

and the energy $\varepsilon$ is related to the dimensionless energy $\omega$ by

$$\varepsilon = \frac{\omega R}{\hbar c} = \frac{\omega}{0.197327} \quad \text{GeV} \tag{G.2}$$

The usual flat Minkowski space metric has been used

$$g^{\nu\mu} = g_{\nu\mu} = \text{diag}\{+1,-1,-1,-1\} \qquad g^{\nu}_{\mu} = \delta^{\nu}_{\mu} \tag{G.3}$$

The Dirac matrices satisfy the Clifford algebra

$$\{\gamma^{\mu}, \gamma^{\nu}\} = 2g^{\mu\nu} \tag{G.4}$$

The gamma matrices in the Dirac representation are used and they are given by

$$\gamma^0 = \begin{pmatrix} I & 0 \\ 0 & -I \end{pmatrix} \quad \gamma^k = \begin{pmatrix} 0 & \sigma^k \\ -\sigma^k & 0 \end{pmatrix} \quad \text{where } k = 1,2,3 \tag{G.5}$$

where $\sigma^k$ are the 2×2 Pauli matrices

$$\sigma^1 = \begin{pmatrix} 0 & 1 \\ 1 & 0 \end{pmatrix} \quad \sigma^2 = \begin{pmatrix} 0 & -i \\ i & 0 \end{pmatrix} \quad \sigma^3 = \begin{pmatrix} 1 & 0 \\ 0 & -1 \end{pmatrix} \tag{G.6}$$

# Bibliography


[1] G. E. Brown and M. Rho, Phys. Lett. **B82** (1979) 177

G. E. Brown, M. Rho and V. Vento, Phys. Lett. **B84** (1979) 383.

[2] A. W. Thomas, Advances in Nuclear Physics, **13** (1983) 1.

[3] R.F. Buser, R.D. Viollier and P. Zimak, International Journal of Theoretical Physics **27** (1988) 925

[4] T. D. Lee, Phys. Rev. **D19** (1979) 1802.

[5] G. U. Schreiber, *The Gluon Self-Energy in Cavity QCD*, PhD thesis, University of Cape Town, May 1991, UCT–TP 172/91, unpublished.

G. U. Schreiber and R. D. Viollier, Phys. Lett. **B279** (1992) 131.

[6] J. A. Cuthbert, *Massive Quark Self-Energy in Cavity QCD*, MSc thesis, University of Cape Town, Sept 1991, unpublished.

[7] M. O'Connor, The Anomalous Magnetic Moment of the Nucleon in Cavity QCD, Ph.D thesis, unpublished, University of Cape Town, 1991, preprint UCT-TP 164/91

[8] J. Sucher, Phys. Rev. **107** (1957) 1448.

[9] A.R. Edmonds, *Angular momentum in Quantum Mechanics*, (Princeton University Press, New Jersey, 1957)

[10] D.A. Varshalovich, A.N. Moskalev and V.K. Khersonskii, *Quantum Theory of Angular Momentum*, (World Scientific, Singapore, 1988)

[11] R.D. Viollier, S.A.Chin and A.K.Kerman, Nucl. Phys. **A407** (1983) 269

[12] R.P. Feynman, Phys. Rev. **76** (1949) 769.

[13] A.J. Stoddart, Renormalisation of Cavity Field Theories, Ph.D thesis, unpublished, University of Cape Town preprint UCT-TP 139/90 1990.

A. J. Stoddart and R. D. Viollier Phys. Lett. **B236** (1990) 387.

[14] A. Chodos, R.L. Jaffe, K. Johnson, C.B. Thorn and V.F. Weisskopf, Phys. Rev. **D9** (1974) 3471.

A. Chodos, R.L. Jaffe, K. Johnson and C.B. Thorn, Phys. Rev. **D10** (1974) 2599.

T. DeGrand, R.L. Jaffe, K.Johnson and J.Kiskis, Phys. Rev. **D12** (1975) 2060.

[15] E. Gillman and H.R. Fiebig, Computers in Physics, Vol. **2** no. 1 (1988) 62.

[16] M. Abramowitz and I.A. Stegun, *Handbook of Mathematical Functions*, (Dover, New York, 1965).

[17] O.V. Maxwell and V. Vento, Nucl. Phys. **A407** (1983) 366.

[18] J.D. Bjorken, Phys. Rev. **179** (1969) 1547.

[19] C.A. Dominguez and E. DeRafael, Ann. of Phys. **174** (1987) 372

[20] C.A. Dominguez, C van Gend and N Paver, Phys. Lett. **B253** (1991) 241

[21] A.L. Fetter and J. D. Walecka, *Quantum theory of Many Particle systems* (McGraw-Hill,New York, 1971).

[22] K. Tsushima, T. Yamaguchi, Y.Kohyama and K. Kubodera, Nucl. Phys. **A489** (1988) 557.

[23] H. Høgaasen and F. Myhrer, Phys. Rev. **D37** (1988) 1950.

[24] K. Ushio, Phys. Lett. **158B** (1985) 71.

[25] M. I. Krivoruchenko, Sov. J. Nucl. Phys. **40** (1984) 514.

[26] A. J. Stoddart and R. D. Viollier, Phys. Lett. **B208** (1988) 65.

[27] P. R. Page, R. J. Lindebaum and R. D. Viollier, Nucl. Phys. **B** (to be published).

[28] M O'Connor, Private communication.